UNIVERSIDADE ESTADUAL DE CAMPINAS
FACULDADE DE ENGENHARIA DE ALIMENTOS

UNICAMP

RAUL FAVARO NASCIMENTO

AGLOMERAÇÃO EM LEITO FLUIDIZADO: DETECÇÃO DOS MECANISMOS DE FORMAÇÃO DE GRÂNULOS E DAS PONTES SÓLIDAS POR VELOCIMETRIA DE FILTRO ESPACIAL E ANÁLISE DE IMAGENS

FLUIDIZED BED AGGLOMERATION: DETECTION OF THE GRANULE FORMATION MECHANISMS AND THE SOLID BRIDGES BY SPATIAL FILTER VELOCIMETRY AND IMAGE ANALYSIS

Campinas-SP

2023

RAUL FAVARO NASCIMENTO

FLUIDIZED BED AGGLOMERATION: DETECTION OF THE GRANULE FORMATION MECHANISMS AND THE SOLID BRIDGES BY SPATIAL FILTER VELOCIMETRY AND IMAGE ANALYSIS

AGLOMERAÇÃO EM LEITO FLUIDIZADO: ANÁLISE DOS MECANISMOS DE FORMAÇÃO DE GRÂNULOS E DAS PONTES SÓLIDAS POR VELOCIMETRIA DE FILTRO ESPACIAL E ANÁLISE DE IMAGENS

Thesis presented to the School of Food Engineering of the University of Campinas in partial fulfillment of the requirements for the degree of Doctor in Food Engineering.

Tese apresentada à Faculdade de Engenharia de Alimentos da Universidade de Campinas como parte dos requisitos exigidos para a obtenção do título de Doutor em Engenharia de Alimentos.

Orientadora: Profª. Drª. Louise Emy Kurozawa

Coorientador: Prof. Dr. Osvaldir Pereira Taranto

ESTE TRABALHO CORRESPONDE À VERSÃO FINAL DA TESE DEFENDIDA PELO ALUNO RAUL FAVARO NASCIMENTO, E ORIENTADA PELA PROFA. DRA. LOUISE EMY KUROZAWA.

Campinas-SP

2023

Ficha catalográfica
Universidade Estadual de Campinas
Biblioteca da Faculdade de Engenharia de Alimentos
Claudia Aparecida Romano - CRB 8/5816

N17f

Nascimento, Raul Favaro, 1988-
Fluidized bed agglomeration : detection of the granule formation mechanisms and the solid bridges by spatial filter velocimetry and image analysis / Raul Favaro Nascimento. – Campinas, SP : [s.n.], 2023.

Orientador: Louise Emy Kurozawa.
Coorientador: Osvaldir Pereira Taranto.
Tese (doutorado) – Universidade Estadual de Campinas, Faculdade de Engenharia de Alimentos.

1. Aglomeração. 2. Leito fluidizado. 3. Bibliometria. 4. Partículas. I. Kurozawa, Louise Emy. II. Taranto, Osvaldir Pereira. III. Universidade Estadual de Campinas. Faculdade de Engenharia de Alimentos. IV. Título.

Informações Complementares

Título em outro idioma: Aglomeração em leito fluidizado : detecção dos mecanismos de formação de grânulos e das pontes sólidas por velocimetria de filtro espacial e análise de imagens
Palavras-chave em inglês:
Agglomeration
Fluidized bed
Bibliometrics
Particles
Área de concentração: Engenharia de Alimentos
Titulação: Doutor em Engenharia de Alimentos
Banca examinadora:
Louise Emy Kurozawa [Orientador]
Gustavo Cesar Dacanal
Fabio Bentes Freire
Marcos Antonio de Souza Barrozo
Juliana Gomes Rosa
Data de defesa: 01-06-2023
Programa de Pós-Graduação: Engenharia de Alimentos

Identificação e informações acadêmicas do(a) aluno(a)
- ORCID do autor: https://orcid.org/0000-0003-1125-6805
- Currículo Lattes do autor: http://lattes.cnpq.br/2063152147699555

COMMITTEE MEMBERS

Prof.ª Dr.ª Louise Emy Kurozawa

Universidade Estadual de Campinas – UNICAMP

Prof. Dr. Gustavo Cesar Dacanal

Universidade de São Paulo – USP

Prof. Dr. Fábio Bentes Freire

Universidade Federal de São Carlos – UFSCar

Prof. Dr. Marcos Antônio de Souza Barrozo

Universidade Federal de Uberlândia – UFU

Prof.ª Dr.ª Juliana Gomes Rosa

Instituto Federal do Espírito Santo – IFES

A ata de defesa com as respectivas assinaturas dos membros encontra-se no SIGA/Sistema de Fluxo de Dissertações e Teses e na Secretaria do Programa da Unidade.

To the child who still lives within me and who may not feel a sense of belonging in this world: believe me, there is a beautiful place meant just for you.

"Education does not change the world, education changes people, people change the world"

Paulo Freire

"Every new discovery is just a reminder: we are small and stupid. And who knows what great new discovery is coming next to make us feel even more insignificant"

Everything Everywhere All At Once

ACKNOWLEDGEMENTS

What are dreams made of? What are accomplishments made of?

Perhaps this is the conclusion of the longest cycle of my life so far. A path that I chose to walk and thought would be lonely. It was not. To everyone who crossed my path and who, in some way, no matter how small, changed my life, I thank you.

I thank God who definitely writes straight on tortuous lines.

I thank my family for their sacrifice, resistance, understanding, and support. For being present even when far away. No distance is too long when you are on the inside.

I thank my friends, from yesterday and today, for their admiration, recognition, and support. Burdens are lighter when shared.

I thank my advisor, Dr. Louise Emy Kurozawa, for seeing in me the professional that I did not see for some time. Thank you for giving me the tools, showing me the way, and definitely guiding me.

I thank my co-advisor, Dr. Osvaldir Pereira Taranto, for his unique contribution to my academic formation.

I thank the committee members for accepting to evaluate and contribute to this work. Undoubtedly, the vast experience in the area and the knowledge about the subject significantly contributed to the improvement of this thesis. Your presence was an honor.

I thank the School of Food Engineering, the School of Chemical Engineering, and the State University of Campinas for providing access to the infrastructure and the opportunity to conduct cutting-edge research on their premises.

I thank you, who still does not know that this work exists, but for whom and for what this work was done. Research should be done looking at what has already been done, but envisioning that someone, somewhere, at some point in the future, will be curious and feel compelled to take a step further based on what was done here. May this work be an inspiration to change someone's life, just as it changed mine. And that is what dreams and accomplishments are made of.

Thank you.

RESUMO

Leitos fluidizados têm sido utilizados para promover a aglomeração em processos industriais, pois melhoram as propriedades do pó. A Velocimetria de Filtro Espacial é uma técnica usada para monitorar, controlar e entender a granulação. O tamanho das gotas de uma solução ligante pulverizada é um fator crucial para o aumento do tamanho da partícula. Para aglomerar um material particulado é necessária a formação de pontes sólidas, mas isso ainda não é bem compreendido. Este trabalho teve como objetivo examinar a evolução do processo em tempo real e a influência das condições operacionais; investigar as propriedades físico-químicas de soluções de maltodextrina, bem como sua influência no tamanho das gotas e no crescimento das partículas; e compreender como a evolução das classes de partículas, os espectros Raman e a microscopia podem auxiliar no entendimento da formação dos grânulos. Inicialmente, foi realizada uma análise bibliométrica e uma revisão bibliográfica para identificar as tendências da aglomeração em leito fluidizado nas últimas quatro décadas. Para todos os experimentos, a celulose microcristalina foi aglomerada com soluções de maltodextrina. Um planejamento experimental Plackett-Burman foi proposto com sete fatores (*C*: concentração de ligante; *Q*: vazão de ligante; *T*: temperatura do ar de fluidização; *v*: velocidade do ar de fluidização; *M*: umidade inicial; *P*: pressão de atomização; *H*: altura do bocal) e três réplicas no ponto central, para avaliar a influência no tamanho médio de partícula. Em outro conjunto experimental, as soluções de ligantes foram caracterizadas em termos de propriedades físico-químicas e tamanho de gotas, e *C*, *Q* e *P* foram avaliados para o crescimento de partículas. No último conjunto experimental, os estados foram classificados em condições úmidas e secas de acordo com a combinação de parâmetros operacionais. Posteriormente, *Q* foi aumentado de tempos em tempos, mantendo *C* e *T* constantes. A ênfase da pesquisa na aglomeração em leitos fluidizados está progredindo para avaliar os parâmetros operacionais de processamento de novos materiais e técnicas de medição modernas. As variáveis *C*, *Q*, *M* e *T* foram significativas a 90% de confiança no primeiro conjunto experimental. Uma nova abordagem foi proposta para delimitar os estágios de aglomeração, baseada na evolução das classes de tamanhos. O segundo conjunto experimental indicou uma grande concentração de gotas com tamanhos pequenos com efeitos semelhantes e positivos de *C* e *Q*, e negativo de *P*. No último conjunto, as condições úmidas levaram a uma formação mais efetiva de partículas pela formação uma camada pegajosa. A análise de dados e imagens permitiu identificar a formação e a estabilidade das pontes sólidas.

Palavras-chave: Aglomeração; Leito fluidizado; Bibliometria; Classes de tamanho de partículas; Tamanho de gotas; Formação de pontes sólidas.

ABSTRACT

Fluidized beds have been used to promote agglomeration in industrial processes, as they improve powder properties. Spatial Filter Velocimetry is a technique used to monitor, control, and understand granulation. The droplet size of a sprayed liquid binder solution is a crucial factor for increased particle size. To agglomerate a particulate material, solid bridge formation is necessary, but this is still not well understood in the agglomeration process. This work aimed to examine the process evolution in real-time and the influence of operating conditions on it and to investigate the physicochemical properties of maltodextrin solutions, as well as their influence on the droplet size and on the particle growth; and to comprehend how particle class evolution, Raman spectra, and microscopy can auxiliary the granule formation understanding. A bibliometric analysis and a bibliographic review were conducted to identify trends in agglomeration in a fluidized bed in the last four decades. Microcrystalline cellulose was agglomerated with maltodextrin solutions for all experiments. A Plackett-Burman design was proposed to evaluate the influence of seven factors (C: binder concentration; Q: binder flow rate; T: fluidizing air temperature; v: fluidizing air velocity; M: powder initial moisture content; P: atomizing pressure; H: nozzle height) and three replicates at the central point condition on the mean particle size. In another experimental set, the binder solutions were characterized in terms of physicochemical properties and droplet size, and following that, the C, Q, and P were evaluated for particle growth. In the last experimental set, the statuses were classified in wet and dry conditions according to the combination of operating parameters. Afterward, Q was increased from time to time while maintaining constant C and T. Research emphasis on agglomeration in fluidized beds is progressing to evaluate the operating parameters of processing new materials and modern measurement techniques to enhance theoretical approaches. The variables C, Q, M, and T were significant at a 90% confidence level in the first experimental set. A new approach was proposed for delimiting the agglomeration stages, based on particle size classes evolution. C is the most outstanding parameter regarding particle growth under experimental conditions. The second experimental set indicated a large concentration of droplets with small sizes. C and Q displayed similar and positive effects on droplet sizes, and P exhibited a negative impact. In the last set, wet conditions led to more effective particle formation by the tendency to form a sticky layer. The examination of data and images enables identifying the solid bridge formation and stability.

Keywords: Agglomeration; Fluidized bed; Bibliometrics; Particle size classes; Droplet size; Solid bridges formation.

LIST OF ILLUSTRATIONS

LIST OF TABLES

LIST OF SYMBOLS AND ABBREVIATIONS

ANOVA	Analysis of variance
BET	Brunauer–Emmett–Teller method
C	Binder concentration
CFD	Computational Fluid Dynamics
CMC	Microcrystalline cellulose
d	Diameter
d_{10}	Percentile 10% of droplet size
d_{50}	Percentile 50% of droplet size
d_{90}	Percentile 90% of droplet size
$D10v$	Percentile 10% of particle size, in volume basis
$D50v$	Percentile 10% of particle size, in volume basis
$D90v$	Percentile 10% of particle size, in volume basis
DC	Dry condition
d_d	Droplet diameter
d_m	Mean droplet size
DSD	Droplet size distribution
E	Experimental assay
F	Focal distance
f_0	Frequency of the burst signal
f_D	High-frequency Doppler component
FBRM	Focused beam reflectance measurement
g	Distance between the two optical fibers
H	Nozzle height
HK	Horvath-Kawazoe method
IF	Impact factor
LD	Laser diffraction
M	Powder initial moisture content
$MD5$	Concentration of maltodextrin in 5% w/w solution
$MD20$	Concentration of maltodextrin in 20% w/w solution
$MD35$	Concentration of maltodextrin in 35% w/w solution
NC	Number of citations

NIR	Near-infrared reflectance
NP	Number of publications
P	Atomizing pressure
PDI	Phase Doppler Interferometry
PSD	Particle size distribution
Q	Liquid binder slow rate
s	Calibration factor
SEM	Scanning electron microscopy
SFV	Spatial filter velocimetry
T	Fluidizing air temperature
t_p	Duration of pulse signal
v	Fluidizing air velocity
v_d	Droplet velocity
v_p	Particle velocity
WC	Wet condition
WoS	Web of Science
x_p	Particle size
γ	Intersection angle between two laser beams
γ	Shear rate
δ	Spacing between the fringes
λ	Wavelength
μ	Viscosity
σ	Shear stress

TABLE OF CONTENTS

CHAPTER I

General Introduction, Objectives, and Thesis Structure

1.1. GENERAL INTRODUCTION

The agglomeration process has produced instant products in the food industry that can quickly reconstitute when mixed with water or milk. The particle size enlargement allows better flowability and appearance features and facilitates the transport and storage conditions [1,2]. The most common foodstuff produced by agglomeration is maize-based (sauces, soups, and infant formulas), instant beverages (soluble coffee and teas), milk-based (chocolate products, milk, and ice cream), and, more recently, plant-based products.

Agglomeration consists of aggregating fine particles by solid bridges to create larger, more porous structures called granules [1,3]. The agglomerates must have a reduced number of fine particles, avoiding the risk of explosions, inhalation, and losses; modification of form and appearance; improvements in flowability, dispersion, and dissolution; minimization of the formation of lumps when stored; and ability to mold itself to specific shapes in further processing [1,2].

Improved safety can occur with a technological bias in mind by reduced dust formation, handling, sensory properties, appearance, dispersion, dissolution, density, and in caking formation during storage when food products are processed by agglomeration [2]. More specifically, in fluidized bed agglomeration, the agglomerated product characteristics presented depend both on the characteristics of the particulate solid and the operating parameters and properties of the binder solution. These factors influence the heat and mass transfer mechanisms between fluid and particles and, consequently, the operations' success. In addition, it is necessary to verify the system requirements and the effect of process conditions on the saturation of agglomerates [4,5].

The fluidized bed agglomeration process consists of atomizing a liquid binder over the fluidized bed of particles. The process is considered as successive humidification and drying operations; at first, the liquid is atomized over the particles causing liquid bridges to be formed; then, the hot air removes water from the particles, forming solid bridges and thus larger granules. Growth only occurs when there is enough liquid to establish the bridges or when the liquid saturation is sufficient to increase the plastic deformation of the agglomerates [4,6].

The choice of adequate operating parameters is essential to obtain the desired quality of the agglomerated product since these significantly influence both the process and the final product. The most important factors that must be considered in the fluidized bed agglomeration process are the binder solution flow rate and concentration, atomization

pressure, fluidization air temperature and flow rate, and relative humidity inside the bed [5,7–12].

Studies have been published on the mechanisms of granule formation at least since the 1970s, first on a qualitative approach [13,14] followed by a quantitative and descriptive investigation based on observations, experiments, and mathematical modeling [1,15,16]. According to Sastry and Fuerstenau [13], the growth of wet nuclei in agglomeration is described by the following mechanisms: nucleation, coalescence, abrasion transfer, breakage, and layering. These mechanisms can occur overlapping and even concurrently, making them difficult to identify when each was proposed. This is because there were no fast and efficient devices to determine some parameters, such as granule size and the number of particles [1]. According to Butensky and Hyman [15], agglomeration can be considered a three-stage process: nucleation, growth and compaction, and drying. This model applies to spherical granules formed by several spherical particles of the same size. A limiting factor in the model proposed by these authors does not consider any immediate and homogeneous liquid dispersion on the particle's surface. The continuity of the steps depends on the degree of liquid dispersion over the powder.

Tardos, Khan, and Mort [16] proposed a scheme that relates the approximation between a drop of liquid and powder particles to understand the degree of liquid dispersion over the powder and how this affects agglomeration. Particle growth can be divided into three stages: nucleation, coalescence, and layer formation. An amount of binder must be present at the point of contact so that there is bridge formation for the mechanisms to occur. Growth is favored if there is a sufficient amount for adhesion; otherwise, it is not. The growth rate depends on the relative sizes of individual particles; in the case of similar sizes, coalescence and nucleation, which produce high growth rates; however, for different sizes, the layer formation is favored. The granules must be strong enough to resist movement within the equipment when they are formed. The granule growth and quality are closely linked to the liquid binder viscosity and the amount of this liquid adhered to the particle surface at the points of contact [16]. Despite the previously well-established models cited above, Iveson et al. [1] updated them through an approach that implies joining stages because they may occur simultaneously.

Also, the limit between the end of one and the beginning of another is not so easy to determine or depends arbitrarily on what is determined by whoever performs the experiment; until then, no physical parameter determines the completion of one of the steps. Despite reducing the steps to three, these authors made them more comprehensive because more than

one physical phenomenon is treated in a single step. Agglomeration was defined according to the following steps: wetting and nucleation, consolidation and growth, and attrition and breakage.

Despite all the orientation of fluidized bed agglomeration studies towards a more technological approach, aiming at the quality of the final product and the influence of process variables, there is a demand for understanding: (i) how these same process variables interfere in the production of granules, (ii) how these factors are interrelated; and (iii) how they can be controlled to produce more stable granules. Some theories are based on observation and mathematical modeling for these reasons. Such theories describe the granule formation mechanisms in agglomeration processes; however, it is necessary to perform more studies that jointly describe, and experimentally confirm these steps that have already been well established.

1.2. OBJECTIVES

The overarching goal of this research was to experimentally identify the constituent stages of the fluidized bed agglomeration process through real-time monitoring of the process parameters listing the mechanisms that govern the agglomeration process and the consequent formation of granules. Furthermore, the study aimed to propose which operating parameters are most suitable for the establishment and permanence of solid bridges. Finally, this study intended to jointly employ advanced techniques for measuring particle size, droplet size, and image analysis to identify solid bridges in agglomerated powder.

The specific objectives of this study were:

- perform a survey on the most important contributions in terms of the number of articles, countries that contributed the most to the field, and most influential journals on the fluidized bed agglomeration theme;

- identify a network of collaborators and different fields of research within the researched theme;

- provide a future perspective of publications on fluidized bed agglomeration;

- analyze the data obtained from the spatial filter velocimetry probe in a set of executed experiments in a fluidized bed agglomeration process, showing the evolution of the process over time and the influence of operating conditions;

- verify the efficiency of the spatial filter velocimetry probe as a tool for real-time monitoring of this process;

- propose a new approach for delimiting the stages of the fluidized bed agglomeration process based on particle size classes;

- analyze the physicochemical properties of maltodextrin solutions used as binder liquids in a fluidized bed agglomeration process;

- verify the influence of maltodextrin solutions on the droplet sizes formed by spraying and their relationship through the growth of microcrystalline cellulose particles during the process;

- monitor the operating parameters during the agglomeration process and evaluate the particle enlargement;

- acquire spectral information about the particulate material before and after the process by a portable bench Raman spectrometer;

- obtain scanning electronic and fluorescence micrographics from the samples to combine methods to establish the solid bridge formation conditions during the agglomeration process.

1.3. THESIS STRUCTURE

The delimitation of the phases and the study of agglomeration mechanisms in a fluidized bed were addressed in this study. Likewise, this research focused on using microcrystalline cellulose as particulate material and maltodextrin solutions as a liquid binder to understand how operating parameters influence agglomeration and affect solid bridge formation and maintenance. Preliminary experiments were carried out aiming to understand the range of the operating parameters as well as the fluid dynamic behavior of the particulate system. This doctoral thesis was divided into seven chapters, and what each one of them deals with is described in the following paragraphs.

This current chapter, **Chapter I – General Introduction, Objectives, and Thesis Structure**, provides a general introduction to the theme, pointing out the overview of the main features of agglomeration in the fluidized bed process, its definition, and how the particles grow during the process. The main mechanisms of particle growth reported in the literature were also

reported in this section. Following that, the general objective of the thesis was presented, as well as the specifics corresponding to what had been described in each paper. Finally, this chapter shows the thesis structure, explaining what was addressed chapter by chapter.

Chapter II – Agglomeration in a fluidized bed: bibliometric analysis, a review, and future perspectives presented the theoretical foundations comprising this study, published by Powder Technology in 2022. It included information on the bibliometric review regarding agglomeration in a fluidized bed, listing the 20 most influential journals and the top 20 most outstanding papers based on the number of citations. A keyword analysis was done to show an overview of the trends in what has been published on the agglomeration and fluidized bed themes. After the first part, a bibliographic review was presented, considering the most cited papers and their theoretical approaches and applications (experimental and/or numerical). Lastly, future outlooks were elaborated on the use of measurement techniques, new materials, and theoretical approaches to agglomeration in a fluidized bed.

A proposal was disclosed for delimiting the fluidized bed agglomeration process stages based on particle size classes obtained from the spatial filter velocimetry probe data in **Chapter III – A new approach for the agglomeration in fluidized bed mechanisms based on spatial filter velocimetry technique**, published by Powder Technology, in 2021. An experimental design was proposed to screen the main operating variables influencing particle growth. The measurement data on spatial filter velocimetry were evaluated to classify the agglomeration steps based on the particle size classes. This article made it possible to define an easily obtainable physical parameter to delimit the stages of agglomeration in a fluidized bed by what had been theoretically proposed in the literature.

It was necessary to characterize a liquid binder from the selected operating parameter performed in the last chapter and explore more effectively how the binder features and spray system properties influence particle growth. These subjects were reported in **Chapter IV – Spray system characterization for evaluating particle size enlargement in fluidized bed agglomeration**, submitted to Powder Technology in 2023. Experiments were conducted to evaluate the influence of the maltodextrin solution used as the binder on the formed droplet size and their relationship to particle growth. The spray system was characterized by employing phase Doppler interferometry under the conditions used in the agglomeration experiments. It was concluded that solution concentration and flow rate were the most prominent parameters in droplet size enlargement. Likewise, the particle size enlargement was strongly dependent on the solid raw material and the liquid binder properties.

Chapter V – The formation of solid bridges during agglomeration in a fluidized bed: investigation by Raman spectroscopy and image analyses was written and published by Powder Technology in 2023 to cluster all the knowledge obtained from the previous chapters and verify the possibility of the existence of a specific condition for the formation of solid bridges. The experimental conditions studied in the previous chapters were presented as two sets of experiments in this current chapter. The first evaluated how dry or wet conditions influence the particle size enlargement, and the second how the increase in the solution flow rate favors the emergence and maintenance of solid bridges from liquid bridges. Raman spectroscopy was used to verify the presence (or not) of maltodextrin on the particle surface; scanning electron microscopy helped to identify the solid bridges; and fluorescence microscopy made it possible to place where the maltodextrin solution remained deposited on the microcrystalline cellulose surface.

The most relevant results of this set of experiments and the aspects to which this thesis contributed to scientific outgrowth are briefly discussed in **Chapter VI – General Discussion**. The main conclusions are presented in **Chapter VII – General Conclusions**.

CHAPTER II

Agglomeration in fluidized bed: bibliometric analysis, a review, and future perspectives

Nascimento, R.F.; Ávila, M.F.; Taranto, O.P.; Kurozawa, L.E.

Agglomeration in fluidized bed: bibliometric analysis, a review, and future perspectives

Raul F. Nascimento[a], Mariana F. Ávila[b], Osvaldir P. Taranto[b], Louise Emy Kurozawa[a]

[a]Department of Food Engineering, School of Food Engineering, University of Campinas, Monteiro Lobato St. 80, Campinas, SP, Brazil

[b]Department of Process Engineering, School of Chemical Engineering, University of Campinas, Albert Einstein Ave. 500, Campinas, SP, Brazil

HIGHLIGHTS

- Bibliometric analysis of agglomeration in fluidized bed.
- China, Sweden, Germany, the USA, and Canada are the most productive countries.
- Both granulation and combustion are trends in agglomeration publications.
- New materials and measurement techniques are the current research emphasis.

ABSTRACT

Fluidized beds have been used as equipment for promoting agglomeration in industrial processes. In general, particle enlargement is desirable because it improves the properties of powders. In some cases, agglomeration can be inconvenient it because can reduce the reaction rate in processes such as combustion. Bibliometric analysis was conducted to examine the global panorama of publications and identify trends in agglomeration in a fluidized bed in the last four decades. China, Sweden, Germany, Canada, and the United States raised their status as the most productive countries in the total number of publications. Keyword analysis showed that fluidization, biomass, granulation, defluidization, and coating were important to agglomeration in fluidized beds. Two main focuses were also identified in publications: granulation and combustion. Research emphasis on agglomeration in fluidized beds is progressing to evaluate the operating parameters of processing new materials and modern measurement techniques to enhance theoretical approaches.

Keywords: Agglomeration; Fluidized bed; Research trends; Granulation; Combustion; Bibliometrics.

2.1. INTRODUCTION

Agglomeration consists of a process capable of increasing particle size in a semipermanent aggregate form, known as granules, where the primary particles can be distinguished [1]. This process comprises a range of processing techniques employing solutions, slurries, melting, and binders [2]. In general, the liquid phase is sprayed onto a solid particle bed that is in constant motion. The liquid makes the surface of the particles stickier and enables mutual particle bonding. The wetted particles remain clustered through a combination of capillarity and viscous forces, and solid bridges are formed by drying or sintering [1].

Pietsch [3] listed a selection of applications of agglomeration methods in different situations but based on the same fundamentals: baking, briquetting, coating, compacting, granulating, instantizing, microencapsulation, pelleting, and sintering. The equipment where agglomeration can be carried out was also cited, namely disc and agglomeration drums, mixers, spray dryers, fluidized beds, and low-density agglomerators. According to Dhanalakshmi et al. [4], agglomeration may be consolidated with other unit operations, and factors such as physical and chemical properties, particle sizes, thermal sensitivity, and final product handling properties are decisive in selecting the agglomeration process. There are some advantages for choosing the fluidized bed as the preferred equipment for particle agglomeration compared to other devices: transporting and handling of solids are facilitated due to the liquid behavior of the fluidized bed, uniform temperature distribution, large solid–gas contact area, high heat transfer, and uniform mixed product [5].

Powders can be agglomerated, as seen, by numerous processes whose objective is improving product safety while handling and by reducing dustiness or conferring good dispersion and dissolution properties and producing a granular form for further processing [6]. Increased particle size is the target of the agglomeration process. However, it is necessary to consider the limits between increasing the size to provide granule strength, minimizing attrition while being transported and handled, and providing proper dispersion and dissolution in a liquid. Additionally, agglomeration is also used to improve appearance in the case of foodstuffs or develop a dense product to facilitate storage in the case of chemicals.

The main problem related to agglomeration is defluidization and all its implications [7]. For example, the combustion of some materials can produce adhesive substances that can provide agglomeration during the process and affect the process responses [8]. In addition to the chemical composition and intrinsic properties of the material (density, size, and surface),

some operating parameters are also essential for the defluidization phenomenon to occur, such as temperature, gas velocity, physical and chemical characteristics, reaction mechanism, and particle size distribution [9–11]. Among these, the particle size distribution may be the most crucial because it influences the minimum fluidization velocity, terminal velocity, elutriation rate, reaction efficiency, hydrodynamic behavior [12], conversion efficiency of the reaction [13], fluidity, conversion, and segregation phenomenon [14].

The bibliometric analysis consists of a systematic literature review originating from the library and information science fields. It can draw an overview scenario about a specific theme, classifying the results based on papers, authors, or journals. This type of analysis has been applied in different research fields, grouping common outcomes, intending to improve the current scenario overview and consequent interpretation of the scientific development. It is noteworthy that no article with this thematic approach presented in this current article was found in the literature. This review applied bibliometric analysis to search for publications referring to fluidized bed agglomeration in the last four decades. The objective was to perform a survey on the most important contributions in terms of the number of articles, countries that contributed the most to the area, and most influential journals, identifying a network of collaborators, followed by identifying different fields of research within the researched theme and, finally providing a future perspective of publications on fluidized bed agglomeration.

2.2. LITERATURE RESEARCH METHODOLOGY

The Web of Science database was used to investigate publications on agglomeration in fluidized beds. The following terms were searched in titles, keywords, and abstracts in the Web of Science (WoS) Core Collection from 1900 to 2021: 'agglomeration' AND 'fluidi*ed bed' (the * indicates that any form of spelling of the word can be considered, in this case, 'fluidized' in American English and 'fluidised' in British English). The Boolean operator AND indicates that each result must present both researched terms. The search was carried out in November 2021. The results were filtered for results in the Chemical Engineering, and Food Science and Technology categories, and a total of 1148 articles (97.6%) and reviews (2.4%) were selected.

The results were extracted based on the year of publication, the country where the research was performed, the 20 most cited articles, the 20 most influential journals, and

keywords. The software VOSviewer (version 1.6.16, Leiden University, The Netherlands) was used to visualize the results from network interaction.

2.3. BIBLIOMETRIC ANALYSIS

2.3.1. General results

When the data were collected, one thousand, one hundred forty-eight articles were published on agglomeration and fluidi*ed bed themes. The first document was published in 1980, and the number of publications increased over the years (Figure 2.1). The number of publications from 2013 to the present corresponds to at least 50% of the total. This means that 601 papers were published in the last nine years, and 547 were published in slightly more than three decades, from 1980 to 2012. If that trend continues, approximately 75 papers will be published in 2022 addressing these themes.
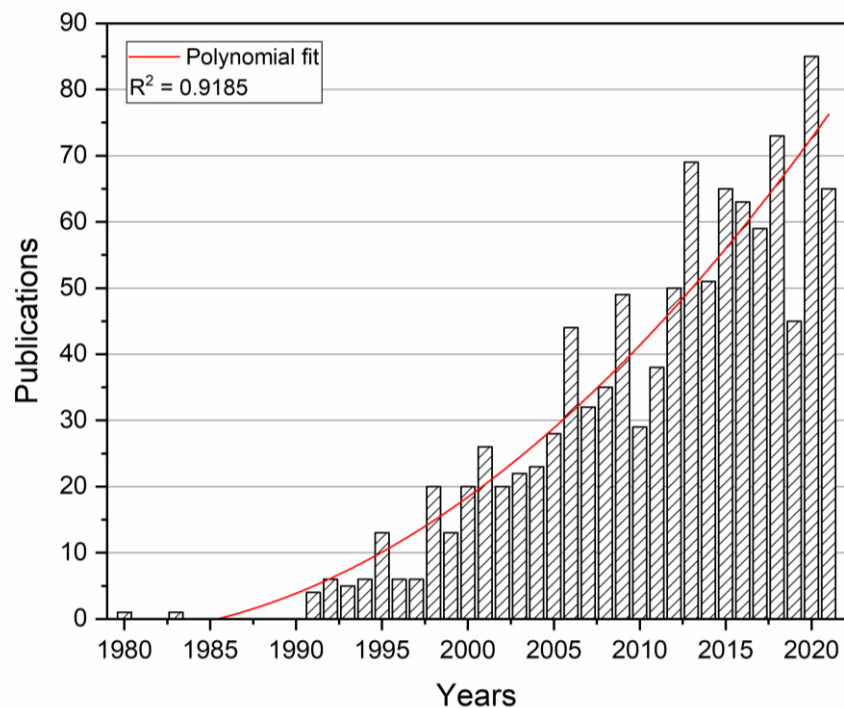
Figure 2.1: Total publication from Web of Science Core Collection, correlating 'agglomeration' and 'fluidi*ed bed', from 1980 to 2021.

Researchers from 60 countries have published studies on agglomeration and fluidized bed themes. Figure 2.2 shows the countries that published the most in these fields of research. The five countries with the highest scientific output are the People's Republic of

China, Sweden, Germany, the United States, and Canada. These five countries, together, published a total of 599 studies. China published its first study on this topic in 2001 and then published an average of three studies per year in the first decade. In the following ten years, it reached the mark of 26 studies published in a single year (2018).
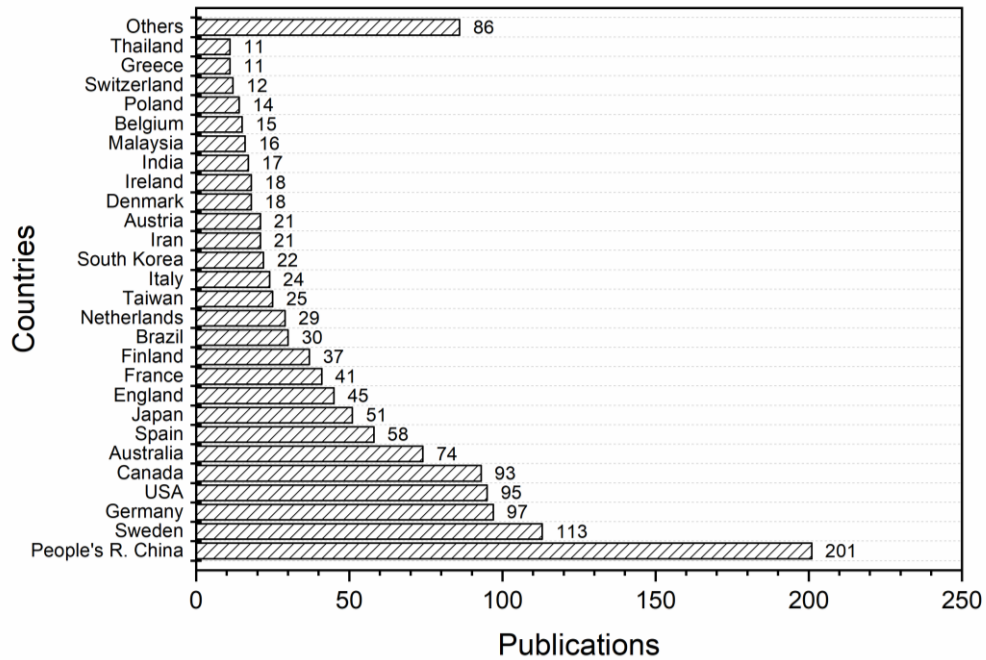
Figure 2.2: Countries with higher production correlating 'agglomeration' and 'fluidi*ed bed' from 1980 to 2021.

On the other hand, the United States was the first country to publish on this theme and only published 13 papers from 1980 to 2000. The most significant number of US publications occurred in 2018 and 2020, when they published 9 and 8 articles, respectively. In this scenario, Brazil was ranked in the thirteenth position as it has published 31 papers. Its first paper was published in 2000.

International research collaborations between all 60 countries, that produce papers in this research field were evaluated by analyzing co-authorship. The social network map of collaborations is displayed in Figure 2.3. The node size indicates the number of publications in this type of analysis. The thicker the line connecting two nodes, the greater the collaboration between them, and the node color indicates the cluster to which the item belongs. In addition to gathering the most significant number of publications, China, Sweden, Germany, Canada, the USA, Australia, Spain, and Japan also have centralized collaboration networks. China has the largest collaboration network through strong interaction with Australia, the USA, and

Canada. Sweden, Germany, Canada, the USA, and Australia rank as the countries with the most collaborations; however, the interaction among them is weak, i.e., there are only collaborations with Sweden-Australia, Sweden-Germany, and Canada-USA. Brazil has a small collaboration network, with only Canada and Spain. The first collaboration addresses the investigation of the feasibility of utilizing time-frequency analysis from a pressure fluctuation time series to characterize system dynamics and flow regimes in wet spouted beds [15]. Moreover, the second report describes the development of impregnated manganese-based oxygen carriers using different supports and their characterization for Chemical Looping Combustion [16].
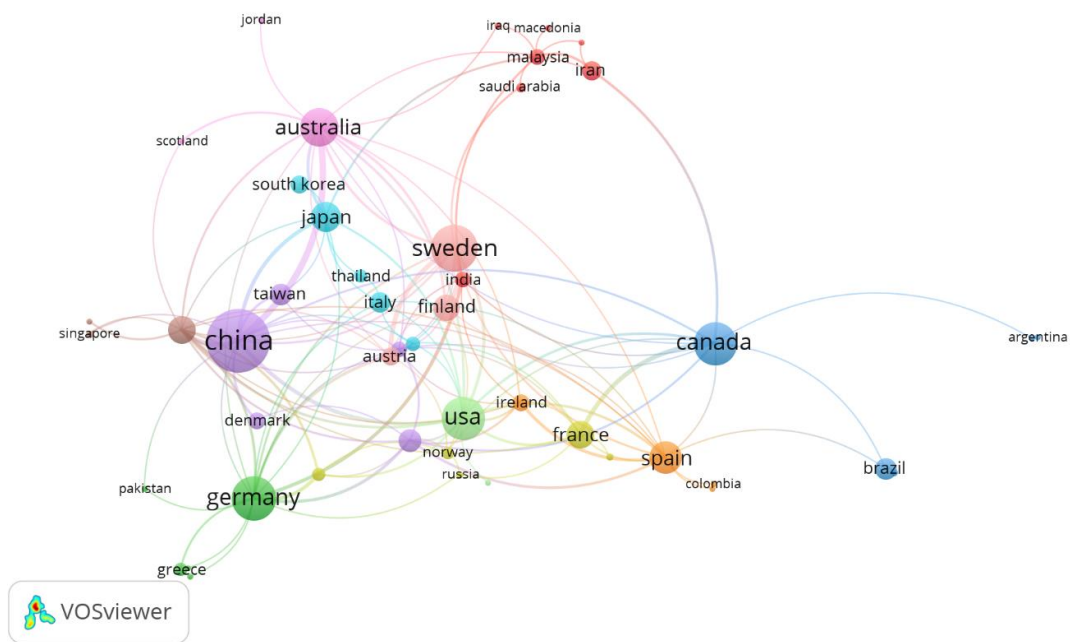
Figure 2.3: Collaboration among the 60 countries from 1980 to 2021 according to co-authorship (Network visualization map).

2.3.2. The most influential journals

The searched terms were published in 92 different journals from 1980 to 2021. Table 2.1 shows the 20 most influential journals in this field of research, ranked by the number of publications (NP). These journals total approximately 80% of all publications when considered jointly. *Powder Technology* (177 papers; impact factor IF = 4.142) is the journal that published 16.11% of the total publications and was mentioned in 5287 citations, followed by *Energy & Fuels* (179 papers; IF = 3.421), *Fuel* (99 papers; IF = 5.578), *Chemical Engineering Science* (73 papers; IF = 3.871), and *Fuel Processing Technology* (66 papers; IF = 4.982).

The first five journals follow the same rank of number of publications (NP) regarding the number of citations (NC). Progress in Energy and Combustions Science (IF = 28.938) is ranked sixth, and it is not one of the top 20 publications. The list goes on to Industrial & Engineering Chemistry Research (IF = 3.573) in the seventh position, and with almost 500 different citations, AICHE Journal (IF = 3.519), in the eighth position. Jointly, the top ten most-cited journals account for 70.7% of all citations; considering the twenty most cited ones, this percentage increases to 77.6%.

2.3.3. The most cited papers

Table 2.2 shows the top 20 most cited papers correlating agglomeration and fluidized bed terms. Seven of them are reviews and deal with themes related to granule formation mechanisms [1], biomass combustion [7,17–19], and the use of fluidized bed combustors [20,21]. The others are original papers contemplating the themes on the characterization of granulation phenomena [2], the feasibility of oxygen carriers in chemical-looping combustion [22–27], biomass combustion [28,29], production of instant soymilk powder [30], oil encapsulation [31], the influence of process variables on growth kinetics [32], and simulation of particle aggregation [33].

The most cited paper was written by Iveson et al. [1], and there were 847 citations according to the WoS Core Collection and was published by Powder Technology (IF = 4.142). This paper reviews the wet agglomeration process and its three key topics: wetting and nucleation, consolidation and growth, and breakage and attrition. The authors also proposed changing the description of the granulation process from a traditional view to what they named the modern approach. These new steps were also discussed in understanding and quantifying the mechanisms that control granule formation attributes.

Table 2.1: Top 20 most influential journals, correlating 'agglomeration' and 'fluidi*ed bed' research, ranked by total number of publications from 1980 to 2021.

Rank	Journal	NP	IF	Rank	Journal	NC	IF
1	Powder Technology	185	4.142	1	Powder Technology	5287	4.142
2	Energy & Fuels	179	3.421	2	Energy & Fuels	5143	3.421
3	Fuel	99	5.578	3	Fuel	4091	5.578
4	Chemical Engineering Science	73	3.871	4	Chemical Engineering Science	2474	3.871
5	Fuel Processing Technology	66	4.982	5	Fuel Processing Technology	2241	4.982
6	Industrial & Engineering Chemistry Research	51	3.573	6	Progress in Energy and Combustion Science	2175	28.938
7	Chemical Engineering Journal	31	10.652	7	Industrial & Engineering Chemistry Research	1294	3.573
8	AICHE Journal	29	3.519	8	AICHE Journal	807	3.519
9	Applied Energy	21	8.558	9	Chemical Engineering Journal	736	10.652
10	Chemical Engineering Research & Design	21	3.350	10	Journal of Food Engineering	626	4.499
11	Canadian Journal of Chemical Engineering	21	1.687	11	Applied Energy	483	8.558
12	Drying Technology	18	2.988	12	Chemical Engineering Research & Design	318	3.350
13	Journal of Food Engineering	18	4.499	13	Drying Technology	308	2.988
14	Advanced Powder Technology	15	1.543	14	Canadian Journal of Chemical Engineering	290	1.687
15	Chemical Engineering & Technology	14	2.787	15	Proceedings of the Combustion Institute	282	5.627
16	Particuology	14	4.217	16	Combustion and Flame	198	4.570
17	Journal of Chemical Engineering of Japan	14	0.651	17	Catalysis Today	191	5.825
18	Chemical Engineering and Processing-Process Intensification	14	3.731	18	Energy & Environmental Science	184	30.289
19	Chemie Ingenieur Technik	9	1.147	19	Innovative Food Science & Emerging Technologies	143	3.731
20	Korean Journal of Chemical Engineering	9	2.690	20	Chemical Engineering and Processing-Process Intensification	138	4.477

NP: number of publications; NC: number of citations; IF: impact factor.

Table 2.2: Top 20 most cited publications, correlating 'agglomeration' and 'fluidi*ed bed' research from 1980 to 2021.

Rank	Title	Authors	Year	NC	Journal	IF
1	Nucleation, growth and breakage phenomena in agitated wet granulation processes: a review	Iveson, S. M.; Litster, J. D.; Hapgood, K.; Ennis, B. J.	2001	847	Powder Technology	4.142
2	Combustion of agricultural residues	Werther, J.; Saenger, M.; Hartge, E. U.; Ogada, T.; Siagi, Z.	2000	762	Progress in Energy and Combustion Science	28.938
3	Biomass combustion in fluidized bed boilers: Potential problems and remedies	Khan, A. A.; de Jong, W.; Jansens, P. J.; Spliethoff, H.	2009	732	Fuel Processing Technology	4.982
4	Comparison of iron-, nickel-, copper- and manganese-based oxygen carriers for chemical-looping combustion	Cho, P.; Mattisson, T.; Lyngfelt, A.	2004	518	Fuel	5.578
5	Ash-related issues during biomass combustion: Alkali-induced slagging, silicate melt-induced slagging (ash fusion), agglomeration, corrosion, ash utilization, and related countermeasures	Niu, Y. Q.; Tan, H. Z.; Hui, S. E.	2016	454	Progress in Energy and Combustion Science	28.938
6	A microlevel-based characterization of granulation phenomena	Ennis, B. J.; Tardos, G.; Pfeffer, R.	1991	430	Powder Technology	4.142
7	Sulfation phenomena in fluidized bed combustion systems	Anthony, E. J.; Granatstein, D. L.	2001	371	Progress in Energy and Combustion Science	28.938
8	Production of instant soymilk powders by ultrafiltration, spray drying and fluidized bed agglomeration	Jinapong, N.; Suphantharika, M.; Jamnong, P.	2008	363	Journal of Food Engineering	4.499
9	Agglomeration in fluidized beds at high temperatures: Mechanisms, detection and prevention	Bartels, M.; Lin, W. G.; Nijenhuis, J.; Kapteijn, F.; van Ommen, J. R.	2008	271	Progress in Energy and Combustion Science	28.938
10	The use of iron oxide as oxygen carrier in a chemical-looping reactor	Abad, A.; Mattisson, T.; Lyngfelt, A.; Johansson, M.	2007	268	Fuel	5.578
11	Multicycle reduction and oxidation of different types of iron oxide particles - Application to chemical-looping combustion	Mattisson, T.; Johansson, M.; Lyngfelt, A.	2004	259	Energy & Fuels	3.421
12	Agglomeration in bio-fuel fired fluidized bed combustors	Lin, W. G.; Dam-Johansen, K.; Frandsen, F.	2003	249	Chemical Engineering Journal	10.652
13	Chemical-looping combustion in a 300 W continuously operating reactor system using a manganese-based oxygen carrier	Abad, A.; Mattisson, T.; Lyngfelt, A.; Ryden, M.	2006	246	Fuel	5.578
14	Chemical looping combustion in a 10 kW(th) prototype using a CuO/Al_2O_3 oxygen carrier: Effect of operating conditions on methane combustion	Adanez, J.; Gayan, P.; Celaya, J.; de Diego, L. F.; Garcia-Labiano, F.; Abad, A.	2006	243	Industrial & Engineering Chemistry Research	3.573
15	Bed agglomeration characteristics during fluidized bed combustion of biomass fuels	Ohman, M.; Nordin, A.; Skrifvars, B. J.; Backman, R.; Hupa, M.	2000	236	Energy & Fuels	3.421

16	Operation of a 10 kWth chemical-looping combustor during 200 h with a CuO-Al$_2$O$_3$ oxygen carrier	de Diego, L. F.; Garcia-Labiano, F.; Gayan, P.; Celaya, J.; Palacios, J. M.; Adanez, J.	2007	230	Fuel	5.578
17	Application of the direct quadrature method of moments to polydisperse gas-solid fluidized beds	Fan, R.; Marchisio, D. L.; Fox, R. O.	2004	219	Powder Technology	4.142
18	Encapsulation of oil in powder using spray drying and fluidised bed agglomeration	Fuchs, M.; Turchiuli, C.; Bohin, M.; Cuvelier, M. E.; Ordonnaud, C.; Peyrat-Maillard, M. N.; Dumoulin, E.	2006	212	Journal of Food Engineering	4.499
19	Fluidized bed coating and granulation: influence of process-related variables and physicochemical properties on the growth kinetics	Hemati, A.; Cherif, R.; Saleh, K.; Pont, V.	2003	185	Powder Technology	4.142
20	Fluidized-bed combustion of alternative solid fuels - status, successes and problems of the technology	Anthony, E. J.	1995	181	Progress in Energy and Combustion Science	28.938

NC: number of citations; IF: impact factor.

2.3.4. Keyword analysis

The analysis of keywords was carried out to show an overview of the trend on what has been published on the themes of agglomeration and fluidized bed. One thousand four hundred seventy-three keywords were used in 1148 papers from 1980 to 2021. The most common keywords were, as expected considering the central theme from the top 20 papers, agglomeration, fluidi*ed bed, fluidization, biomass, granulation, defluidization, coating, combustion, gasification, and modeling. These ten combined keywords represent 21.6% of all occurrences. Keywords such as CO_2 capture, oxygen carrier, chemical looping combustion, fluidized bed combustion, oxy-fuel combustion, biomass gasification, biomass ash, coal ash, coal gasification, and co-combustion indicate that the majority of the research was focused on energy production and thermal systems. On the other hand, keywords such as growth, food powders, microencapsulation, aggregation, drying, kinetics, optimization, viscosity, population balances, granules, and droplet sizes, although less frequent, show another trend in most papers, i.e., these keywords are more focused on process analysis for understanding the characteristics of the raw material and products than on the process application for technological purposes.

Figure 2.4 shows the network visualization map for all keywords used in the selected papers. The formation of five distinct clusters of words can be seen (the same color indicates the same cluster, i.e., nodes closely related), and each cluster assembles and relates the keywords from the same subject. For example, fluidization (green cluster) is related to granulation, growth or population balances (all from blue cluster), but, in terms of thematic area, it is closer to velocity or hydrodynamics (also from green cluster).

2.4. LITERATURE REVIEW

Among the top 20 most cited papers, two research trends were identified: Granulation and Combustion. The review was sectioned into theoretical approaches and applications (experimental and/or numerical) for each trend. Furthermore, the most recent research studies and their main results were also highlighted.
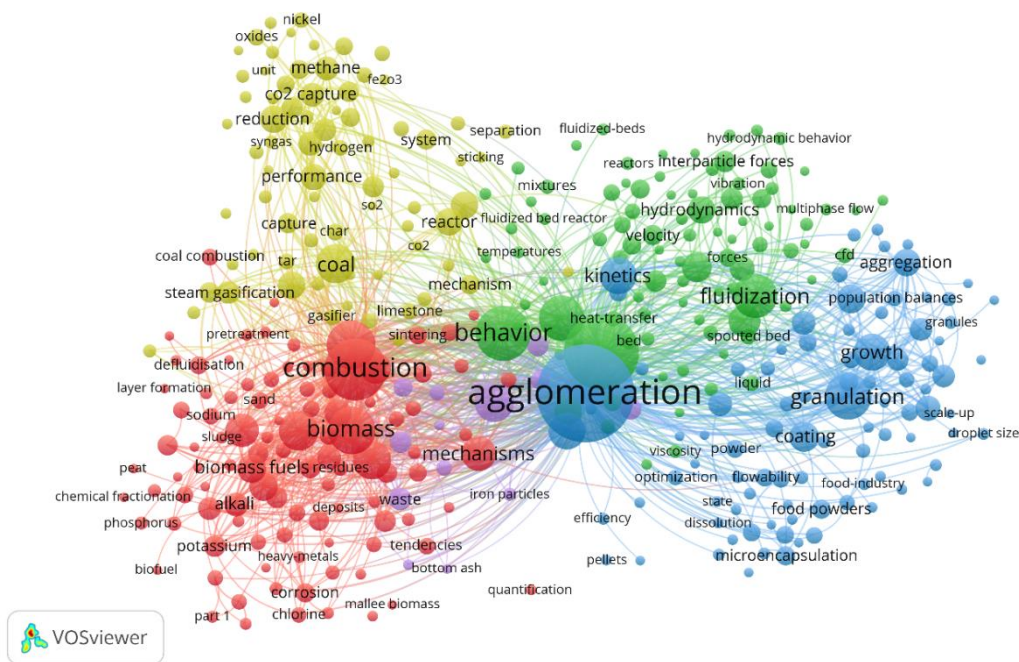
Figure 2.4: Network visualization map of key words used in the bibliographic production correlating 'agglomeration' and 'fluidi*ed bed' from 1980 to 2021.

2.4.1. Granulation

Fluidized bed granulation has been recognized as a widely used unit operation in industries at least, since 1991, in several applications, such as granulation of food products, fertilizers, energy conversion, pharmaceutical and chemical products, iron metallurgy, and mineral processing [1,2,34–46]. The common factor in all these works is that granulation implies particle enlargement for improving powder end-use handling properties.

Perhaps Iveson et al. [1] and Ennis et al. [2] are the most important papers on granulation published in recent years. This is mainly because Ennis et al. [2] focused efforts on understanding the granulation mechanisms from the microscale based on relative particle kinetic energy and collisional dissipation instead of the macroscale approach, and the consequences of operating variables have been studied until then. Approximately ten years later, Iveson et al. [1] introduced a more comprehensive view of granulation. These authors critically proposed and defined a modern approach to granulation based on three phenomena. Both works together are an essential tool for understanding granulation more thoroughly. It is not surprising that they are the two most cited reviews on this theme.

Hemati et al. [32] published experimental work on the influence of process variables and physicochemical properties on the growth kinetics regarding granulation applications. A few years later, Fuchs et al. [31] and Jinapong et al. [30] also published research studies on the combined use of spray drying and agglomeration in fluidized bed techniques to verify the viability of encapsulating vegetal oil and the combined sequence of the three techniques to produce instant soymilk powder. In this selection, Fan et al. [33] published only one study on numerical applications, dealing with the combined use of aggregation and breakage models in the direct quadrature method of moments to evaluate particle size distribution (PSD) evolution.

Considering that granulation is a complex process, it is indispensable to evaluate as many factors as possible that can interfere with the process. For example, Hemati et al. [32] evaluated process variables (gas velocity, atomizer location, liquid flow rate, liquid concentration, and atomizing air flow rate) and physicochemical properties (viscosity of solutions, wettability of the liquid on the solid, initial particle mean size, and porosity) to understand their effect on agglomeration kinetics. The more variables there are, the more complex their joint analysis is; thus, the conclusions on the subject are more comprehensive. They used sand, glass beads, alumina, and silica as solid materials and carboxymethylcellulose and NaCl solutions as binders for that purpose. The results reported by these authors suggested that liquid and atomizing air flow rates positively favor the agglomeration process because an increase in the air relative humidity can be observed by the formation of a larger number of droplets with smaller sizes and the consequent formation of a more compact and homogeneous layer over the particle. Additionally, the agglomeration was favored by using fine particles and increasing the adhesion strength of the solution on a solid surface. The agglomeration of porous particles identified a nongrowing period by comparing porous and nonporous particles. First, binder liquid was used to fill the particle pores, and then growth occurred in the same way as nonporous particles.

According to the WoS Core Collection, at least 20 papers have cited Hemati et al. [32] in recent years. These works deal with chemical engineering, materials science, pharmacology, and food science technology. In general, they address themes related to modeling and simulation [47–52], evaluation of powder and binder solution properties [53–62], dust cyclone collector efficiency [63,64], microencapsulation [65], and regime map creation [66]. Hemati et al. [32] managed to cover publications on other topics, either by comparing their results or exemplifying the discussed theoretical concepts, even though it is strictly a

research study for evaluating parameters in the granulation process. This situation is recurrent because granulation is a unit operation following well-defined and known physical behavior, even when applied to different materials.

Similar to the findings of Hemati et. al [32], encapsulation is one of the technological fields that has stood out the most. Fuchs et al. [31] tested the viability to produce encapsulated vegetal oil, using a technological approach. Thus, they assessed three manners for producing the powders: the first one, by atomizing a suspension composed of acacia gum, maltodextrin, and oil in water using a spray dryer; the second one, by atomizing water onto the powder produced by a spray dryer using a fluidized bed; and, finally, by agglomerating maltodextrin using acacia gum, oil, and water as a liquid binder in a fluidized bed. The main objective was acquiring a powder with good end-use properties; for that reason, several properties were evaluated. These authors concluded that the three processes efficiently prepared formulations using encapsulated oil in acacia gum and a maltodextrin matrix, with low oil losses. Depending on the technique used, they obtained samples with 2% and 6% total oil on the surface. Furthermore, the powders displayed good mechanical properties, wettability, and flowability, besides in addition to increased particle size when agglomeration was used combined with spray drying.

Jinapong et al. [30] followed a technological approach and reported using a three-stage process to produce instant soymilk powders. They used ultrafiltration, spray drying, and fluidized bed agglomeration in sequence to produce instant soymilk powders and evaluated the solid concentration in the spray-drying step and liquid binder concentration in the agglomeration step. The results of this work were promising, as ultrafiltration could concentrate the liquid up to 20% and spray drying could generate satisfactory-sized particles ($<25\ \mu$m), but it did not provide good handling properties. The fluidized bed agglomeration increased the particle size (260 μm using 10% maltodextrin solution) and improved the wettability.

Fuchs et al. [31] and Jinapong et al. [30] were cited together 84 times in 2020, mainly by research studies on food science technology, chemical engineering, and mechanical engineering. Fuchs et al. [31] work is mainly based on oil encapsulation [67–74], vegetable extract encapsulation [75–79], new route uses [80], a new emulsifier [81], a new approach to the stability and solubility of nanocapsules [82], and microencapsulation using foam [83]. There were also results found in studies on adsorption [84], agglomeration [56,85–87], coating [88], and freeze-drying [89]. All these studies are subject to experimental and technological bias. In the case of Jinapong et al. [30], the trend is the same. However, most of their studies are no

longer about encapsulation; now, most of them deal with applications in food products [90–103], using different techniques for producing powder, for example, microencapsulation by spray drying [68,70,81,104–110], fluidized bed [45,56,85,87,111–114], drying by spray [93,115–122], in addition to heat treatment and bioaccessibility [123], and particle size impact [124–126]. It can be noted that both papers are used as a basis for a range of recent works focused on applications of granulation, even if they were published over a decade ago.

Regarding the numerical approach, Fan et al. [33] reported a study applying the quadrature method of moments by computational fluid dynamics (CFD), considering that the solid phase is polydisperse and governed by aggregation and breakage phenomena. For that reason, they incorporated the population balance equation into the continuity and momentum balance equations. First, complex mathematical modeling was presented, which comprises interactions between phenomena such as multiphase flow dynamics, mass transfer, heat transfer, chemical reactions, and particulate processes (aggregation and breakage). Continuity, momentum, energy, and chemical species equations require concurrent resolution. After that, they applied the models to aggregation and breakage models, considering that they cause PSD changes. Last, they described the mathematical model and incorporated it into multifluid CFD to describe some gas–solid flows. These authors proved that this type of mathematical approach was effective in representing the PSD evolution. Moreover, for real systems, other features can be added to the models, such as information on heat and mass transfer and chemical reactions, but no framework change is needed.

Most authors who also study modeling and simulation have cited Fan et al. [33]. Last year, at least 12 papers were produced on the population balance model and its applications, e.g., using an open-source package to solve quadrative-based moment methods [127], evaluating water flow impact, temperature, and median size in wellheads [128], breakage modeling [129], bioengineering processes [130], the kinetic model for gas–solid flows [131], air pollution simulation [132], the comparison between one-dimensional CFD results and analytical solution [133], the cluster distribution size effect on interfacial drag in fluidized bed [134], the simulation of the actual microscopic behavior of salt-out particles [135], and solving the population balance by the dual quadrature method of moments [136,137] or disperse multiphasic systems [138]. Research on modeling or simulation also often has a technological aspect, as seen in the works mentioned above, although fewer in number.

As one can see, granulation covers a wide variety of topics, whether due to the process itself and the various techniques and equipment used or its practical application in the

development of experimental or simulated products. This trend is still essential for industrial processes and their applications.

2.4.2. Combustion

The six most cited review papers on combustion cover a substantial part of the subject. Werther et al. [17] provide an overview of agricultural residue combustion and its potential for use, the main problems associated with these raw materials as fuels, and finally, a discussion on design considerations for combustion facilities. Khan et al. [7], Niu et al. [19], and Bartels et al. [18] also discuss combustion-related problems. The first authors list problems and solutions related to biomass combustion, regarding its chemical composition, since they contain a high content of alkalis, chlorines, and ash. Despite this, the authors note that fluidized beds are essential equipment for biomass combustion, as they are flexible and highly efficient. The following authors are more specific when dealing with ash-related issues, such as alkali-induced slagging, silicate melt-induced slagging, agglomeration, corrosion, and ash utilization. The authors also explore viable solutions for performing formation mechanisms and measurement analyses to mitigate these undesirable situations. Finally, the latter exclusively explores agglomeration at elevated temperatures, their mechanisms, detection, and strategies to avoid this. The authors cite using pressure and temperature measurements to help identify agglomeration and list actions to reduce the agglomeration phenomenon, such as additives, alternative materials such as biomass, and improvements in the reactor design.

Anthony [20] made a considerable contribution to this field when he published using fluidized bed combustion as an alternative to using solid fuels. The author emphasized the economic importance of using petroleum coke, coal wastes, wood pulp sludge, and biomass residues. He reported that a number of challenges are still present, e.g., N_2O emissions, agglomeration, and fouling. Years later, based on recent literature and personal experiments, Anthony et al. [21] focused their efforts on identifying mechanisms associated with the sulfation phenomena in fluidized bed combustion systems. The authors highlighted a disagreement regarding the understanding of sulfur capturing efficiency at maximum temperatures and that oxidizing and reducing conditions are much more critical to sorbent performance than previously reported in the literature. Perhaps these two concepts are the most important contributions of this paper.

Cho et al. [22] reported on chemical-looping combustion and using oxygen carriers in this process regarding experimental and technological applications. They compared seven different carriers of CuO, Fe_2O_3, Mn_3O_4, and NiO supported on aluminum oxide or kaolin for that purpose. Clearly, these kinds of support materials affect the carrier strength and reactivity. Moreover, Ni-, Cu-, and Fe-based oxygen carriers supported on aluminum oxide display high reactivity, and in the latter, there were signs of agglomeration. The authors concluded that copper carriers are unsuitable, and nickel carriers are potentially significant if the particle strength increases. These results are noteworthy since it was possible to develop a simple laboratory method to evaluate and compare the reactivity of metal-based oxygen carriers on industrial applications.

Furthermore, Abad et al. [26] tested the Fe-based oxygen carriers' ability to operate continuously at 300 W at four different temperatures in a chemical-looping reactor. Fe_2O_3 was used as an Fe-based oxygen carrier, and it was supported on aluminum oxide. The main results are related to the absence of agglomeration during the process and not decreased mass. Additionally, the authors verified that the process did not significantly affect the reactivity and crushing strength. These results suggest that how the reactor was operated, the friction between the particles was very low and, therefore, high durability. Syngas was more promising than natural gas regarding the gas used since it reached high efficiencies at the tested temperatures.

Mattisson et al. [23] also reported results on chemical-looping combustion and the use of iron-based carriers supported by five inert materials and analyzed the reducing and oxidizing conditions. The authors investigated the reactivity utilizing crushing strength, surface structure, and chemical composition. They proved that the sintering temperature influences reactivity, e.g., the particles sintered at 950 °C and 1100 °C displayed the highest reactivity, except Fe_2O_3 supported on Al_2O_3 which showed the best results when sintered at 1300 °C. Some exhibit agglomeration during the process, indicating that they may not be suitable for chemical-looping reactor systems.

Abad et al. [24] tested the feasibility of a manganese-based oxygen carrier. The authors evaluated this carrier supported on zirconia in this study and its use in chemical-looping combustion with natural gas or syngas as fuel in a continuously operating reactor. A range of thermal power, fuel flow, airflow, air ratio, and temperature were tested. The results show that the Mn-based oxygen carrier sintered at approximately 1150 °C was the most suitable, due to the nonexistence of agglomeration, little attrition, and a low mass-loss rate. They also revealed

that these particles were more appropriate for syngas than natural gas combustion since high efficiencies were achieved at all temperatures tested.

Adanez et al. [25] studied Cu-based oxygen carriers supported on alumina under several conditions adhering to the research trend on metallic carriers. The researchers used two interconnected bubbling fluidized bed reactors to demonstrate the chemical-looping combustion technology. The authors analyzed the experimental conditions, such as the oxygen carrier-to-fuel ratio, gas velocity, particle size, and temperature. They noticed that the oxygen carrier-to-fuel ratio and temperature were the most remarkable factors affecting methane conversion. No observed operating problems were informed, i.e., there was no agglomeration or carbon deposition. CuO proved to be an acceptable oxygen carrier, as it displayed high durability, attrition rate, and reactivity.

De Diego et al. [27] also studied chemical-looping combustion and CuO-supported alumina as the oxygen carrier. In this study, the authors evaluated two different sizes of the support material for methane combustion in a fluidized bed reactor. They performed the experiments at 800 °C for 200 hrs. of continuous operation to check the evolution of the oxygen carrier behavior and its structure. The oxygen carrier-to-fuel ratio was the most important parameter, and the absence of carbon deposition and agglomeration was consistent with the results reported by Adanez et al. [25]. The particles remained highly reactive even after 100 hrs. of operation, and the initial attrition rate was high and stabilized at low values throughout the process. According to the authors, the prototype displayed good performance, and the Cu-based oxygen carrier exhibited enough features to be used as a carrier in the chemical combustion process.

These are the six most cited papers in the Combustion theme addressing experimental results. It was noteworthy that they all mutually contribute to one another, i.e., there is an evident collaboration network. Furthermore, these works are similar in their results, as they all researched the use of metal carriers for converting fuel to CO_2 and water-using chemical-looping combustion. These results, jointly, make a significant contribution to the field of fluidized bed combustion, which is indisputable considering the total number of citations in these papers. These research studies were identified as being cited at the same time by five other papers, namely, Gao et al. [139], Iggland et al. [140], Adánez et al. [141], Rydén et al. [142], and Nandy et al. [143]. Two of these papers are reviews referring to the significant advances in chemical-looping combustion and chemical-looping reformation, highlighting the progress in developing these technologies related to using gaseous, solid, and liquid fuels, oxygen carriers,

modeling, and reactor systems [141,143]. The others are experimental papers investigating the usefulness of NiO oxygen carriers in chemical-looping combustion in a range of temperatures [139]; the particle size influences the reaction rate of coal combustion through the development of a method able to stop the reaction and measure the particle size [140] and establishing a method to examine carrier particles previously submitted to continuous operations compared with experimental data [142].

Two older studies complete this list of the top 20 most cited, Öhman et al. [28] and Lin et al. [144]. Both study agglomeration during the combustion of biomass fuels in fluidized beds. They were interested in elucidating bed agglomeration during the combustion of different biomass fuels. While Öhman et al. [28] used eight types of biomasses, Lin et al. [144] focused their efforts on only one. The results discussed by Öhman et al. [28] suggested that elements from the fuel formed a homogeneous ash layer in the coating, and the sticky layer formed from melting the coating material was responsible for agglomeration and defluidization. In turn, Lin et al. [144] suggested that their agglomeration and defluidization results were caused by high potassium concentrations in the ash, whereas potassium was converted from organic forms to inorganic forms during combustion. Furthermore, increased temperature favors agglomeration and defluidization because it promotes faster sintering between the carrier and the support material. Both agree that their results were very promising, but, at the time, further research should be done to obtain a more comprehensive view of agglomeration and defluidization phenomena.

Öhman et al. [28] and Lin et al. [144] have been cited at least 64 times jointly according to the WoS Core Collection. These works improved the understanding of aspects related to agglomeration and defluidization phenomena in chemical-looping combustion. In the last five years, papers that used them as references reported on a general investigation of agglomeration phenomenon [145–150], the impact of inorganic elements [151], CO_2, N_2, O_2, and steam [152], refractory materials [153] on agglomeration, physicochemical aspects [154], layer formation [155–160], combustion and steam gasification [161–163], in addition to describing the performance of pilot-scale reactor [164], development of a new device [165], defluidization inhibitors [166], and a more technological approach studying coarse particle fluidization effect on agglomeration, deposition, and defluidization [167], temperature influences on ash fouling and slagging during combustion [168], parameters influence on yield, composition, mineral phase, and physicochemical properties [169], hydrodynamic in extreme

conditions [170], inorganic transformation at high temperatures [171], and chemical equilibrium applications [172].

2.5. FUTURE OUTLOOKS

More research in the field of fluidized bed agglomeration could further contribute to the development of this research field. It is noticeably clear that a vast amount of literature addresses the influence of process parameters on final product characteristics or process efficiency. However, there is a gap in understanding, for example, how such parameters influence the process microscale, in view of the 20 most cited papers inspected in the bibliometric analysis. This void in the literature is probably due to no lack of interest in the subject but the limitation of more advanced techniques that are available only recently. It is noteworthy that among the papers studied in the bibliometric analysis (Table 2.2), the major part of them was published in the last twenty years, and maybe due to this, they appear as the most cited. This does not mean that among all the others papers listed by the bibliometric filtering, there is no research being carried out with a focus on the parameters influence in the process microscale, or the usage of advanced techniques for particle size measurement, for example.

There is broad knowledge regarding operating parameter evaluation, as has already been disclosed, using measurement techniques, new materials, and theoretical approaches on agglomeration in a fluidized bed. The effect on varying operating parameters is perhaps the most common type of research in this field, and it is closely linked to using new materials or new measurement techniques. Binder concentration and flow rate, fluidizing air velocity and temperature, nozzle height, solid material load, and atomizing air pressure are the most common parameters analyzed in the case of granulation. Some authors evaluated these parameters in their studies on soymilk [30], sand [32], glass beads [32,173], zein [174], sawdust [175], and lactose [176], among others. The most common is evaluating fuel and carrier types, temperature, oxygen-to-fuel rate, fuel gas velocity, and particle size in the case of combustion. Those studies checked the combustion parameters using metal carriers such as iron [22,23,26], copper [22,25,27,177], nickel [22,177], manganese [22,26], or biomass [19,28,178,179]. There is a strong trend to employ the granulation of plant-based materials and the combustion of agro-industrial residues using the abovementioned operating parameters.

Additionally, there is also the trend toward using robust and modern measurement techniques based on in-line measurements by tools that can be coupled to the fluidized bed. These methods are advantageous because they can provide real-time process feedback, making it possible to overview the process as it occurs. Infrared moisture sensors [180], near infrared spectroscopy [181–184], pressure fluctuations [185], optical imaging processing [180,186–188] acoustic emission [189–193], electrical capacitance tomography [194], spatial filter velocimetry [195–200], Raman spectroscopy [201], focused beam reflectance measurement [184,202], microwave resonance technology [203], triboelectric probes [204,205], and positron emission particle tracking [206,207] are examples of these techniques. These techniques can help improve theories by proposing innovative approaches for agglomeration in a fluidized bed or the formation of useful databases for process modeling and simulation.

2.6. FINAL REMARKS

An appreciable number of studies have discussed using agglomeration in fluidized beds for several applications in chemical processes. The bibliometric analysis made it possible to recognize the most frequent keywords, influential journals, the most cited papers, productive countries and network collaboration according to co-authorship, and innovation trends in granulation and combustion research based on the top 20 most cited papers. The studies examined theoretical approaches and experimental and/or numerical applications regarding granulation and combustion. The review revealed a considerable range of fluidized bed applications, whether for producing foodstuffs or using gas combustion to separate inherent greenhouse gases. It was also possible to verify the duality of particle agglomeration, which is desirable for granulation, as the objective is to increase particle size for improved handling properties. In contrast, combustion is an undesirable aspect, as the increase in particles negatively impacts reactor efficiency. Thus, it represents an opportunity for identifying new potential ways of employing this technique in industrial processes.

ACKNOWLEDGMENTS

REFERENCES

[1] S. M. Iveson, J. D. Litster, K. Hapgoog, B. J. Ennis. Nucleation, growth and breakage phenomena in agitated wet granulation processes: a review. Powder Technology, 117, 3-39, 2001. https://doi.org/10.1016/S0032-5910(01)00313-8.

[2] B. J. Ennis, G. Tardos, R. Pfeffer. A microlevel-based characterization of granulation phenomena. Powder Technology, 65, 257-272, 1991. https://doi.org/10.1016/0032-5910(91)80189-P.

[3] W. Pietsch. An interdisciplinary approach to size enlargement by agglomeration. Powder Technology, 130, 1-3, 8-13, 2003. https://doi.org/10.1016/S0032-5910(02)00218-8.

[4] K. Dhanalakshmi, S. Ghosal, S. Bhattacharya. Agglomeration of food powder and applications. Critical Reviews in Food Science and Nutrition, 51, 5, 432-441, 2011. https://doi.org/10.1080/10408391003646270.

[5] J. Werther. Fluidized-bed reactors. Ullmann's Encyclopedia of Industrial Chemistry. 2007. https://doi.org/10.1002/14356007.b04_239.pub2.

[6] P. C. Knight. Structuring agglomerated products for improved performance. Powder Technology, 119, 1, 14-25, 2001. https://doi.org/10.1016/S0032-5910(01)00400-4.

[7] A. A. Khan, W. de Jong, P. J. Jansens, H. Spliethoff. Biomass combustion in fluidized bed boilers: potential problems and remedies. Fuel Processing Technology, 90, 21-50, 2009. https://doi.org/10,1016/j.fuproc.2008.07.012.

[8] C. L. Lin, T. H. Peng, W. J. Wang. Effect of particle size distribution on agglomeration/defluidization during fluidized bed combustion. Powder Technology, 207, 1-3, 290-295, 2011. https://doi.org/10.1016/j.powtec.2010.11.010.

[9] B. G. Langston, F. M. Stephens Jr. Self-agglomeration fluidized-bed reduction. JOM, 12, 312-316, 1960. https://doi.org/10.1007/BF03377976.

[10] J. L. Moseley, T. J. O'Brien. A model for agglomeration in a fluidized bed. Chemical Engineering Science, 48, 17, 3043-3050, 1993. https://doi.org/10.1016/0009-2509(93)80170-U.

[11] J. R. Wank, S. M. George, A. W. Weimer. Vibro-fluidization of fine boron nitride powder at low pressure. Powder Technology, 121, 2-3, 195-204, 2001. https://doi.org/10.1016/S0032-5910(01)00337-0.

[12] M. Pell, J. C. Williams, T. Allen. Handbook of Powder Technology. Amsterdam: Elsevier, 1990.

[13] G. Sun, J. R. Grace. Effect of particle size distribution in different fluidization regimes. AIChE Journal, 38, 5, 716-722, 1992. https://doi.org/10.1002/aic.690380508.

[14] D. Gauthier, S. Zerguerras, G. Flamant. Influence of the particle size distribution of powders on the velocities of minimum and complete fluidization. Chemical Engineering Journal, 74, 3, 181-196, 1999. https://doi.org/10.1016/S1385-8947(99)00075-3.

[15] W. P. Oliveira, C. R. F. Souza, C. J. Lim, J. R. Grace. Identification of the state of a wet spouted bed through time-frequency analysis of pressure fluctuation time series. The Canadian Journal of Chemical Engineering, 87, 2, 289-297, 2009. https://doi.org/10.1002/cjce.20159.

[16] T, R. Costa, P. Gayán, A. Abad, F. García-Labiano, L. F. de Diego, D. M. A. Melo, J. Adánez. Mn-based oxygen carriers prepared by impregnation for Chemical Looping Combustion with diverse fuels. Fuel Processing Technology, 178, 236-250, 2018. https://doi.org/10.1016/j.fuproc.2018.05.019.

[17] J. Werther, M. Saenger, E. U. Hartge, T. Ogada, Z. Siagi. Combustion of agricultural residues. Progress in Energy and Combustion Science, 26, 1-27, 2000. https://doi.org/10.1016/S0360-1285(99)00005-2.

[18] M. Bartels, W. Lin, J. Nijenhuis, F. Kapteijn, J. R. van Ommen. Agglomeration in fluidized beds at high temperatures: mechanisms, detection and prevention. Progress in Energy and Combustion Science, 34, 633-666, 2008. https://doi.org/10.1016/j.pecs.2008.04.002.

[19] Y. Niu, H. Tan, S. Hui. Ash-related issues during biomass combustion: Alkali-induced slagging, silicate melt-induced slagging (ash fusion), agglomeration, corrosion, ash utilization, and related countermeasures. Progress in Energy and Combustion Science, 52, 1-61, 2016. https://doi.org/10.1016/j.pecs.2015.09.003.

[20] E. J. Anthony. Fluidized bed combustion of alternative solid fuels; status, successes and problems of the technology. Prog. Energy Combust. Sci., 21, 239-268, 1995. https://doi.org/0360-1285(95)0005-4.

[21] E. J. Anthony, D. L. Granatstein. Sulfation phenomena in fluidized bed combustion systems. Progress in Energy and Combustion Science, 27, 215-236, 2001. https://doi.org/S0360-1285(00)00021-6.

[22] P. Cho, T. Mattisson, A. Lyngfelt. Comparison of iron-, nickel-, copper- and manganese-based oxygen carriers for chemical-looping combustion. Fuel, 83, 1215-1225, 2004. https://doi.org/10.1016/j.fuel.2003.11.013.

[23] T. Mattisson, M. Johansson, A. Lyngfelt. Multicycle reduction and oxidation of different types of iron oxide particles – application to chemical-looping combustion. Energy & Fuels, 18, 628-637, 2004. https://doi.org/10.1021/ef0301405.

[24] A. Abad, T. Mattisson, A. Lyngfelt, M. Rydén. Chemical-looping combustion in a 300 W continuously operating reactor system using a manganese-based oxygen carrier. Fuel, 85, 9, 1174-1185, 2006. https://doi.org/10.1016/j.fuel.2005.11.014.

[25] J. Adánez, P. Gayán, J. Celaya, L. F. de Diego, F. García-Labiano, A. Abad. Chemical Looping Combustion in a 10 kWth prototype using a CuO/Al2O3 oxygen carrier: effect of operating conditions on methane combustion. Ind. Eng. Chem. Res., 45, 6075-6080, 2006. https://doi.org/0.1021/ie060364l.

[26] A. Abad, J. Adánez, F. García-Labiano, L. F. de Diego, P. Gayán, J. Celaya. Mapping of the range of operational conditions for Cu-, Fe-, and Ni-based oxygen carriers in chemical-looping combustion. Chemical Engineering Science, 62, 1-2, 533-549, 2007. https://doi.org/10.1016/j.ces.2006.09.019.

[27] L. F. de Diego, F. García-Labiano, P. Gayán, J. Celaya, J. M. Palacios, J. Adánez. Operation of a 10 kWth chemical-looping combustor during 200 h with a CuO-Al2O3 oxygen carrier. Fuel, 86, 1036-1045, 2007. https://doi.org/10.1016/j.fuel.2006.10.004.

[28] M. Öhman, A. Nordin, B. J. Skrifvars, R. Backman, M. Hupa. Bed agglomeration characteristics during fluidized bed combustion of biomass fuels. Energy & Fuels, 14, 169-178, 2000. https://doi.org/10.1021/ef90107b.

[29] J. N. Knudsen, P. A. Jensen, W. Lin, F. J. Frandsen, K. Dam-Johansen. Sulfur transformations during thermal conversion of herbaceous biomass. Energy Fuels, 18, 3, 810-819, 2004. https://doi.org/10.1021/ef034085b.

[30] N. Jinapong, M. Suphantharika, P. Jamnong. Production of instant soymilk powders by ultrafiltration, spray drying and fluidized bed agglomeration. Journal of Food Engineering, 84, 194-205, 2008. https://doi.org/10.1016/j.jfoodeng.2007.04.032.

[31] M. Fuchs, C. Turchiuli, M. Bohin, M. E. Cuvelier, C. Ordonnaud, M. N. Peyrat-Maillard, E. Dumoulin. Encapsulation of oil in powder using spray frying and fluidized bed agglomeration. Journal of Food Engineering, 75, 27-35, 2006. https://doi.org/10.1016/j.jfoodeng.2005.03.047.

[32] M. Hemati, R. Cherif, K. Saleh, V. Pont. Fluidized bed coating and granulation: influence of process-related variables and physicochemical properties on the growth kinetics. Powder Technology, 130, 18-34, 2003. https://doi.org/S0032-5910(02)00221-8.

[33] R. Fan, D. L. Marchisio, R. O. Fox. Application of the direct quadrature method of moments to polydisperse gas-solid fluidized beds. Powder Technology, 139, 7-20, 2004. https://doi.org/10.1016/j.powtec.2003.10.005.

[34] M. H. Hariri, H. Arastoopour, A. Rehmat. Agglomeration of polyolefin particles in a fluidized bed with a central jet Part I. Experimental study. Powder Technology, 74, 3, 231-238, 1993. https://doi.org/10.1016/0032-5910(93)85031-4.

[35] I. A. Al Amin, A. K. Biń. Application of the fluidized bed process for formulation of WG-type pesticide granules. Powder Technology, 79, 2, 135-146, 1994. https://doi.org/10.1016/0032-5910(94)80008-1.

[36] S. Watano, K. Miyanami. Image processing for on-line monitoring of granule size distribution and shape in fluidized bed granulation. Powder Technology, 83, 55-60, 1995. https://doi.org/10.1016/0032-5910(94)02944-J.

[37] K. Dewettinck, A. Huyghebaert. Fluidized bed coating in food technology. Trends in Food Science & Technology, 10, 4-5, 163-168, 1999. https://doi.org/10.1016/S0924-2244(99)00041-2.

[38] H. Kage, M. Dohzaki, H. Ogura. Powder coating efficiency of small particles and their agglomeration in circulating fluidized bed. Korean J. Chem. Eng., 16, 5, 630-634, 1999. https://doi.org/10.1007/BF02708143.

[39] J. R. van Ommen, J. C. Schouten, M. O. Coppens, C. M. van der Bleek. Monitoring fluidization by dynamic pressure analysis. Chemical Engineering Technology, 22, 9, 1999. https://doi.org/10.1002/(SICI)1521-4125(199909)22:9<773::AID-CEAT773>3.0.CO;2-I.

[40] J. M. Rodríguez, J. R. Sanchéz, A. Alvaro, D. F. Florea, A. M. Estévez. Fluidization and elutriation of iron oxide particles. A study of attrition and agglomeration processes in fluidized beds. Powder Technology, 111, 218-230, 2000. https://doi.org/10.1016/S0032-5910(99)00292-2.

[41] S. Palzer. The effect of glass transition on the desired and undesired agglomeration of amorphous food powders. Chemical Engineering Science, 60, 14, 3959-3968, 2005. https://doi.org/10.1016/j.ces.2005.02.015.

[42] C. Turchiuli, R. Smail, E. Dumoulin. Fluidized bed agglomeration of skim milk powder: Analysis of sampling for the follow-up of agglomerate growth. Powder Technology, 238, 161-168, 2013. https://doi.org/10.1016/j.powtec.2012.02.030.

[43] F. Parveen, C. Briens, F. Berruti, J. McMillan. Effect of particle size, liquid content and location on the stability of agglomerates in a fluidized bed. Powder Technology, 237, 376-385, 2013. https://doi.org/10.1016/j.powtec.2012.12.021.

[44] J. Ji, K. Cronin, J. Fitzpatrick, S. Miao. Enhanced wetting behaviours of whey protein isolate powder: The different effects of lecithin addition by fluidised bed agglomeration and coating processes. Food Hydrocolloids, 71, 94-101, 2016. https://doi.org/10.1016/j.foodhyd.2017.05.005.

[45] G. R. Custódio, L. F. G. de Souza, M. Nitz, K. Andreola. A protein powder agglomeration process using acai pulp as the binder: An analysis of the process parameters. Advanced Powder Technology, 31, 8, 3551-3561, 2020. https://doi.org/10.1016/j.apt.2020.07.001.

[46] M. Langner, I. Kitzmann, A. L. Ruppert, I. Wittich, B. Wolf. In-line particle size measurement and process influences on rotary fluidized bed agglomeration. Powder Technology, 364, 673-679, 2020. https://doi.org/10.1016/j.powtec.2020.02.034.

[47] E. Zhalehrajabi, K. K. Lau, K. KuShaari, W. H. Tay, T. Hagemeier, A. Idris. Modelling of urea aggregation efficiency via particle tracking velocimetry in fluidized bed granulation. Chemical Engineering Science, 223, 2020. https://doi.org/10.1016/j.ces.2020.115737.

[48] A. Tabeei, A. Samimi, D. Mohebbi-Kalhori. CFD modeling of an industrial scale two-fluid nozzle fluidized bed granulator. Chemical Engineering Research & Design, 159, 605-614, 2020. https://doi.org/10.1016/j.cherd.2020.05.020.

[49] M. S. Salehi, M. Askarishahi, S. Radl. Quantification of solid mixing in bubbling fluidized beds via two-fluid model simulations. Industrial & Engineering Chemistry Reserarch, 59, 22, 10606-10621, 2020. https://doi.org/10.1021/acs.iecr.9b06343.

[50] P. Bachmann, K. Chen, A. Buck, E. Tsotsas. Prediction of particle size and layer-thickness distributions in a continuous horizontal fluidized-bed coating process. Particuology, 50, 1-12, 2020. https://doi.org/10.1016/j.partic.2019.06.005.

[51] I. C. Kemp, A. van Millingen, H. Khaled. Development and verification of a novel design space and improved scale-up procedure for fluid bed granulation using a mechanistic model. Powder Technology, 361, 1021-1037, 2020. https://doi.org/10.1016/j.powtec.2019.10.093.

[52] C. Rieck, A. Buck, E. Tsotsas. Estimation of the dominant size enlargement mechanism in spray fluidized bed processes. AIChE Journal, 66, 5, 2020. https://doi.org/10.1002/aic.16920.

[53] C. Shin, J. H. Choi, J. H. Kim, K. T. Hwang, J. H. Kim. Influence of flowability of ceramic tile granule powders on sintering behavior of relief ceramic tile. Korean Journal of Materials Research, 30, 10, 550-557, 2020. https://doi.org/10.3740/MRSK.2020.30.10.550.

[54] G. Strenzke, R. Durr, A. Buck, E. Tsotsas. Influence of operating parameters on process behavior and product quality in continuous spray fluidized bed agglomeration. Powder Technology, 375, 210-220, 2020. https://doi.org/10.1016/j.powtec.2020.07.083.

[55] F. Sahnen, J. P. Kamps, K. Langer. Conversion of indomethacin nanosuspensions into solid dosage forms via fluid bed granulation and compaction. European Journal of Pharmaceutics and Biopharmaceutics, 154, 89-97, 2020. https://doi.org/10.1016/j.ejpb.2020.06.020.

[56] J. G. Rosa, R. F. Nascimento, K. Andreola, O. P. Taranto. Acacia gum fluidized bed agglomeration: use of inulin as a binder and process parameters analysis. Journal of Food Process and Engineering, 43, 7, 2020. https://doi.org/10.1111/jfpe.13409.

[57] J. Du, A. Buck, E. Tsotsas. Influence of process variables on spray agglomeration process in a continuously operated horizontal fluidized bed. Powder Technology, 363, 195-206, 2020. https://doi.org/10.1016/j.powtec.2020.01.008.

[58] G. Tian, Y. D. Wei, J. Zhao, W. L. Li, H. B. Qu. Application of pulsed spray and moisture content control strategies on quality consistency control in fluidized bed granulation: A comparative study. Powder Technology, 363, 232-244, 2020. https://doi.org/10.1016/j.powtec.2019.11.118.

[59] S. Pathi, R. Kumar, V. K. Surasani. Investigantion of agglomeration kinetics of acetaminnophen using fluidized bed wet granulation. Asia-Pacific Journal of Chemical Engineering, 15, 2, 2020. https://doi.org/10.1002/apj.2416.

[60] M. Askarishahi, M. Maus, D. Schröder, D. Slade, M. Martinetz, D. Jajcevic. Mechanistic modelling of fluid bed granulation, Part I: Agglomeration in pilot scale process. International Journal of Pharmaceutics, 573, 118837, 2020. https://doi.org/10.1016/j.ijpharm.2019.118837.

[61] P. Sureshi, N. S. Reddy, R. Hariharan, I. Sreedhar. Studies on fluid bed granulation of lactose-MCC mixture. Materials Today-Proceedings, 24, 519-530, 2020.

[62] N. Le Bolay, R. Lakhal, M. Hemati. Production of hematite micro- and nanoparticles in a fluidized bed process-mechanism study. Kona Powder and Particle Journal, 37, 244-257, 2020. https://doi.org/10.14356/kona.2020014.

[63] B. Wang, H. Y. Liu, C. L. Zhou, H. H. Huo, K. J. Dong, Y. C. Jiang. Enhancing the collection efficiency of a gas cyclone with atomization and electrostatic charging. Powder Technology, 364, 562-571, 2020. https://doi.org/10.1016/j.powtec.2020.01.062.

[64] C. W. Wang, Y. M. Zhang, K. J. Dong, B. Wang, S. Q. Li, R. B. Xi, Y. C. Jiang. Enhanced collection of fine particles in a cyclone using ultrasonic vapor with surfactants. Advanced Powder Technology, 31, 6, 2207-2214, 2020. https://doi.org/10.1016/j.apt.2020.03.015.

[65] M. Arenas-Jal, J. M. Suñé-Negre, E. García-Montoya. An overview of microencapsulation in the food industry: opportunities, challenges, and innovations. European Food Research and Technology, 246, 1371–1382, 2020. https://doi.org/10.1007/s00217-020-03496-x.

[66] S. Pohl, P. Kleinebudde. A review of regime maps for granulation. International Journal of Pharmaceutics, 587, 2020. https://doi.org/10.1016/j.ijpharm.2020.119660.

[67] A. S. Abed, M. Rismanchi, M. H. Moosavi, A. M. Khaneghah, A. Mohammadi, M. Mahmoudzadeh. A mixture of modified starch and maltodextrin for spray drying encapsulation of Nigella sativa seeds oil containing thymoquinone. Starch-Stärke, 73, 3-4, 1900225, 2020. https://doi.org/10.1002/star.201900255.

[68] H. B. de Souza, A. L. D. Dessimoni, M. L. A. Ferreira, D. A. Botrel, S. V. Borges, L. C. Viana, C. R. de Oliveira, A. M. T. Lago, R. V. D. Fernandes. Microparticles obtained by spray-drying technique containing ginger essential oil with the addition of cellulose nanofibrils extracted from the ginger vegetable fiber. Drying Technology, 1-15, 2020. https://doi.org/10.1080/07373937.2020.1851707.

[69] T. S. de Oliveira, O. Freitas-Silva, A. M. Kluczovski, P. H. Campelo. Potential use of vegetable proteins to reduce Brazil nut oil oxidation in microparticle systems. Food Research International, 137, 2020. https://doi.org/10.1016/j.foodres.2020.109526.

[70] I. S. M. Zaidul, T. K. Fahim, F. Sahena, A. K. Azad, M. A. Rashid, M. S. Hossain. Dataset on applying HPMC polymer to improve encapsulation efficiency and stability of the fish oil: In vitro evaluation. Data in Brief, 32, 2020. https://doi.org/10.1016/j.dib.2020.106111.

[71] A. M. de Melo, R. C. T. Barbi, W. F. C. de Souza, L. C. Luna, H. B. Souza, G. L. Lucena, M. R. Quirino, S. de Souza. Microencapsulated lemongrass (Cymbopogon flexuosus) essential oil: A new source of natural additive applied to Coalho cheese. Journal of Food Processing and Preservation, 44, 10, 2020. https://doi.org/10.1111/jfpp.14783.

[72] B. Başyiğit, H. Sağlam, Ş. Kandemir, A. Karaaslan, M. Karaaslan. Microencapsulation of sour cherry oil by spray drying: Evaluation of physical morphology, thermal properties, storage stability, and antimicrobial activity. Powder Technology, 364, 654-663, 2020. https://doi.org/10.1016/j.powtec.2020.02.035.

[73] M. Pattnaik, H. N. Mishra. Effect of microwave treatment on preparation of stable PUFA enriched vegetable oil powder and its influence on quality parameters. Journal of food Processing and Preservation, 44, 4, 2020. https://doi.org/10.1111/jfpp.14374.

[74] J. Ndayishimiye, G. Ferrentino, H. Nabil, M. Scampicchio. Encapsulation of oils recovered from brewer's spent grain by particles from gas saturated solutions technique. Food and Bioprocess Technology, 13, 2, 256-264, 2020. https://doi.org/10.1007/s11947-019-02392-x.

[75] V. D. Quintero-Castano, J. F. Vasco-Leal, L. Cuellar-Nunez, I. Luzardo-Ocampo, F. Castellanos-Galeano, C. Alvarez-Barreto, L. A. Bello-Perez, M. Cortes-Rodriguez. Novel OSA-modified starch from Gros Michel banana for encapsulation of Andean blackberry concentrate: production and storage stability. Starch-Starke, 73, 3-4, 2020. https://doi.org/10.1002/star.202000180.

[76] L. M. de Macedo, E. M. dos Santos, L. Militão, L. L. Tundisi, J. A. Ataide, E. B. Souto, P. G. Mazzola. Rosemary (Rosmarinus officinalis L., syn Salvia rosmarinus Spenn.) and its topical applications: A review. Plants-Basel, 9, 5, 2020. https://doi.org/10.3390/plants9050651.

[77] M. S. Navidad-Murrieta, A. Perez-Larios, J. A. Sanchez-Burgos, J. A. Ragazzo-Sanchez, G. Luna-Barcenas, S. G. Sayago-Ayerdi. Use of a Taguchi Design in Hibiscus sabdariffa extracts encapsulated by spray-drying. Foods, 9, 2, 2020. https://doi.org/10.3390/foods9020128.

[78] E. Rahpeyma, S. S. Sekhavatizadeh. Effects of encapsulated green coffee extract and canola oil on liquid kashk quality. Foods and Raw Materials, 8, 1, 40-51, 2020. https://doi.org/10.21603/2308-4057-2020-1-40-51.

[79] O. Alfaro-Galarza, E. O. López-Villegas, N. Rivero-Perez, D. Tapia-Maruri, A. R. Jiménez-Aparicio, H. M. Palma-Rodríguez, A. Vargas-Torres. Protective effects of the use of taro and rice starch as wall material on the viability of encapsulated Lactobacillus paracasei subsp. Paracasei. LWT, 117, 108686, 2020. https://doi.org/10.1016/j.lwt.2019.108686.

[80] M. Stasse, E. Laurichesse, M. Vandroux, T. Ribaut, V. Heroguez, V. Schmitt. Cross-linking of double oil-in-water-in-oil emulsions: A new way for fragrance encapsulation with tunable sustained release. Colloids and Surfaces A – Physicochemical and Engineering Aspects, 607, 2020. https://doi.org/10.1016/j.colsurfa.2020.125448.

[81] C. C. Loi, G. T. Eyres, P. Silcock, E. J. Birch. Preparation and characterisation of a novel emulsifier system based on glycerol monooleate by spray-drying. Journal of Food Engineering, 285, 2020. https://doi.org/10.1016/j.jfoodeng.2020.110100.

[82] Y. Wang, Z. J. Zheng, K. Wang, C. H. Tang, Y. F. Liu, J. W. Li. Prebiotic carbohydrates: Effect on physicochemical stability and solubility of algal oil nanoparticles. Carbohydrates Polymers, 228, 2020. https://doi.org/10.1016/j.carbpol.2019.115372.

[83] A. Lewandowski, I. Zbicinki, M. Jaskulski. Microencapsulation in foam spray drying. Drying Technology, 38,1-2, 55-70, 2020. https://doi.org/10.1080/07373937.2019.1614047.

[84] C. Mutlu, A. Koc, M. Erbas. Some physical properties and adsorption isotherms of vacuum-dried honey powder with different carrier materials. LWT-Food Science and Technology, 134, 2020. https://doi.org/10.1016/j.lwt.2020.110166.

[85] H. Yuksel, S. N. Dirim. Application of the agglomeration process on spinach juice powders obtained using spray drying method. Drying Technology, 39, 1, 19-34, 2020. https://doi.org/10.1080/07373937.2020.1832515.

[86] K. Haas, T. Dohnal, P. Andreu, E. Zehetner, A. Kiesslich, M. Volkert, P. Fryer, H. Jaeger. Particle engineering for improved stability and handling properties of carrot concentrate powders using fluidized bed granulation and agglomeration. Powder Technology, 370, 104-115, 2020. https://doi.org/10.1016/j.powtec.2020.04.065.

[87] R. F. Nascimento, J. G. Rosa, K. Andreola, O. P. Taranto. Wettability improvement of pea protein isolate agglomerated in pulsed fluid bed. Particulate Science and Technology, 38, 4, 511-521, 2020. https://doi.org/10.1080/02726351.2019.1574940.

[88] D. Kontziampasis, M. S. Manga, D. W. York. Coating particles using liquids and foams based on viscous formulations with industrial mixers: Batch operation. Particuology, 50, 13-24, 2020. https://doi.org/10.1016/j.partic.2019.06.002.

[89] S. Pandey, Aparna, K. S. Varghese, A. K. Chauhan, M. Singh. Development of phytonutrient enriched avocado milkshake powder and its quality evaluation. Indian Journal of Dairy Science, 73, 6, 556-565, 2020. https://doi.org/10.33785/IJDS.2020.v73i06.007.

[90] Z. Hardy, V. A. Jideani. Functional characteristics and microbiological viability of foam-mat dried Bambara groundnut (Vigna subterranea) yogurt from reconstituted Bambara groundnut milk powder. Food Science & Nutrition, 8, 10, 5238-5248, 2020. https://doi.org/10.1002/fsn3.951.

[91] G. V. Marson, R. P. Saturno, T. A. Comunian, L. Consoli, M. T. D. Machado, M. D. Hubinger. Maillard conjugates from spent brewer's yeast by-product as an innovative encapsulating material. Food Research International, 136, 2020. https://doi.org/10.1016/j.foodres.2020.109365.

[92] Z. A. Ozbek, P. G. Ergonul. Optimisation of wall material composition of freeze-dried pumpkin seed oil microcapsules: Interaction effects of whey protein, maltodextrin, and gum Arabic by D-optimal mixture design approach. Food hydrocolloids, 107, 2020. https://doi.org/10.1016/j.foodhyd.2020.105909.

[93] L. Lipan, B. D. Rusu, E. L. Simon, E. Sendra, F. Hernandez, D. C. Vodnar, M. Corell, A. Carbonell-Barrachina. Chemical and sensorial characterization of spray dried hydroSOStainable almond milk. Journal of the Science of Food and Agriculture, 101, 4, 1372-1381, 2020. https://doi.org/10.1002/jsfa.10748.

[94] G. C. Koc, A. N. Yuksel, E. Bas, S. L. Erdogan. Foam mat drying of taro (Colocasia esculenta): The effect of ultrasonic pretreatment and drying techniques on the drying behavior, flow, and reconstitution properties of taro flour. Journal of Food Process Engineering, 43, 11, 2020. https://doi.org/10.1111/jfpe.13516.

[95] C. Zhang, S. L. A. Khoo, P. Swedlund, Y. Ogawa, Y. Shan, S. Y. Quek. fabrication of spray-dried microcapsules containing noni juice using blends of maltodextrin and gum acacia: physicochemical properties of powders and bioaccessibility of bioactives during in vitro digestion. Foods, 9, 9, 2020. https://doi.org/10.3390/foods9091316.

[96] E. Ermis, M. Ozkan. Sugar beet powder production using different drying methods, characterization and influence on sensory quality of cocoa-hazelnut cream. Journal of Food Science and Technology-Mysore, 58, 6, 2068-2077, 2020. https://doi.org/10.1007/s13197-020-04715-9.

[97] S. B. Cinar, G. C. Koc, S. N. Dirim, G. Unal, A. S. Akalin. Textural and sensorial characteristics of set-type yogurt containingBifidobacterium animalissubsp.lactisBb-12 and quince powder. Journal of Food Measurement and Characterization, 14, 6, 3067-3077, 2020. https://doi.org/10.1007/s11694-020-00552-8.

[98] H. H. Ding, W. Yu, I. Boiarkina, N. Depree, B. R. Young. Effects of morphology on the dispersibility of instant whole milk powder. Journal of Food Engineering, 276, 2020. https://doi.org/10.1016/j.jfoodeng.2019.109841.

[99] S. Mounir, A. Ghandour, R. Mustafa, K. Allaf. Can hydro-thermo-mechanical treatment by instant controlled pressure-drop (DIC) be used as short time roasting process? Effect of processing parameters on sensory, physical, functional, and color attributes of Egyptian carob powder. Journal of Food Science and Technology-Mysore, 58, 2, 451-464, 2020. https://doi.org/10.1007/s13197-020-04553-9.

[100] G. C. Koc. The effect of different drying techniques and microwave finish drying on the powder properties of the red pepper powder (Capsicum annuum L.). Journal of Food Science and Technology-Mysore, 57, 12, 4576-4587, 2020. https://doi.org/10.1007/s13197-020-04496-1.

[101] Y. Yang, D. D. Pan, Y. Wang, J. He, Y. Yue, Q. Xia, G. H. Zhou, J. X. Cao. Effect of reconstituted broth on the taste-active metabolites and sensory quality of stewed and roasted pork-hock. Foods, 9, 4, 2020. https://doi.org/10.3390/foods9040513.

[102] B. Safdar, Z. H. Pang, X. Q. Liu, M. T. Rashid, M. A. Jatoi. Structural and functional properties of raw and defatted flaxseed flour and degradation of cynogenic contents using different processing methods. Journal of Food Process Engineering, 43, 6, 2020. https://doi.org/10.1111/jfpe.13406.

[103] F. M. Yilmaz, A. Z. Bastioglu. Production of phenolic enriched mushroom powder as affected by impregnation method and air drying temperature. LWT-Food Science and Technology, 122, 2020. https://doi.org/10.1016/j.lwt.2020.109036.

[104] A. Dantas, S. Verruck, G. R. de Liz, E. Hernandez, E. S. Prudencio. Lactose-free skim milk and prebiotics as carrier agents of Bifidobacterium BB-12 microencapsulation: physicochemical properties, survival during storage and in vitro gastrointestinal condition behavior. International Journal of Food Science and Technology, 56, 5, 2132-2145, 2020. https://doi.org/10.1111/ijfs.14823.

[105] J. D. Figueiredo, M. A. Teoxeira, P. H. Campelo, A. M. T. Lago, T. P. de Souza, M. I. Yoshida, C. R. de Oliveira, A. P. A. Pereira, G. M. Pastore, E. A. Sanches, D. A. Botrel, S. V. Borges. Encapsulation of camu-camu extracts using prebiotic biopolymers: Controlled release of bioactive compounds and effect on their physicochemical and thermal properties. Food Research International, 137, 2020. https://doi.org/10.1016/j.foodres.2020.109563.

[106] N. Kanha, S. Surawang, P. Pitchakarn, T. Laokuldilok. Microencapsulation of copigmented anthocyanins using double emulsion followed by complex coacervation: Preparation, characterization and stability. LWT-Food Science and Technology, 133, 2020. https://doi.org/10.1016/j.lwt.2020.110154.

[107] S. C. Lourenco, M. Moldao-Martins, V. D. Alvez. Microencapsulation of pineapple peel extract by spray drying using maltodextrin, inulin, and Arabic gum as wall matrices. Foods, 9, 6, 2020. https://doi.org/10.3390/foods9060718.

[108] M. S. Noghabi, M. Molaveisi. The effect of wall formulation on storage stability and physicochemical properties of cinnamon essential oil microencapsulated by spray drying. Chemical Papers, 74, 10, 3455-3465, 2020. https://doi.org/10.1007/s11696-020-01171-9.

[109] Y. W. Chi, D. X. Wang, M. Jiang, S. H. Chu, B. Wang, Y. E. Zhi, P. Zhou, D. Zhang. Microencapsulation of Bacillus megaterium NCT-2 and its effect on remediation of secondary salinization soil. Journal of Microencapsulation, 37, 2, 134-143, 2020. https://doi.org/10.1080/02652048.2019.1705409.

[110] T. A. Comunian, A. G. D. Anthero, E. O. Bezerra, I. C. F. Moraes, M. D. Hubinger. Encapsulation of pomegranate seed oil by emulsification followed by spray drying: evaluation of different biopolymers and their effect on particle properties. Food and Bioprocess technology, 13, 1, 53-66, 2020. https://doi.org/10.1007/s11947-019-02380-1.

[111] J. Park, B. Yoo. Particle agglomeration of gum mixture thickeners used for dysphagia diets. Journal of Food Engineering, 279, 2020. https://doi.org/10.1016/j.jfoodeng.2020.109958.

[112] R. F. Nascimento, J. G. Rosa, M. F. Ávila, O. P. Taranto. Pea protein isolate fluid dynamics and characterization obtained by agglomeration in pulsed fluidized bed. Particulate Science and Technology, 2020. https://doi.org/10.1080/02726351.2020.1830209.

[113] H. Lee, B. Yoo. Agglomerated xanthan gum powder used as a food thickener: Effect of sugar binders on physical, microstructural, and rheological properties. Powder Technology, 362, 301-306, 2020. https://doi.org/10.1016/j.powtec.2019.11.124.

[114] S. Wu, J. Fitzpatrick, K. Cronin, V. Maidannyk, S. Miao. Effects of spraying surfactants in a fluidised bed on the rehydration behaviour of milk protein isolate powder. Journal of Food Engineering, 266, 2020. https://doi.org/10.1016/j.jfoodeng.2019.109694.

[115] S. Zamani, A. Morris. Effect of droplet collisions on evaporation in spray-drying. Drying Technology, 2020. https://doi.org/10.1080/07373937.2020.1866006.

[116] M. Sobulska, I. Zbicinski. Advances in spray drying of sugar-rich products. Drying Technology, 2020. https://doi.org/10.1080/07373937.2020.1832513.

[117] A. Marinopoulou, V. Karageorgiou, D. Petridis, S. N. Raphaelides. Physical properties of starch-paracetamol molecular inclusion complexes produced by the spray drying process on an industrial scale. Drying Technology, 2020. https://doi.org/10.1080/07373937.2020.1815764.

[118] M. Z. Islam, O. Ayami, Y. Kitamura, M. Kokawa, K. Takeshi, K. Masayuki, H. Norihiro. Micro wet milling and spray drying of whole mandarin powder and its characterization. Journal of Food Measurement and Characterization, 15, 1, 851-861, 2020. https://doi.org/10.1007/s11694-020-00679-8.

[119] N. D. Mendes, P. P. S. Coimbra, M. C. B. Santos, L. C. Cameron, M. S. L. Ferreira, M. D. Buera, E. C. B. A. Gonçalves. Capsicum pubescens as a functional ingredient: Microencapsulation and phenolic profiling by UPLC-MSE. Food Research International, 135, 2020. https://doi.org/10.1016/j.foodres.2020.109292.

[120] K. Samborska, A. Baranska, K. Szulc, E. Jankowska, M. Truszkowska, E. Ostrowska-Ligeza, R. Wolosiak, E. Szymanska, A. Jedlinska. Reformulation of spray-dried apple concentrate and honey for the enhancement of drying process performance and the physicochemical properties of powders. Journal of the Science of Food and Agriculture, 100, 5, 2224-2235, 2020. https://doi.org/10.1002/jsfa.10247.

[121] D. X. Cuong. Antioxidant nano phlorotannin powder from brown algae sargassum serratum: spray drying, antioxidant activities, physic-chemical characterization. Journal of Pharmaceitucal Research International, 32, 9, 71-85, 2020. https://doi.org/10.9734/JPRI/2020/v32i930484.

[122] A. F. McDonagh, L. Tajber. The control of paracetamol particle size and surface morphology through crystallisation in a spray dryer. Advanced Powder Technology, 31, 1, 287-299, 2020. https://doi.org/10.1016/j.apt.2019.10.021.

[123] M. J. Rodriguez-Roque, B. De Ancos, R. Sanchez-Vega, C. Sanchez-Moreno, P. Elez-Martinez, O. Martin-Belloso. In vitro bioaccessibility of isoflavones from a soymilk-based beverage as affected by thermal and non-thermal processing. Innovative Food Science & Emerging Technologies, 66, 2020. https://doi.org/10.1016/j.ifset.2020.102504.

[124] D. A. Turker, M. G. Sarac, M. Dogan. Influence of sucrose reduction and starch type on bulk and powder properties of ready-to-use powdered dessert. European Food Research International, 247, 2, 453-464, 2020. https://doi.org/10.1007/s00217-020-03638-1.

[125] G. H. Jiang, Z. G. Wu, K. Ameer, S. J. Li, K. Ramachandraiah. Particle size of ginseng (Panax ginseng Meyer) insoluble dietary fiber and its effect on physicochemical properties and antioxidant activities. Applied Biological Chemistry, 63, 1, 2020. https://doi.org/10.1186/s13765-020-00558-2.

[126] N. Savlak, B. Turker. Particle size affects physical properties and antioxidant activity of unripe banana peel. Fresenius Environmental Bulletin, 29, 3, 1677-1685, 2020.

[127] S. H. Bryngelson, T. Colonius, R. O. Fox. QBMMlib: A library of quadrature-based moment methods. Softwarex, 12, 2020. https://doi.org/10.1016/j.softx.2020.100615.

[128] G. L. Li, C. J. Li, J. Wang, N. N. Xia, X. L. Chen. Study on growth and change of solid particles with water flow in oilfield water-injection pipeline. Tehnicki Vjesnik-Technical Gazette, 27, 3, 996-1005, 2020. https://doi.org/10.17559/TV-20191129074559.

[129] A. Das, A. Buck, J. Kumar. Original Research Paper Selection function in breakage processes: PBM and Monte Carlo modeling. Advanced Powder Technology, 31, 4, 1457-1469, 2020. https://doi.org/10.1016/j.apt.2020.01.002.

[130] R. Durr, A. Buck. Approximate moment methods for population balance equations in particulate and bioengineering processes. Processes, 8, 4, 2020. https://doi.org/10.3390/pr8040414.

[131] B. Kong, R. O. Fox. A moment-based kinetic theory model for polydisperse gas-particle flows. Powder Technology, 365, 92-105, 2020. https://doi.org/10.1016/j.powtec.2019.04.031.

[132] L. Y. Zhang, J. W. Su, Y. Huang, Q. Y. Wang, R. J. Zhang, Y. F. Wu, Y. Zhang, Y. Cheng, Y. P. He, S. Lee, C. Yu, Z. L. Gu. Examining the physical and chemical contributions to size spectrum evolution during the development of hazes. Scientific Reports, 10, 1, 2020. https://doi.org/10.1038/s41598-020-62296-1.

[133] A. Passalacqua, F. Laurent, R. O. Fox. A second-order realizable scheme for moment advection on unstructured grids. Computer Physics Communications, 248, 2020. https://doi.org/10.1016/j.cpc.2019.106993.

[134] S. W. Hu, X. H. Liu. A CFD-PBM-EMMS integrated model applicable for heterogeneous gas-solid flow. Chemical Engineering Journal, 383, 2020. https://doi.org/10.1016/j.cej.2019.123122.

[135] P. F. Hu, L. H. Cao, J. K. Su, Q. Li, Y. Li. Distribution characteristics of salt-out particles in steam turbine stage. Energy, 192, 2020. https://doi.org/10.1016/j.energy.2019.116626.

[136] F. P. Santos, P. L. C. Lage, J. L. Favero, I. Senocak. GPU-accelerated simulation of polydisperse multiphase flows using dual-quadrature-based moment methods. Canadian Journal of Chemical Engineering, 98, 5, 1211-1224, 2020. https://doi.org/10.1002/cjce.23697.

[137] A. K. Gilfanov, R. R. Salakhov, T. S. Zaripov. Mathematical modeling of the dynamics of inertial polydisperse particles in a vortex flow. Uchenye Zapiski Kazanskogo Universiteta-Seriya Fiziko-Matematicheskie Nauki, 162, 2, 120-136, 2020. https://doi.org/10.26907/2541-7746.2020.2.120-136.

[138] M. Shiea, A. Buffo, M. Vanni, D. Marchisio. Numerical methods for the solution of population balance equations coupled with computational fluid dynamics. Annual Review of Chemical and Biomolecular Engineering, 11, 339-366, 2020. https://doi.org/10.1146/annurev-chembioeng-092319-075814.

[139] Z. Gao, L. Shen, J. Xiao, C. Qing, Q. Song. Use of coal as fuel for chemical-looping combustion with Ni-based oxygen carrier. Ind. Eng. Chem. Res. 47, 23, 9279-9287, 2008. https://doi.org/10.1021/ie800850p.

[140] M. Iggland, H. Leion, T. Mattisson, A. Lyngfelt. Effect of fuel particle size on reaction rate in chemical looping combustion. Chemical Engineering Science, 65, 22, 5841-5851, 2010. https://doi.org/10.1016/j.ces.2010.08.001.

[141] J. Adánez, A. Abad, F. Garcia-Labiano, P. Gayán, L. F. de Diego. Progress in chemical-looping combustion and reforming technologies. Progress in Energy and Combustion Science, 38, 2, 215-282, 2012. https://doi.org/10.1016/j.pecs.2011.09.001.

[142] M. Rydén, P. Moldenhauer, S. Lindqvist, T. Mattisson, A. Lyngfelt. Measuring attrition resistance of oxygen carrier particles for chemical looping combustion with a customized jet cup. Powder Technology, 256, 75-86, 2014. https://doi.org/10.1016/j.powtec.2014.01.085.

[143] A. Nandy, C. Loha, S. Gu, P. Sarkar, M. K. Karmakar, P. K. Chatterjee. Present status and overview of Chemical Looping Combustion technology, 59, 597-619, 2016. https://doi.org/10.1016/j.rser.2016.01.003.

[144] W. Lin, K. Dam-Johansen, F. Frandsen. Agglomeration in bio-fuel fired fluidized bed combustors. Chemical Engineering Journal, 96, 171-185, 2003. https://doi.org/10.1016/j.cej.2003.08.008.

[145] F. Scala. Particle agglomeration during fluidized bed combustion: Mechanisms, early detection and possible countermeasures. Fuel Processing Technology, 171, 31-38, 2018. https://doi.org/10.1016/j.fuproc.2017.11.001.

[146] E. Ghiasi, A. Montes, F. Ferdosian, H. Tran, C. Xu. Bed material agglomeration behavior in a bubbling fluidized bed (BFB) at high temperatures using KCl and K2SO4 as simulated molten ash. International Journal of Chemical Reactor Engineering, 16, 4, 2018. https://doi.org/10.1515/ijcre-2017-0033.

[147] J. D. Morris, S. S. Daood, S. Chilton, W. Nimmo. Mechanisms and mitigation of agglomeration during fluidized bed combustion of biomass: A review. Fuel, 230, 452-473, 2018. https://doi.org/10.1016/j.fuel.2018.04.098.

[148] C. Sevonius, P. Yrjas, D. Lindberg, L. Hupa. Impact of sodium on agglomeration in a laboratory fluidized bed. Fuel, 245, 305-315, 2019. https://doi.org/10.1016/j.fuel.2019.02.034.

[149] C. Sevonius, P. Yrjas, D. Lindberg, L. Hupa. Agglomeration tendency of a fluidized bed during addition of different phosphate compounds. Fuel, 268, 2020. https://doi.org/10.1016/j.fuel.2020.117300.

[150] J. D. Morris, S. S. Daood, W. Nimmo. Agglomeration and the effect of process conditions on fluidized bed combustion of biomasses with olivine and silica sand as bed materials: Pilot-scale investigation. Biomass and Bioenergy, 142, 2020. https://doi.org/10.1016/j.biombioe.2020.105806.

[151] V. Narayan, P. A. Jensen, U. B. Henriksen, P. Glarborg, W. Lin, R. G. Nielsen. Defluidization in fluidized bed gasifiers using high-alkali content fuels. Biomass and Energy, 91, 160-174, 2016. https://doi.org/10.1016/j.biombioe.2016.05.009.

[152] T. Ma, C. Fan, L. Hao, S. Li, W. Song, W. Lin. Biomass-ash-induced agglomeration in a fluidized bed. part 1: experimental study on the effects of a gas atmosphere. Energy Fuels, 30, 8, 6395-6404, 2016. https://doi.org/10.1021/acs.energyfuels.6b00164.

[153] R. Michel, J. Kaknics, E. Bilbao, J. Poirier. The mechanism of agglomeration of the refractory materials in a fluidized-bed reactor. Ceramics International, 42, 2, 2570-2581, 2016. https://doi.org/10.1016/j.ceramint.2015.10.060.

[154] J. Kaknics, R. Michel, J. Poirier. Miscanthus ash transformation and interaction with bed materials at high temperature. Fuel Processing Technology, 141, 2, 178-184, 2016. https://doi.org/10.1016/j.fuproc.2015.08.041.

[155] H. He, X. Ji, D. Boström, R. Backman, M. Öhman. Mechanism of quartz bed particle layer formation in fluidized bed combustion of wood-derived fuels. Energy Fuels, 30, 3, 227-2232, 2016. https://doi.org/10.1021/acs.energyfuels.5b02891.

[156] M. Kuba, H. He, F. Kirnbauer, N. Skoglund, D. Boström, M. Öhman, H. Hofbauer. Mechanism of layer formation on olivine bed particles in industrial-scale dual fluid bed gasification of wood. Energy Fuels, 30, 9, 7410-7418, 2016. https://doi.org/10.1021/acs.energyfuels.6b01522.

[157] H. He, N. Skoglund, M. Öhman. Time-dependent crack layer formation in quartz bed particles during fluidized bed combustion of woody biomass. Energy Fuels, 31, 2, 1672-1677, 2017. https://doi.org/10.1021/acs.energyfuels.6b02980.

[158] H. He, N. Skoglund, M. Öhman. Time-dependent layer formation on K-feldspar bed particles during fluidized bed combustion of woody fuels. Energy Fuels, 31, 11, 12848-12856, 2017. https://doi.org/10.1021/acs.energyfuels.7b02386.

[159] Z. He, D. J. Lane, W. L. Saw, P. J. van Eyk, G. J. Nathan, P. J. Ashman. Ash–Bed Material Interaction during the Combustion and Steam Gasification of Australian Agricultural Residues. Energy Fuels, 32, 4, 4278-4290, 2018. https://doi.org/10.1021/acs.energyfuels.7b03129.

[160] Z. He, W. L. Saw, D. J. Lane, P. J. van Eyk, R. de Nys, G. J. Nathan, P. J. Ashman. The ash-quartz sand interaction behaviours during steam gasification or combustion of a freshwater and a marine species of macroalgae. Fuel, 263, 2020. https://doi.org/10.1016/j.fuel.2019.116621.

[161] P. Ninduangdee, V. I. Kuprianov. A study on combustion of oil palm empty fruit bunch in a fluidized bed using alternative bed materials: Performance, emissions, and time-domain changes in the bed condition. Applied Energy, 176, 34-48, 2016. https://doi.org/10.1016/j.apenergy.2016.05.063.

[162] V. I. Kuprianov, P. Ninduangdee, P. Suheri. Co-firing of oil palm residues in a fuel staged fluidized-bed combustor using mixtures of alumina and silica sand as the bed material. Applied Thermal Engineering, 144, 371-382, 2018. https://doi.org/10.1016/j.applthermaleng.2018.08.089.

[163] Z. He, W. L. Saw, P. J. van Eyk, G. J. Nathan, P. J. Ashman. Effect of calcium and phosphorus on interactions between quartz sand and K-salt-doped wood under both steam gasification and combustion atmospheres. Energy Fuels, 34, 3, 3210-3222, 2020. https://doi.org/10.1021/acs.energyfuels.9b02992.

[164] P. J. van Eyk, A. Kosminski, P. J. Mullinger, P. J. Ashman. control of agglomeration during circulating fluidized bed gasification of a South Australian low-rank coal: pilot scale testing. Energy Fuels, 30, 3, 1771-1782, 2016. https://doi.org/10.1021/acs.energyfuels.5b02267.

[165] G. Lardier, J. Kaknics, A. Dufour, R. Michel, B. Cluet, O. Authier, J. Poirier, G. Mauviel. Gas and bed axial composition in a bubbling fluidized bed gasifier: results with miscanthus and olivine. Energy Fuels, 30, 10, 8316-8326, 2016. https://doi.org/10.1021/acs.energyfuels.6b01816.

[166] J. Shabanian, P. Sauriol, A. Rakib, J. Chaouki. Defluidization prediction and prevention during cocombustion of reengineered feedstock with coal in a bubbling fluidized bed combustor. Energy Fuels, 33, 1603-1621, 2019. https://doi.org/10.1021/acs.energyfuels.8b03875.

[167] J. Shabanian, J. Chaouki. Fluidization characteristics of a bubbling gas-solid fluidized bed at high temperature in the presence of interparticle forces. Chemical Engineering Journal, 288, 344-358, 2016. https://doi.org/10.1016/j.cej.2015.12.016.

[168] X. Yao, K. Xu, F. Yan, Y. Liang. The influence of ashing temperature on ash fouling and slagging characteristics during combustion of biomass fules. BioResources, 12, 1, 1593-1610, 2017.

[169] X. Yao, K. Xu, Y. Liang. Comparative analysis of the physical and chemical properties of different biomass ashes produced from various combustion conditions. BioResources, 12, 2, 3222-3235, 2017. https://doi.org/10.15376/biores.12.2.3222-3235.

[170] J. Shabanian, J. Chaouki. Effects of temperature, pressure, and interparticle forces on the hydrodynamics of a gas-solid fluidized bed. Chemical Engineering Journal, 313, 580-590, 2017. https://doi.org/10.1016/j.cej.2016.12.061.

[171] J. Kaknics, R. Michel, J. Poirier, E. Bilbao. Experimental study and thermodynamic modelling of high temperature interactions between molten miscanthus ashes and bed particles in fluidized bed reactors. Waste and Biomass Valorization, 8, 2771–2790, 2017. https://doi.org/10.1007/s12649-017-9828-x.

[172] B. Gattering, J. Karl. Application of chemical equilibrium calculations for the prediction of ash-induced agglomeration. Biomass Conv. Bioref. 9, 117–128, 2019. https://doi.org/10.1007/s13399-018-0325-7.

[173] T. Jimenez, C. Turchiuli, E. Dumolin. Particles agglomeration in a conical fluidized bed in relation with air temperature profiles. Chemical Engineering Science, 61, 18, 5954-5961, 2006. https://doi.org/10.1016/j.ces.2006.05.007.

[174] C. Turchiuli, Z. Eloualia, N. El Mansouri, E. Demoulin. Fluidised bed agglomeration: Agglomerates shape and end-use properties. Powder Technology, 157, 1-3, 168-175, 2005. https://doi.org/10.1016/j.powtec.2005.05.024.

[175] K. L. Clarke, T. Pugsley, G. A. Hill. Fluidization of moist sawdust in binary particle systems in a gas-solid fluidized bed. Chemical Engineering Science, 60, 24, 6909-6918, 2005. https://doi.org/10.1016/j.ces.2005.06.004.

[176] G. M. Walker, G. Andrews, D. Jones. Effect of process parameters on the melt granulation of pharmaceutical powders. Powder Technology, 165, 3, 161-166, 2006. https://doi.org/10.1016/j.powtec.2006.03.024.

[177] P. Gayán, I. Adanéz-Rubio, A. Abad, L. F. de Diego, F. García-Labiano, J. Adánez. Development of Cu-based oxygen carriers for Chemical-Looping with Oxygen Uncoupling (CLOU) process. Fuel, 96, 226-238, 2012. https://doi.org/10.1016/j.fuel.2012.01.021.

[178] M. Zevenhoven-Onderwater, R. Backman, B. J. Skrifvars, M. Hupa. The ash chemistry in fluidised bed gasification of biomass fuels. Part I: predicting the chemistry of melting ashes and ash-bed material interaction. Fuel, 80, 10, 1489-1502, 2001. https://doi.org/10.1016/S0016-2361(01)00026-6.

[179] K. O. Davidsson, L. E. Amand, B. M. Steenari, A. L. Elled, D. Eskilsson, B. Leckner. Countermeasures against alkali-related problems during combustion of biomass in a circulating fluidized bed boiler. Chemical Engineering Science, 63, 21, 5314-5329, 2008. https://doi.org/10.1016/j.ces.2008.07.012.

[180] S. Watano, Y. Sato, K. Miyanami. Optimization and validation of an image processing system in fluidized bed granulation. Advanced Powder Technology, 8, 4, 269-277, 1997. https://doi.org/10.1016/S0921-8831(08)60600-7.

[181] P. Frake, D. Greenhalgh, S. M. Grierson, J. M. Hempenstall, D. R. Rudd. Process control and end-point determination of a fluid bed granulation by application of near infra-red spectroscopy. International Journal of Pharmaceutics, 151, 1, 75-80, 1997. https://doi.org/10.1016/S0378-5173(97)04894-1.

[182] S. G. Goebel, K. J. Steffens. Online-measurement of moisture and particle size in the fluidized-bed processing with the near-infrared spectroscopy. Pharm. Ind. 60, 889-895, 1998.

[183] W. P. Findlay, G. R. Peck, K. R. Morris. Determination of fluidized bed granulation end point using near-infrared spectroscopy and phenomenological analysis. Journal of Pharmaceutical Sciences, 94, 604-612, 2005. https://doi.org/10.1002/jps.20276.

[184] A. Tok, X. P. Goh, W. Ng, R. Tan. Monitoring granulation rate process using three Pat tools in a pilot-scale fluidized bed. AAPS PharmSciTech, 9, 1038-1091, 2008. https://doi.org/10.1208/s12249-008-9145-6.

[185] M. R. Parise, O. P. Taranto, P. R. G. Kurka, L. B. Benetti. Detection of the minimum gas velocity region using Gaussian spectral pressure distribution in a gas-solid fluidized bed. Powder Technology, 182, 3, 453-458, 2008. https://doi.org/10.1016/j.powtec.2007.07.014.

[186] S. Watano, Y. Sato, K. Miyanami. Control of granule growth in fluidized bed granulation by an image processing system. Chemical and pharmaceutical Bulletin, 44, 8, 1556-1560, 1996. https://doi.org/doi.org/10.1248/cpb.44.1556.

[187] S. Watano, T. Numa, K. Miyanami, Y. Osako. On-line monitoring of granule growth in high shear granulation by an image processing system. Chemical and Pharmaceutical Bulletin, 48, 1154-1159, 2000. https://doi.org/10.1248/cpb.48.1154.

[188] S. Watano. Direct control of wet granulation process by image processing system. Powder Technology, 117, 163-172, 2001. https://doi.org/10.1016/S0032-5910(01)00322-9.

[189] M. Halstensen, P. Bakker, K. H. Esbensen. Acoustic chemometric monitoring of an industrial granulation production process - a PAT feasibility study. Chemometrics and Intelligent Laboratory Systems, 84, 1-2, 88-97, 2006. https://doi.org/10.1016/j.chemolab.2006.05.012.

[190] N. Naelapää, P. Veski, J. G. Pederson, D. Anov, P. Jørgensen, H. G. Kristersen, P. Bertelsen. Acoustic monitoring of a fluidized bed coating process. International Journal of Pharmaceutics, 332, 1-2, 90-97, 2007. https://doi.org/10.1016/j.ijpharm.2006.09.036.

[191] H. Tsujimoto, T. Yokoyama, C. C. Huang, I. Sekiguchi. Monitoring particle fluidization in a fluidized bed granulator with an acoustic emission sensor. Powder Technology, 113, 1-2, 88-96, 2000. https://doi.org/10.1016/S0032-5910(00)00205-9.

[192] L. Briens, M. Bojarra. Monitoring fluidizing bed drying of pharmaceutical granules. AAPS PharmSciTech, 11, 4, 1612-1618, 2010. https://doi.org/10.1208/s12249-010-9538-1.

[193] S. Matero, S. Poutiainen, J. Leskinen, K. Järvinen, J. Ketolainen, S. P. Reinikainen, M. Hakulinen, R. Lappalainen, A. Poso. The feasibility of using acoustic emissions for monitoring of fluidized bed granulation. Chemometrics and Intelligent Laboratory Systems, 97, 1, 75-81, 2009. https://doi.org/10.1016/j.chemolab.2008.11.001.

[194] G. Chaplin, T. Pugslay. Application of electrical capacitance tomography to the fluidized bed drying of pharmaceutical granule. Chemical Engineering Science, 60, 24, 7022-7033, 2005. https://doi.org/10.1016/j.ces.2005.06.029.

[195] D. Petrak. Simultaneous measurement of particle size and particle size velocity by the Spatial Filtering Technique. Particle & Particle systems Characterization, 19, 6, 391-400, 2002. https://doi.org/10.1002/ppsc.200290002.

[196] S. Schmidt-Lehr, H. U. Moritz, K. C. Jürgens. Online control of particle size during fluidized bed granulation. Pharm. Ind., 69, 4, 478-484, 2007.

[197] T. Närvänen, T. Lipsanen, O. Antikainen, H. Räikkönen, J. Yliruusi. Controlling granule size by granulation liquid feed pulsing. International Journal of Pharmaceutics, 357, 132-138, 2008. https://doi.org/10.1016/j.ijpharm.2008.01.060.

[198] H. Ehlers, A. Liu, H. Räikkönena, J. Hataraa, O. Antikainema, J. Heinämäkia, H. Loub, J. Yliruusi. Granule size control and targeting in pulsed spray fluid bed granulation. International Journal of Pharmaceutics, 377, 1-2, 9-15, 2009. https://doi.org/10.1016/j.ijpharm.2009.04.041.

[199] A. Burggraeve, T. van der Kerkhof, M. Hellings, J. P. Remon, C. Vervaet, T. de Beer. Evaluation of in-line spatial filter velocimetry as PAT monitoring tool for particle growth during fluid bed granulation. European Journal of Pharmaceutics and Biopharmaceutics, 76, 1, 138-146, 2010. https://doi.org/10.1016/j.ejpb.2010.06.001.

[200] P. Dieter, D. Stefan, E. Gunter, K. Michael. In-line particle sizing for real-time process control by fibre-optical spatial filtering technique (SFT). Advanced Powder Technology, 22, 2, 203-208, 2011. https://doi.org/10.1016/j.apt.2010.11.002.

[201] G. Walker, S. E. J. Bell, M. Vann, D. S. Jones, G. Andrews. Fluidised bed characterisation using Raman spectroscopy: Applications to pharmaceutical processing. Chemical Engineering Science, 62, 14, 3832-3838, 2007. https://doi.org/10.1016/j.ces.2007.04.017.

[202] X. Hu, J. C. Cunningham, D. Winstead. Study growth kinetics in fluidized bed granulation with at-line FBRM. International Journal of Pharmaceutics, 347, 54-61, 2008. https://doi.org/10.1016/j.ijpharm.2007.06.043.

[203] C. Buschmüller, W. Wiedey, C. Doscher, J. Dressler, J. Breitkreutz. In-line monitoring of granule moisture in fluidized-bed dryers using microwave resonance technology. European Journal of Pharmaceutics and Biopharmaceutics, 69, 1, 380-387, 2008. https://doi.org/10.1016/j.ejpb.2007.09.014.

[204] F. Portoghese, F. Berruti, C. Briens. Use of triboelectric probes for on-line monitoring of liquid concentration in wet gas-solid fluidized beds. Chemical Engineering Science, 60, 22, 6043-6048, 2005. https://doi.org/10.1016/j.ces.2005.03.042.

[205] W. Brennan, M. Jacobson, G. Book, C. Briens, L. Briens. Development of a triboelectric procedure for the measurement of mixing and drying in a vibrated fluidized bed. Powder Technology, 181, 2, 178-185, 2008. https://doi.org/10.1016/j.powtec.2006.12.002.

[206] S. H. Schaafsma, P. Vonk, N. W. F. Kossen, A. C. Hoffmann. A model for the spray zone in early-stage fluidized bed granulation. AIChE Journal, 52, 8, 2736-2741, 2006. https://doi.org/10.1002/aic.10864.

[207] F. Depypere, J. G. Pieters, K. Dewettinck. PEPT visualization of particle motion in a tapered fluidized bed coater. Journal of Food Engineering, 93, 3, 324-336, 2009. https://doi.org/10.1016/j.jfoodeng.2009.01.042.

CHAPTER III

A new approach to the mechanisms of agglomeration in fluidized beds based on Spatial Filter Velocimetry measurements

Nascimento, R.F.; Ávila, M.F.; Taranto, O.P.; Kurozawa, L.E.

A new approach to the mechanisms of agglomeration in fluidized beds based on Spatial Filter Velocimetry measurements

Raul F. Nascimento[a], Mariana F. Ávila[b], Osvaldir P. Taranto[b], Louise Emy Kurozawa[a]

[a]Department of Food Engineering, School of Food Engineering, University of Campinas, Monteiro Lobato St. 80, Campinas, SP, Brazil

[b]Department of Process Engineering, School of Chemical Engineering, University of Campinas, Albert Einstein Ave. 500, Campinas, SP, Brazil

HIGHLIGHTS

- *D50v* and PSD increase due to high binder concentration.
- SFV probe provides particle chord length throughout the agglomeration process.
- Particle size classes delimit the agglomeration steps.
- The SFV measurements and particle size classes determine a new approach to agglomeration.

ABSTRACT

Spatial Filter Velocimetry (SFV) is a technique that has been used for agglomeration processes during the past few years as it can monitor, control, and understand granulation and its implications in particle size distribution. This work has considered and aimed to analyze the evolution of the process as time goes on and in real-time and the influence of operating conditions on the process. A Plackett-Burman design was proposed with seven factors and three replicates at the central point condition, using microcrystalline cellulose (CMC) as the raw material and a maltodextrin solution as a liquid binder. Binder concentration, binder flow rate, powder initial moisture content, and fluidizing air temperature were significant at a 90% confidence level. A new approach was proposed for delimiting the stages of the fluidized bed agglomeration process, based on particle size classes that were obtained from the SFV probe data.

Keywords: Fluidization; Particle size classes; Wetting; Nucleation; Coalescence; Stabilization.

3.1. INTRODUCTION

The agglomeration process can be defined as the transformation of fine particles into agglomerated particles. It is widely utilized in food, chemical, and pharmaceutical industries for producing instant products. This process consists of pulverizing binder liquid onto a fluidized bed of particles, whereas after wetting, the particles will be united by liquid bridges. Depending on the type of binder, the liquid bridge can solidify by cooling, or dry by heating in order to form a solid bridge [1], causing increased particle size. The particle size enlargement provides improved flowability and appearance and facilitates transport and storage [2,3]. The characteristics are more precisely and closely related to the fluidized bed agglomeration process that depends on solid particulate properties and operating parameters, and binder solution features. These factors influence heat and mass transfer mechanisms between the fluid and the particles and, consequently, operational success [4].

Agglomeration depends on numerous variables as it is a complex process. Properties of the equipment, the particles, and the binding liquid can interfere with particle growth and the success of the agglomeration operation. The most important aspects are mechanical properties, air temperature, and humidity [5]. Parameters such as size and shape of the agglomeration chamber, air distributor, and type and position of the atomizing nozzle impact the operational parameters of particle load, flow, and temperature of the fluidizing air, binder liquid flow, and drop size, respectively. Such parameters directly reflect the agglomerated product properties such as composition, particle size, density, composition, and the sprayed liquid temperature [5,6]. Additionally, other factors should be considered in the fluidized bed agglomeration process are binder solution and concentration flow, atomization pressure, temperature and flow of the fluidizing air, and relative humidity within the bed [7–9].

Tan et al. [1] reported a limitation on the knowledge of agglomeration rates, granulation kinetics, and quantification of growth behavior submitted to different operational conditions. Nevertheless, some authors have made efforts to minimize this limitation. Cronin et al. [10] also affirmed that predict about the process is not possible due to the lack of understanding about granulation kinetics, which in turns it is related to the complex network of micro-processes that occur in series and in parallel during fluidized bed agglomeration. These authors developed a model for the time-dependent component applicable to fluidized bed agglomeration with continuous addition of liquid binder. Terrazas-Velarde et al. [11] reported how the agglomerates are formed, by means the model based on the single micro-level interactions between primary particles and liquid droplets, such as droplet capture, continuous

binder addition, deposited binder drying, equilibrium between agglomeration and rebound, and rupture. Their results summarize that under the conditions analyzed, the micro-scale approach was a favorable manner to comprehend the agglomerate formation through simulation. Villa et al. [12] evaluated the final particle size distribution (PSD) curves and the growth behavior to predict the coating and agglomeration regimes, first by mathematical modelling, and then by dimensionless analysis. Results such as these can be useful and serve as a basis for inquiries regarding agglomeration rates, granulation kinetics and fluidized bed granule growth behavior.

The knowledge of agglomeration kinetics becomes necessary as the agglomeration process targets particle size growth. The Spatial Filter Velocimetry (SFV) is an in-line particle size technique monitoring that displays both granule growth and breakage as a function of granulation time based on the measurement of the particle chord lengths. This technique is a relatively new method, and it has been successfully used in recent studies [13–15]. SFV is similar to the focused beam reflectance measurement (FBRM). Both use granule size expressed in chord length distribution [13], FBRM by backscattered light, and SFV by generated shadow. Particle size monitoring during the fluidized bed process has proven that SFV has been considered a significant, robust, and efficient technique compared to others [13,14,16,17].

There have been several reviews on the use of techniques such as SFV for monitoring, controlling, and understanding granulation and its implications; those were for evaluating PSD and fluidization regimes [16–19] performed during the past decade. PSD is a critical parameter to determine product quality related to moisture content, drying behavior, solubility, and the establishment of agglomerates [20]. In those cases, SFV particle size monitoring could improve knowledge on what favored increased particle size or breakage, providing relevant information for the study of granulation kinetics.

Although these studies have used the SFV probe as a tool for monitoring and controlling the agglomeration process, none of them has analyzed the data obtained during the process to evaluate the particulate growth or the evolution of PSD. Thus, this work has aimed to analyze the data obtained from the SFV probe in a set of executed experiments in a fluidized bed agglomeration process. Firstly, this shows the evolution of the process over time and the influence of operating conditions. Secondly, it verifies the efficiency of the SFV probe as a tool for real-time monitoring of this process. Finally, it proposes a new approach for delimiting the stages of the fluidized bed agglomeration process based on particle size classes.

3.2. MATERIAL AND METHODS

3.2.1. Material

Microcrystalline cellulose (CMC) (Microcel®, Blanver Farmoquímica, Brazil) was used as the raw material. Its moisture content and density were 7.28 ± 0.05% and 1.5485 ± 0.0010 g/cm^3, respectively. The particle size was measured by laser diffraction (Mastersizer S, Malvern Instruments, Germany) and represented by *D10v*, *D50v*, and *D90v* percentiles, was 119.8 ± 9.0, 290.2 ± 6.6, and 517.8 ± 8.5 μm, respectively.

Maltodextrin (MOR-REX® 1910, Ingredion, USA) is a binder solution used for the agglomeration process. Distilled water and maltodextrin both were subjected to magnetic stirring until completely dissolved and prepared at room temperature of around 27 °C. Binder solution concentration varied according to the experimental design (Table 3.1).

Table 3.1: Levels and results of Plackett-Burman experimental design.

Run	*Independent variables*							*Response*
	C	*Q*	*T*	*v*	*M*	*P*	*H*	*D50v*
1	35.0(+1)	1.0(−1)	90(+1)	0.12(−1)	5.3(−1)	10(−1)	0.4(+1)	442.2
2	35.0(+1)	4.0(+1)	60(−1)	0.26(+1)	5.3(−1)	10(−1)	0.3(−1)	479.4
3	5.0(−1)	4.0(+1)	90(+1)	0.12(−1)	7.3(+1)	10(−1)	0.3(−1)	338.5
4	35.0(+1)	1.0(−1)	90(+1)	0.26(+1)	5.3(−1)	20(+1)	0.3(−1)	439.4
5	35.0(+1)	4.0(+1)	60(−1)	0.26(+1)	7.3(+1)	10(−1)	0.4(+1)	495.4
6	35.0(+1)	4.0(+1)	90(+1)	0.12(−1)	7.3(+1)	20(+1)	0.3(−1)	501.2
7	5.0(−1)	4.0(+1)	90(+1)	0.26(+1)	5.3(−1)	20(+1)	0.4(+1)	360.7
8	5.0(−1)	1.0(−1)	90(+1)	0.26(+1)	7.3(+1)	10(−1)	0.4(+1)	355.7
9	5.0(−1)	1.0(−1)	60(−1)	0.26(+1)	7.3(+1)	20(+1)	0.3(−1)	350.7
10	35.0(+1)	1.0(−1)	60(−1)	0.12(−1)	7.3(+1)	20(+1)	0.4(+1)	514.8
11	5.0(−1)	4.0(+1)	60(−1)	0.12(−1)	5.3(−1)	20(+1)	0.4(+1)	359.9
12	5.0(−1)	1.0(−1)	60(−1)	0.12(−1)	5.3(−1)	10(−1)	0.3(−1)	345.0
13	25.0(0)	2.5(0)	75(0)	0.19(0)	6.3(0)	15(0)	0.35(0)	393.5
14	25.0(0)	2.5(0)	75(0)	0.19(0)	6.3(0)	15(0)	0.35(0)	386.8
15	25.0(0)	2.5(0)	75(0)	0.19(0)	6.3(0)	15(0)	0.35(0)	376.6

The independent variables correspond to the real values. Values enclosed parentheses correspond to the coded values. *C* is binder concentration (% w/w); *Q* is binder flow rate (mL/min); *T* is fluidizing air temperature (°C); *v* is fluidizing air velocity (m/s); *M* is powder initial moisture content (%); *P* is atomizing pressure (Psi); *H* is nozzle height (m); *D50v* is the median particle size in volume (μm).

3.2.2. Fluidized bed agglomeration process

The agglomeration experiments were carried out in a lab-scaled fluidized bed. Andreola et al. [21] and Rosa et al. [22] describe the details of the equipment and the data acquisition system. The fluidized bed-chamber was composed of a conical base (0.075 m inlet air diameter and 0.15 m of height) and a cylindrical column (0.15 m diameter and 0.60 m height), both constructed from transparent acrylic Plexiglass®. The experimental apparatus and the position of the Parsum probe in the bed-chamber can be observed in Nascimento et al. [23].

The temperature data was collected using a thermoresistance (PT100, Novus, Brazil) installed in the conical part of the bed-chamber, just above the distribution plate. The relative humidity was also measured using a thermos-hygrometer sensor (RHT-XS, Novus, Brazil) placed at the top position of the bed-chamber. The pressure drop was measured by a differential pressure transmitter (98073-12, Cole Parmer, USA) based on the difference between the pressures at two positions: near the inlet air at the bottom of the conical chamber and outside of the bed-chamber (atmospheric pressure). Data was collected every 5.12 seconds and sent to the LabVIEW™ 8.6 software.

3.2.3. Plackett-Burman experimental design

According to a Plackett-Burman design, the experimental runs were performed based on seven factors with three replicates at the central point condition. There was a total of 15 trials (Table 3.1). The following interval levels were used as independent variables as follows: binder concentration (C) from 5% to 35% (w/w); binder flow rate (Q) from 1.0 to 4.0 mL/min; fluidizing air temperature (T) from 60 to 90 °C; fluidizing air velocity (v) from 0.12 to 0.26 m/s; powder initial moisture content (M) from 5.3% to 7.3%; atomizing pressure (P) from 10 to 20 Psi; and nozzle height (H) from 0.3 to 0.4 m. The minimum fluidization air velocity was 0.07 m/s, captured from the bed pressure drop measurement as a function of the air velocity, which did not undergo binder atomization. The experimental response (dependent variable) was the *D50v* percentile. The execution time of each experiment (20, 32, and 80 min) varied according to the binder flow rate to keep the amount of liquid constant at 80 mL. 0.4 kg of raw material was established in preliminary tests for each assay. The analysis of variance (ANOVA) was carried out using the Statistica 7.0 software (StatSoft, Tusla, USA).

3.2.4. SFV probe measurements

The in-line particle size was monitored by the SFV probe (Parsum IPP 70S, Chemnitz, Germany). According to Langner et al. [24], the SFV probe measures the particle velocity (v_p) from the frequency of the burst signal (f_0) and the distance between the two optical fibers (g). Furthermore, a t_p duration pulse signal is generated from another single fiber as diameter d. The particle size (x_p), defined by chord length, is calculated using the direct relations in Eq. (3.1) and (3.2) [24].

$$v_p = f_0 \times g \tag{3.1}$$

$$x_p = t_p \times v_p - d \tag{3.2}$$

Silva and Taranto [14] and Andreola et al. [21] describe equipment details, accessories, and methodology. The system recorded the particle size and PSD every 5.12 seconds, and data was sent to the LabVIEW™ 8.16 software via OPC Server protocol, developed by Silva and Taranto [14]. According to preliminary tests (data not shown) and Silva and Taranto [14], 2,000 particles were used as the ring buffer size in the SFV probe measurements. The median particle size in volume ($D50v$) was evaluated throughout the agglomeration process, whereas the last ten measurements for each run (Table 3.1) were used to calculate the $D50v$ agglomerated mean.

The size measurement validation was done by comparing the data obtained from the SFV probe and laser diffraction for the raw material without binder atomization. A similar validation was performed by Silva and Taranto [14], Andreola et al. [21], and Rosa et al. [22].

Moreover, information on particle diameter and PSD was collected by the SFV probe and data was displayed according to the Tyler sieves. The retained fractions (% volume) were measured for the particle diameter and recorded over time for the following particle size classes: class I corresponds to fines ($D50v < 300$ μm), class II to intermediate (300 μm $\leq D50v < 600$ μm), and class III to coarse ($D50v \geq 600$ μm). The retained fraction was analyzed for PSD by the relative particle amount based on the size of each experimental run. The PSD curve evolution was evaluated compared to the processing time in the same run. Those curves were plotted considering the moving average from fifteen results to avoid more significant data fluctuations and make the trend line more evident.

3.3. RESULTS AND DISCUSSION

3.3.1. Fluid dynamics behavior

The fluid dynamics behavior of CMC was similar to the theoretical curve of the pressure drop as a function of air velocity, probably because CMC is classified as Geldart group B, i.e., during fluidization, there is bubble formation since the air velocity exceeds the minimum fluidizing air velocity [25]. The experimental minimum fluidizing air velocity is estimated by comparing the maximum pressure drop reached before the linear behavior in the pressure drop profile.

Figure 3.1 displays the bed pressure drop as a function of the air velocity increased and decreased curves. The pressure drop increased as the air velocity increased until it reached the maximum pressure drop (384 Pa). After that, the homogeneous behavior was visually observed, and even though there was an air velocity increase, the pressure drop demonstrated slight variation, oscillating around 300 Pa. Thus, the minimum fluidizing air velocity was selected as the corresponding velocity for the peak pressure drop, 0.07 m/s (marked in Figure 3.1 by a dotted line). According to the experiment design levels, the fluidization velocity was kept above the minimum fluidization velocity so that defluidization would not occur during experimental runs, according to the experiment design levels (Table 3.1).
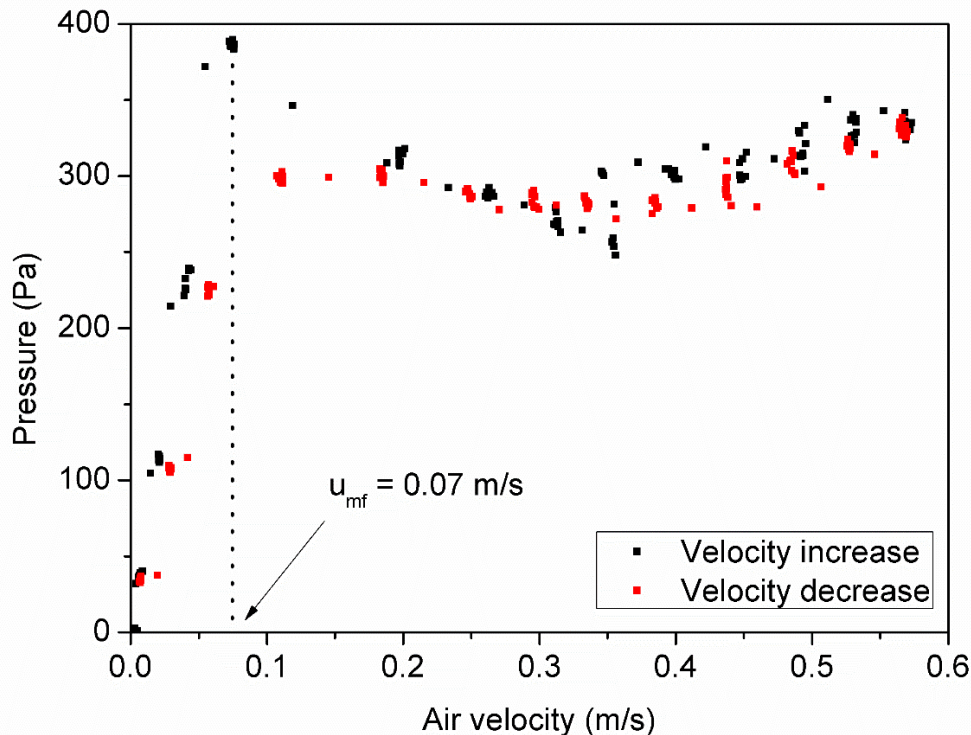
Figure 3.1: Bed pressure drop as a function of air velocity during fluidization of CMC.

3.3.2. Plackett-Burman experimental design

The effect of binder concentration (C), binder flow rate (Q), fluidizing air temperature (T), fluidizing air velocity (v), powder initial moisture content (M), atomizing pressure (P), and nozzle height (H) (independent variables) on agglomeration process was evaluated according to the Plackett-Burman experimental design levels (Table 3.1).

The *D50v* percentile varied from 338.5 to 514.8 μm (Table 3.1). Analysis of variance (ANOVA) showed that the levels C, M, T, and Q were statistically significant at a 90% confidence level to the D50v response. The coefficient of determination (R^2) representing the experimental data fitting was 93.4%.

Table 3.2 shows the coded results of the experimental design for the *D50v* response. Binder concentration (C) made the highest impact on the response, followed by the M, T, and Q factors. Moreover, this parameter positively affected particle size, indicating that an increase in concentration level provided an increase in particle size. Since higher C suggests a greater amount of solids in the binder solution, this fact may have favored the particle agglomeration process [7–9,15,26]. M and Q also had a positive influence, meaning that wetter particles tend to reach larger diameters at the end of the process [27]; T, in turn, caused an opposite effect, whereas the increase of T decreased *D50v*. Higher binder flow rate and lower temperatures favor the formation of the wetting-active zone, allowing more particles to penetrate this area and have their surface wetted by liquid binder droplets. This phenomenon favors agglomeration, leading to larger and heavier particles and preventing elutriation [28].

Table 3.2: Coded results of the design of experiments for the response *D50v*.

Factor	Effect	p-value
Mean/Intercept	409.320	~0.000
Binder concentration (C)	126.983	0.002
Powder initial moisture content (M)	21.617	0.048
Fluidizing air temperature (T)	−17.917	0.068
Binder flow rate (Q)	14.550	0.098
Nozzle height (H)	12.417	NS
Atomizing pressure (P)	11.750	NS
Fluidizing air velocity (v)	−3.383	NS

NS: non-significant ($p > .10$).

Two experimental runs were selected and compared in each case to exhibit the effect of the significant variables on PSD. For example, the analysis of the binder concentration, run 2 and run 11 were executed with significant effects (*M*, *T*, and *Q*) constant at the same levels; the *C* effect changed its levels from +1 to –1. The same was adopted to verify the effect of *M* and *T*. In the case of the *Q* effect analysis, there were not only two experimental runs in which only the *Q* factor changed. Then, runs 1 and 2 were chosen wherein the *T* factor also varied, which was the second less significant factor.

The binder concentration displayed a more noticeable effect by analyzing the PSD curves (Figure 3.2 (a)). The curves are located in unequal positions and are shaped differently, indicating the median particle sizes are distinct in these two experimental runs. The PSD curves for the other significant factors are similar (Figure 3.2 (b)–(d)), indicating that despite these factors are significant, their importance is much less than the concentration.
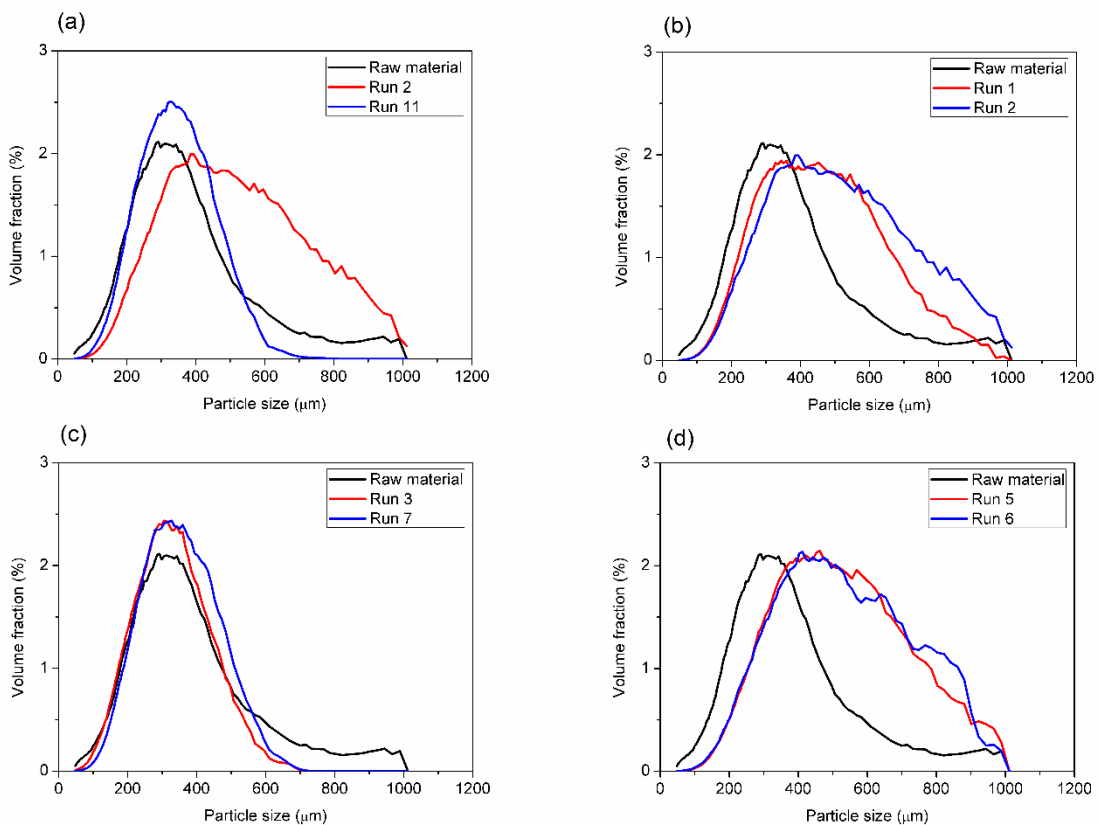
Figure 3.2: Effect of (a) binder solution concentration (level +1: run 2; level –1: run 11); (b) binder solution flow rate (level +1: run 2; level –1: run 1); (c) initial moisture content (level +1: run 3; level –1: run 7); (d) fluidizing air temperature (level +1: run 6; level –1: run 5) on particle size distribution.

Tan et al. [1] describe some mechanisms summarizing what occurs in the agglomeration process in a fluidized bed regarding the operating parameter evaluation. According to the proposed theory, the binder droplets touch solid particles and wet them in a region inside a column named the spray zone. Up to now, this mechanism has been governed by liquid binder properties and the operating variables linked to it, such as concentration and flow rate. According to Du et al. [29], a higher concentration provides a more viscous liquid. When it touches the solid particle, it can form a viscous liquid layer around the particle. The increased concentration makes the binder solution stickier. This binder layer can dissipate the kinetic energy of particle-particle collisions, favoring the formation of agglomerates through larger and stronger solid bridges [30].

The influence of temperature is more remarkable when switching to the binder solidification step as the solid bridge formation is related to water evaporation. However, if the agglomerate is dried and the bonds are not strong enough, solid bridges will likely weaken and rupture [1]. Dadkhah and Tsotsas [30] and Du et al. [29] confirm that fact by stating that temperature has an opposite influence on size enlargement since higher temperatures cause binder evaporation just after the drops emerge from the atomizing nozzle and reduce the size of the droplets previously placed on the solid particle surface. The probability of a droplet to wet and make a footprint on a solid particle surface at higher temperature is smaller than at a lower temperature.

3.3.3. SFV probe measurements

3.3.3.1. Validation of size results

SFV probe measurements were obtained without binder atomization that maintained the fluidization regime in stable conditions. The SFV probe measured the CMC values compared with those determined by laser diffraction (LD), as Silva and Taranto [14], Andreola et al. [21], and Rosa et al. [22] had already done using the same probe as used in this current work. This validation was performed to verify whether the particle size from the SFV probe corresponded to that obtained by LD, first for the raw material and then the agglomerates. Table 3.3 shows the comparison between the $D10v$, $D50v$, and $D90v$ percentiles in both techniques, and Figure 3.3 shows the cumulative curves in each case. These curves are similar, although the data in Table 3.3 were statistically different. That difference is mainly due to the measurement of the particles in each technique as the SFV probe measures the size of the chord,

which is a set of distances between the center of gravity of the particle and the edge. In contrast, the LD technique measures the particle volume and compares that to the size of a sphere with the same volume [31].

Table 3.3: Particle size measured in-line by SFV probe and off-line by laser diffraction for the raw material.

Technique	*D10v* (μm)	*D50v* (μm)	*D90v* (μm)
Laser diffraction	119.8 ± 9.0[a]	290.2 ± 6.6[a]	517.8 ± 8.5[a]
SFV	185.2 ± 12.7[b]	329.7 ± 13.3[b]	486.4 ± 23.2[b]

Data are expressed as mean ± standard deviation. Values in a column with the same letter were not significantly different (p < .05) according to Tukey's test.
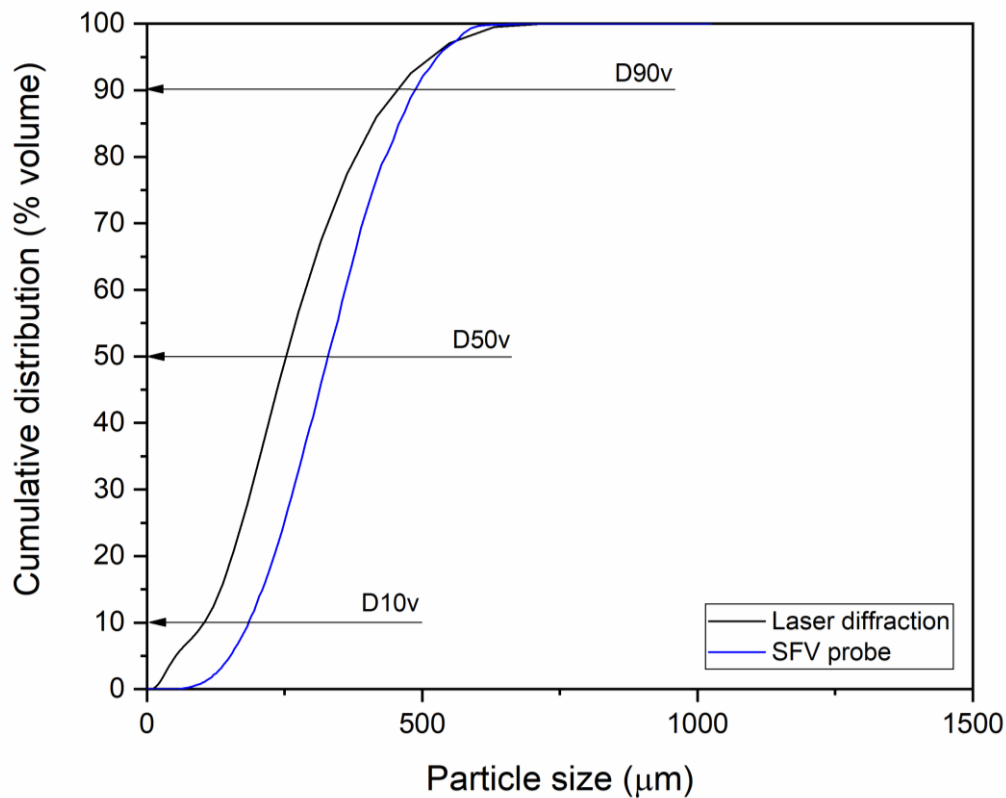
Figure 3.3: Comparison between cumulative curves obtained by laser diffraction (black line) and SFV probe (blue line).

All the Plackett-Burman experimental designs had their percentiles compared to these two techniques. Figure 3.4 shows a strong correlation of *D50v* and *D90v* percentiles between both methods (R^2 = 0.92 and 0.90, respectively), and a fair correlation for *D10v* (R^2 =

0.71). It confirms the SFV probe is suitable for in-line agglomeration measures in fluidized bed processes, corroborating what has already been reported by Langner et al. [24].
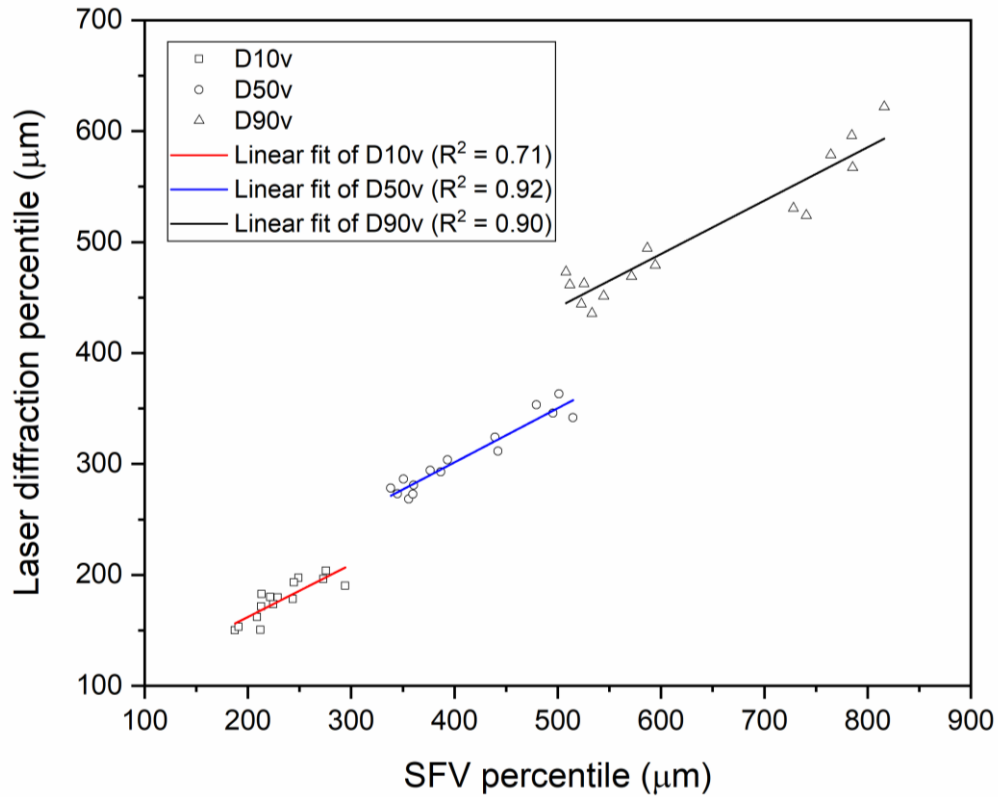
Figure 3.4: Laser diffraction percentiles versus SFV probe at the end of the process for all 15 batches in the experimental design.

3.3.3.2. Particle growth and growth kinetics

The particle growth kinetics for each run of the Plackett-Burman experimental design (Table 3.1) is shown in Figure 3.5. According to binder flow rates, the runs were carried out for 20, 32, and 80 min, since the same amount of inserted liquid in the bed-chamber was used during the process in all experiments. Although the data represents the mean diameter as a function of time, the graphs were plotted with the x-axis representing process percentage for improved comparison among the results in all runs. The growth kinetics for the other percentiles can be consulted in the Supplementary Material.
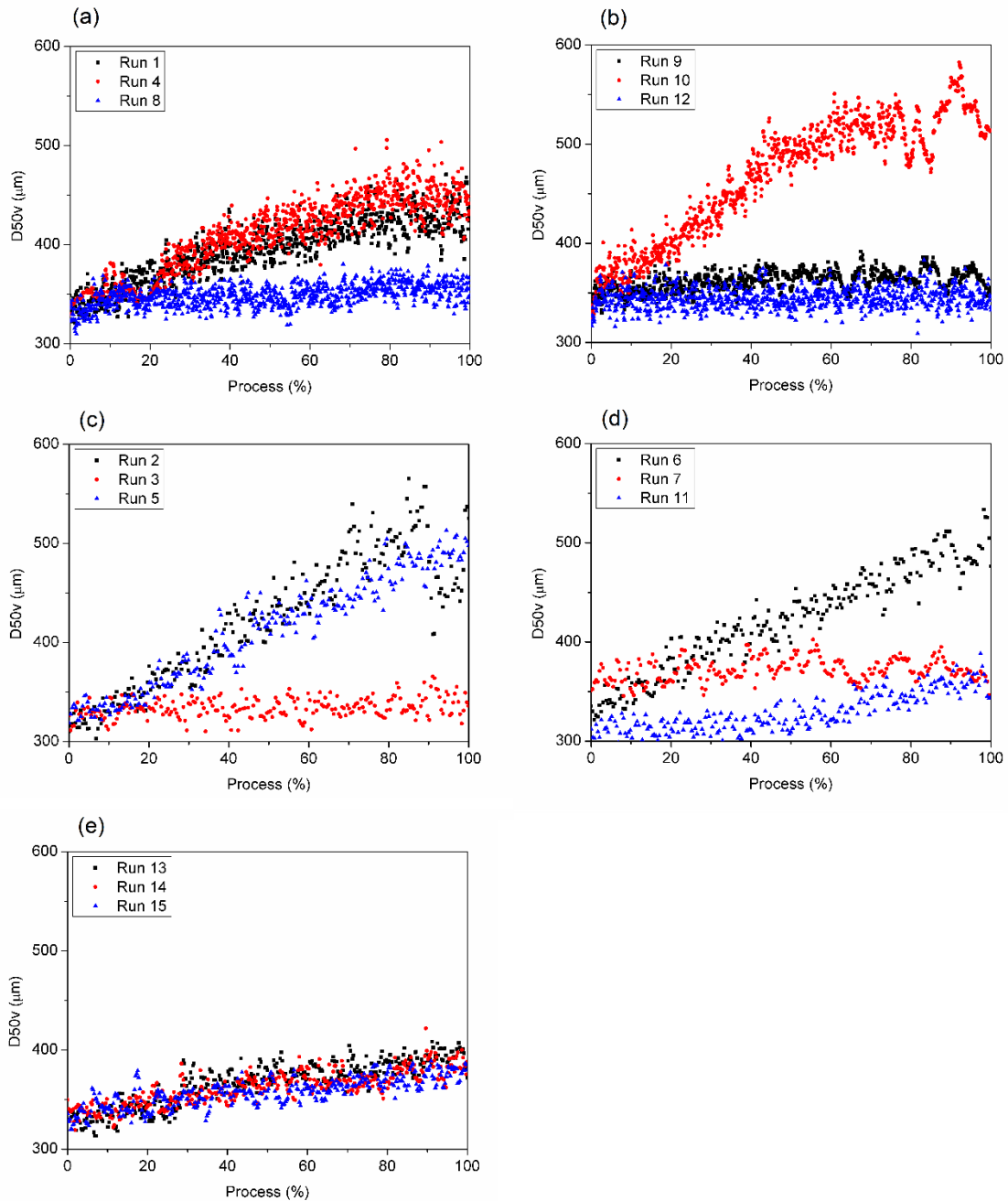
Figure 3.5: The particle growth kinetics for each run of the Plackett-Burman experimental design: (a) runs 1, 4, and 8 (80 min); (b) Runs 9, 10, and 12 (80 min); (c) Runs 2, 3, and 5 (20 min); (d) runs 6, 7, and 11 (20 min); (e) runs 13, 14, and 15 (32 min). The time in parentheses represents the total time process.

There was particle enlargement during all runs, as one can see in Figure 3.5. Runs 2, 5, 6, and 10 provided a final *D50v* value of 479.4, 495.4, 501.2, and 514.8 μm, respectively. These values were the highest ones among all experiments. On the contrary, the conditions from

runs 9 and 11 proved to be less efficient in promoting size enlargement, reaching 350.7 and 359.9 µm particle sizes, respectively. The data adhered to the same enlargement trend at the central point condition, pointing out that runs (13–15) were reproducible.

Figure 3.5 shows three distinct particle growth kinetic behaviors. In runs 1, 4, and 10, there was growth stabilization after some time. In trials 2, 5, 6, 11, and the three replicates at the central point (13–15), growth continued to occur until the process ended. The curves remained stable throughout the process in further tests (3, 7, 8, 9, and 12). One must understand that growth stabilization behavior does not indicate that there is no longer an increase in the particle size but the growth balance. That is because the experimental points in the graphs correspond to an average chord length between 2,000 particles. Additionally, the growth stabilization trend indicates that the balance between particles breaking and agglomerating is close to zero.

Likewise, when there is an increase in the particle size during the process, then there is positive growth balance, i.e., the number of particles increasing in size through agglomeration is greater than the number of aggregates breaking down. According to Tan et al. [1], fluidized bed melt granulation comprises a sequence of events regulated by operating parameters. This sequence was divided into two categories – *Aggregation* and *Breakage* – more detailed than the steps proposed by Iveson et al. [2]. *Aggregation* is made up by the following events (1) *droplet capture*; (2) *particle wetting*; (3a) *particle collision*; (3b) *binder solidification*; (4a) *particle aggregation with liquid binder*; (4b) *unsuccessful aggregation*; (5a) *binder solidification*; (5b) *liquid bridge rupture*. *Breakage* is made up of (6) *solid bridge rupture*. Clearly, the parameters regulating these phenomena are mainly moisture (expressed by binder flow rate and concentration), temperature, and turbulence (related to the particle moving velocity and passage through the spray zone).

The same growth trend is viewed when comparing runs 1 and 4 (Figure 3.5 (a)) (the particle growth occurred in up to about 25% of the process and after that became less accentuated), both experiments were performed at the same significant levels (Table 3.1). It indicates the experiments were reproducible, and the statistical analysis effect of the variables is consistent with the experimental result. The combination of high C and T and low Q and M provided an increase in the growth balance of particles throughout at least 25% of the process, and after that, it became less effective.

The internal bed-chamber temperature had not reached a steady state until after 20% of the process or 16 min in both cases (Figure 3.6 (a)) and relative humidity was already in equilibrium (Figure 3.6 (d)). The agglomeration events proposed by Tan et al. [1] can be explained by analyzing the relation between internal temperature and relative humidity. The increase in temperature induces a slow rate of binder solidification, and it remains molten for longer. This fact makes the events (2) *particle wetting* and (3a) *particle collision* more evident, indicating they were undergoing the aggregation phenomenon. It means there was more time for the binder to promote more aggregation of particles before solidification, leading to rapid particle growth through increasing bed temperature [1]. This behavior is observed for about the first 25% of the process when the slope of the particle growth curve is more accentuated than the curve after 25%. The situation is believed to have changed after the temperature reached a steady state. The (5a) *binder solidification* became the most important event as the stabilization of temperature is more essential for drying liquid bridges [1,29,30].
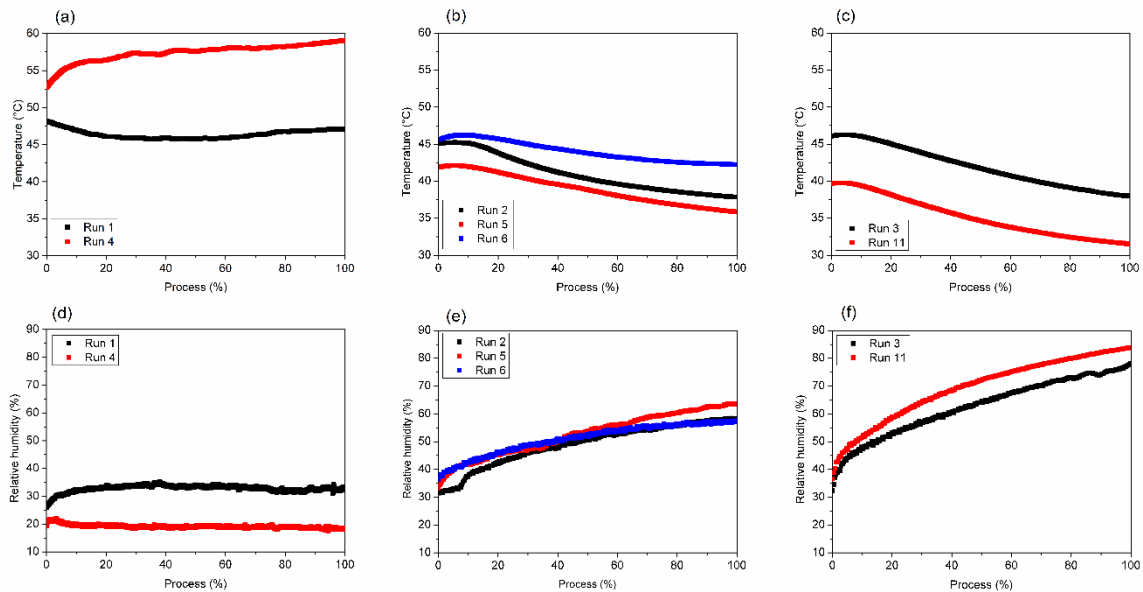
Figure 3.6: Evolution of parameters temperature (above) and relative humidity (below) during the agglomeration process for runs 1 and 4 (a, d); runs 2, 5, and 6 (b, e), and runs 3 and 11 (c, f).

A constant and linear growth was observed throughout the process when analyzing runs 5 and 6 (Figure 3.5 (c) and (d)), practically attaining the same size value as at the end of the process (495.4 and 501.2 μm, respectively). Unlike the other runs, run 2 (Figure 3.5 (c)) showed an increase in the particle size up to 85% of the process, followed by a decrease,

reaching approximately the same final values as the other two runs. This drop indicates that the growth balance was negative, i.e., the breakdown rate of the aggregates was greater than the agglomeration rate of the particles, probably suggested by the change in event (5a) *binder solidification* to the event (6) *solid bridge rupture*. These runs (2, 5, and 6) were carried out under the same C (+1) and Q (+1) levels, but comparing run 2 and run 5 there was a change from –1 to +1 of M levels and little or no change in the process response. Likewise, when comparing runs 5 and 6, there was only a change in the T factor, from –1 to +1, and also, as seen in Figure 3.5, no or little change in the particle-growth behavior. These changes do not affect the growth balance, making it clear that these factors, though statistically significant, are not substantially important, i.e., a change in the M and T levels does not cause an expressive change in the response since the final sizes are practically the same.

The constant growth in particle size in runs 5 and 6 shows that events in the Aggregation category occur sequentially and neither one was more evident than the other, unlike the situation reported in runs 1 and 4, as proposed in the sequence by Tan et al. [1]. The temperature drops and humidity increase (Figure 3.6 (b) and (e)) by not reaching stability confirmation then as well. However, this does not mean that the (6) *solid bridge rupture* event does not occur; on the contrary, it only happens on a smaller scale than Aggregation events, causing positive growth balance. In run 2, after nearly 95% of the process, there was a behavioral change in the growth kinetics, showing the breakdown balance was higher than the growth balance. There has also likely been a change in the events impelling growth, from (5a) *binder solidification* to (6) *solid bridge rupture*. However, no evident behavior was observed in the temperature and humidity curves based on the processing time, thus guaranteeing this proposed change.

Runs 3 and 11 (Figure 3.5 (c) and (d), respectively) resulted in similar final *D50v* values (338.5 and 339.8 μm, respectively), although the kinetic particle growth displayed different behavior. While run 3 remained as steady growth balance, in run 11, the particle size remained almost constant until around 50% of the process, followed by a slight growth until the end of the process.

It was impossible to identify any definite temperature and relative humidity behavior explaining this difference between runs 3 and 11. In Figure 3.6 (c) and (f), these temperature and relative humidity variables seem to maintain the same trend in each case throughout the experiments. The change in the kinetic particle growth behavior can possibly be due to the simultaneous change in the M and T levels. In run 3, the particles were initially wetter,

and the air temperature was higher; the sequence of events occurred, according to Tan et al. [1], yet no step stood out more than any other. The same behavior was supposed to happen in run 11; however, as the initial moisture content of particles and the temperature were lower, probably the amount of liquid inserted in the chamber was initially used to wet the particle surface, making the growth balance close to zero. After that, the binder solution was used to form liquid stronger bridges than previously, leading to a positive balance in particle enlargement.

3.3.3.3. Wet granulation mechanisms based on particle size classes

Sastry and Fuerstenau [32] proposed the first approach for wet granulation mechanisms. A modern approach was conceived by Iveson et al. [2], reducing the mechanisms from five to three steps. Some steps were merged from the previous model in the newest one as some occur simultaneously. Also, the limit between the end of one of them and the beginning of the next is not so easy to determine or depends arbitrarily on what is determined by those who perform the experiment, i.e., there is no awareness of a physical parameter to assess the completion of one of the steps [2]. More recently, Tan et al. [1] described an aggregation model to account for the process of net particle growth considering aggregation, binder solidification, and breakage processes. Despite that, by analyzing particle classes, a change of trend in particle size evolution can be identified throughout the process. So, it is possible to classify the steps more clearly through a new approach. Thus, in this work, we suggest a new approach based on particle size classes, whereas the agglomeration process can be divided into 4 steps, as shown in Figure 3.7 (a). A scheme based on the definition of the four regions is displayed in Figure 3.7 (b).

Figure 3.7 summarizes these steps and shows the evolution of particle size classes expressed by the remaining fraction in sieves. The use of the SFV technique was essential for defining these steps.

It was possible to monitor the evolution of sizes, separating the particles into classes based on the sieving data by which the technique is based (see Section 3.2.4). So, it was possible to overview the process as it progressed.
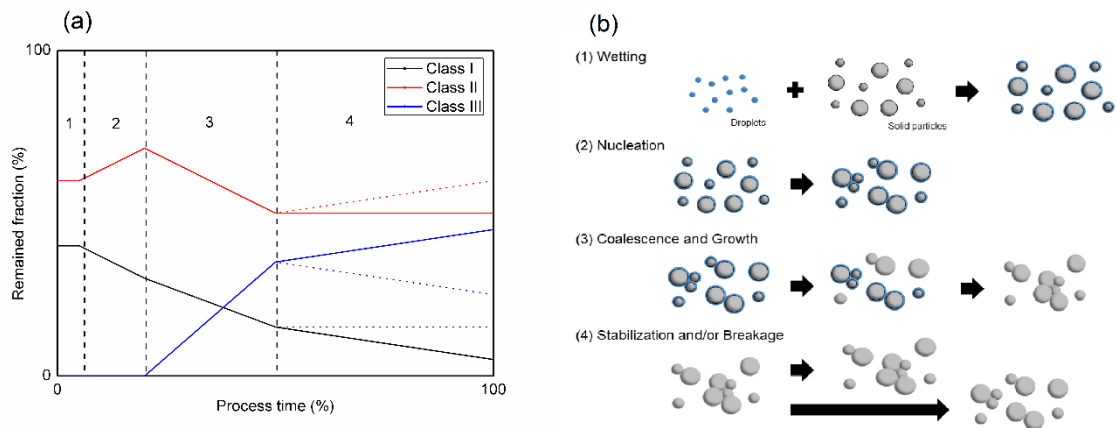
Figure 3.7: Particle size classes evolution for agglomeration. (a) Regions 1, 2, 3, and 4 correspond to wetting, nucleation, coalescence and growth, and stabilization (indicated by continuous lines) and/or breakage (indicated by dashed lines). Classes I, II, and III correspond to fine, intermediate, and coarse particles. (b) agglomeration process schematic.

The structure of our new approach is based on particle size classes as following:

(1) Wetting;

(2) Nucleation;

(3) Coalescence and growth;

(4) Stabilization and/or breakage.

Phase 1, named *wetting*, does not differ from what Iveson et al. [2] proposed., but it is only separated by the nucleation step. The separation of the steps occurred because two different behaviors can occur at the beginning of the process. Wetting is characterized by no change in the percentage of fine and intermediate particles, and there are no coarse particles present either. The particles are only wetted without growth in this period. It is the shortest one compared to the following steps, however, sometimes it is impossible to identify. The wetting phase depends on the degree of dispersion of liquid over the powder [33]. Additionally, a sufficient amount of liquid binder must be available where it gets in contact for the bridge to form. If it occurs, there is adherence in the following steps, and growth is favored. Otherwise, the particles are rebounded [6]. The contact angle between liquid and particles and the spread of the liquid phase over the solid phase is the main limiting parameter in this phase [2].

The percentage of fine particles decreases, and the percentage of intermediate particles gradually increases in Phase 2, *nucleation*, as the percentage of coarse particles are negligible or null. It is an initial period of particle growth, marked by the lowest growth rate. The collision between small particles produces intermediate or new primary particles, which provides a slight increase in the average particle size. This collision occurs due to capillary attraction between wet particles, whereas the surface tension of the liquid binder is one of the main factors keeping the particles together [32,33]. The kinetics of primary particle formation is governed by parameters such as particle size and droplet size [2,6] since this step only occurs due to the presence of a liquid binder on the powder surface.

There is a sharp and continuous decrease in the percentage of fine particles and a regular increase in the rate of the coarse ones in Phase 3, *coalescence and growth*. The fraction of intermediate particles reaches a maximum percentage throughout the process, followed by a decreasing trend, while the coarse fraction increases and continues to rise. The particle growth rate is greater than in Phase 2, with a significant increase in the average particle size value. There is probably a predominance of coalescence mechanism and consolidation of the particles in this period. Species are produced here by collisions between two or more particles. The collision results in a species by which the mass is the sum of the individual masses [32]. The particles only join if they are sufficiently moist, i.e., the porous surface of the granules must be saturated with liquid, and the granules must be adequately malleable to deform and form bridges [2,6,33].

Finally, in Phase 4, *stabilization and/or breakage*, the granule size reduces due to friction and/or breakage, or stabilization when consolidation occurs. First, the percentage of coarse particles decreases while the percentage of fine and/or intermediate classes increase resulting in a decrease in the average particle size (dashed lines in Figure 3.7). When the change in the percentage of the three classes is not so significant that results in a low reduction and/or stabilization in the average particle size value (solid lines in Figure 3.7), then, there is a predominance of consolidation in drying. This phase is characterized by the formation of fragments by the breaking up of wet granules. It causes a change in the number of particles but not mass, interfering with size distribution [2,32]. The break-up is due to the collision and wear of weak primary particles, between primary particles and other primary particles or between primary particles and equipment. Both friction and fragmentation form tiny small secondary particles used as primary particles to form new granules. Impacted granules can break into larger fragments by breakage and smaller ones by attrition [34]. Exponential growth is initiated

due to wetting the solid portion and the consequent densification of the secondary primary particles until there is insufficient liquid, making the breakage step more significant than the stabilization [2,35].

The evolution of particle size classes is shown in Figure 3.8 (a) and (c), from runs 3 and 10, displaying the smallest and the highest increase in particles, respectively. Figure 3.8 (b) and (d) represent the PSD curves from the same experimental runs.
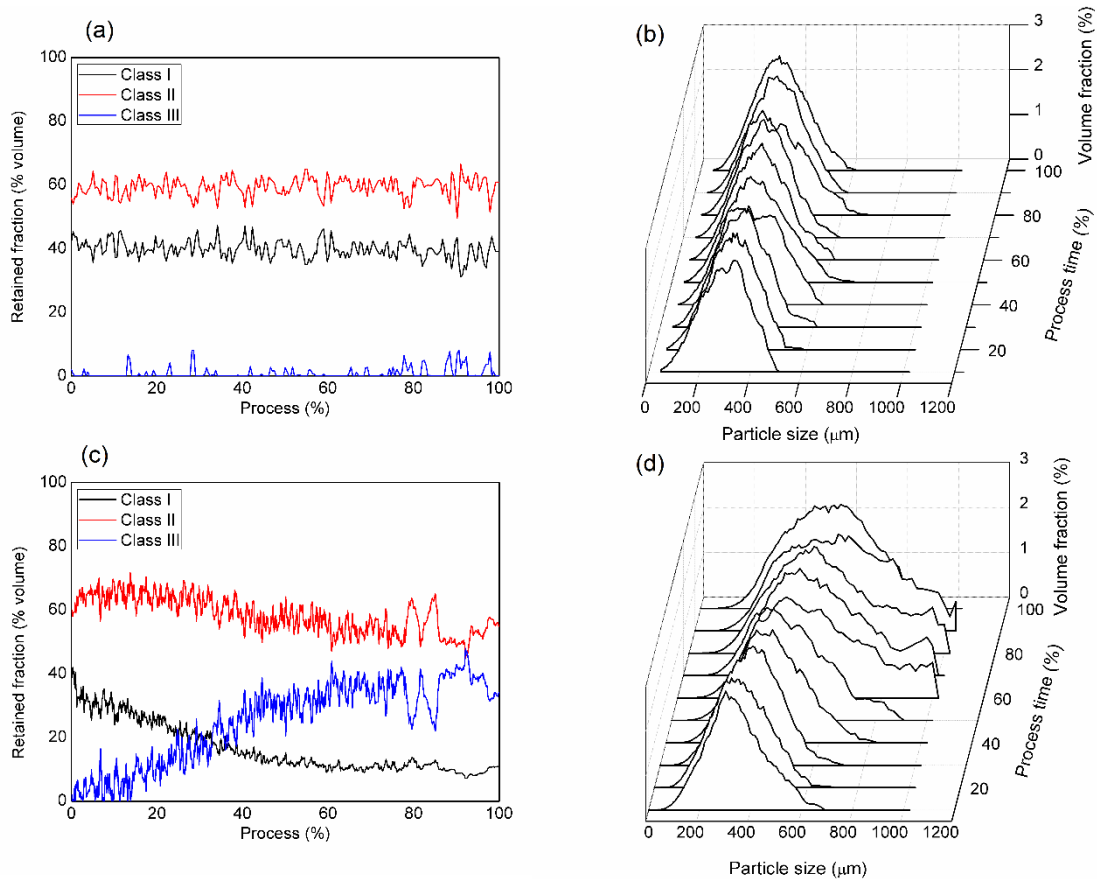
Figure 3.8: Evolution of particle size classes (left) and particle size distribution (right) during agglomeration process observed in run 3 (a, b), and run 10 (c, d). Classes I, II, and III correspond to fine, intermediate, and coarse particles.

Figure 3.8 (a) shows no particle growth under the experimental conditions from run 3, nor evolution of size classes. According to the new approach presented in this work, the agglomeration process in run 3 where only wetting occurred as there was no class evolution, i.e., the values of retained fractions fluctuate around 40%, as a constant value, in Class I and

60% in Class II. Furthermore, the retained Class III fraction was considered to fluctuate about 0%, even though some particles over 600 μm were sometimes identified.

The comparison between the particle size classes and the PSD curves confirm that the particle enlargement was too small for run 3 (Figure 3.8 (b)) since the curves representing the processing time of 30%, 60%, and at the end of the process were practically coincident. It shows that the operating conditions used (Table 3.1) were not able to cause particle agglomeration. Additionally, the nucleation step was most likely negatively impacted due to the high wetting rate provided by the less concentrated binder solution. Indeed, the binder concentration was the most crucial factor for the agglomeration of CMC in the Plackett-Burman experimental design (Table 3.2).

The evolution of size classes during the process is evident in run 10, Figure 3.8 (c). There was a sharp decrease in the smaller particle frequency during the process. In contrast, the frequency of the intermediate particle increased slightly from 60% to 75% and then decreased, giving rise to the formation of coarse particles. The frequency of the coarse particles constantly increased to around 60% in the process, after that reaching a plateau. Up to 15% of the process occurs in steps 1 (*wetting*) and 2 (*nucleation*), according to the new presented approach, but it is only possible to separate them by analyzing the data and not by graphic analysis.

The wetting phase happened very quickly (around 10% of the process or less), and the nucleation phase started before 10% of the process and went on until 15%; after that, the coarse particles began to appear. It is still not possible to separate the two phases from existing data. After going through the wetting zone, it is believed that particles are available for nucleus formation; however, due to the operating conditions of this experiment, the primary particles are still weak. There is a cyclical behavior between wetting and nucleation. The balance between the formation of stable and non-stable primary particles is positive; at that time, nucleation becomes more evident than wetting. The occurrence of the *coalescence and growth* event (Phase 3) ranges from 15% to 60% marked by the appearance and constant increase of coarse particles rate formation. Thenceforth, the process entered Phase 4 (*stabilization and/or breakage*). However, a tendency to break the granules was not identified. Therefore, after 60% of the process, it was already possible to stabilize the agglomeration, highlighted by the practically constant behavior of around 40% of coarse particles.

There has been a change in PSD curves throughout the process, thereby confirming what was evidenced from run 10. The displacement of the curves on the positive side of the x-

axis (Figure 3.8 (d)) confirms the change of the PSD curves throughout the process. There was an increase in particle size in at least 60% of the processing time, as compared to the 0%, 30%, and 60% curves. After that, the sizes maintained regular, as noted by the similarity between the 60% process time curve and also at the end of the process curve.

3.4. CONCLUSIONS

The experimental design made it possible to demonstrate the agglomeration process as technically feasible for improving the CMC particle size. This process occurs due to the pulverization of a maltodextrin solution, used as a liquid binder, on the surface of CMC particles. Particle surfaces were wetted and dried, resulting in the agglomerated structure consolidates, leading to particle enlargement.

Increased concentration, initial moisture content, and binder flow rate result in the production of larger granules. Additionally, when the fluidizing air temperature increased, D50v decreased. These data were confirmed by growth kinetics obtained from the SFV technique.

The SFV technique proved efficient and effective for real-time monitoring of particle size in the CMC agglomeration with maltodextrin. In addition to analyzing the data it was possible to demonstrate the evolution of PSD curves also in real time. PSD curves are considered as one of the critical parameters in the particulate material agglomeration and, thus, process in-line follow-up and introduce relevant advances in this research field.

Finally, it was possible to define a physical parameter to delimit the previously proposed agglomeration steps in the literature. The most significant progress in this work was to present a new approach considering particle size classification of particulate material divided into size classes and the joint use of the SFV technique.

REFERENCES

[1] H.S. Tan, A.D. Salman, M.J. Hounslow, Kinetics of fluidised bed melt granulation I: The effect of process variables, Chem. Eng. Sci. 61 (2006) 1585–1601. http://doi.org/10.1016/j.ces.2005.09.012.

[2] S.M. Iveson, J.D. Litster, K. Hapgood, B.J. Ennis, Nucleation, growth and breakage phenomena in agitated wet granulation processes: a review, Powder Technol. 117 (2001) 3–39. http://doi.org/10.1016/S0032-5910(01)00313-8.

[3] P.C. Knight, Structuring agglomerated products for improved performance, Powder Technol. 119 (2001) 14–25. http://doi.org/10.1016/S0032-5910(01)00400-4.

[4] D.M. Lipps, A.M. Sakr, Characterization of wet granulation process parameters using response surface methodology. 1 Top-Spray Fluidized Bed, J. Pharm. Sci. 83 (1994) 937–947. https://doi.org/10.1002/jps.2600830705.

[5] C. Avilés-Avilés, E. Dumoulin, C. Turchiuli, Fluidised bed agglomeration of particles with different glass transition temperatures, Powder Technol. 270 (2014) 445–452. http://doi.org/10.1016/j.powtec.2014.03.026.

[6] G.I. Tardos, M.I. Khan, P.R. Mort, Powder technology critical parameters and limiting conditions in binder granulation of fine powders, Powder Technol. 94 (1997) 245–258. http://doi.org/10.1016/S0032-5910(97)03321-4.

[7] G.C. Dacanal, F.C. Menegalli, Selection of operational parameters for the production of instant soy protein isolate by pulsed fluid bed agglomeration, Powder Technol. 203 (2010) 565–573. http://doi.org/10.1016/j.powtec.2010.06.023.

[8] G.C. Dacanal, T.A.M. Hirata, F.C. Menegalli, Fluid dynamics and morphological characterization of soy protein isolate particles obtained by agglomeration in pulsed-fluid bed, Powder Technol. 247 (2013) 222–230. http://doi.org/10.1016/j.powtec.2013.07.001.

[9] V.G. Machado, T.A.M. Hirata, F.C. Menegalli, Agglomeration of soy protein isolate in a pulsed fluidized bed: experimental study and process optimization, Powder Technol. 254 (2014) 248–255. http://doi.org/10.1016/j.powtec.2014.01.040.

[10] K. Cronin, F.J.G. Ortiz, D. Ring, F. Zhang, A new time-dependent rate constant of the coalescence kernel for the modelling of fluidised bed granulation, Powder Technol. 379 (2021) 321–334. http://doi.org/10.1016/j.powtec.2020.10.083.

[11] K. Terrazas-Velarde, M. Peglow, E. Tsotsas, Stochastic simulation of agglomerate formation in fluidized bed spray drying: A micro-scale approach, Chem. Eng. Sci. 64 (2009) 2631–2643. http://doi.org/10.1016/j.ces.2009.02.041.

[12] M.P. Villa, D.E. Bertin, I.M. Cotabarren, J. Piña, V. Bucalá, Fluidized-bed melt granulation: Coating and agglomeration kinetics and growth regime prediction, Powder technol. 300 (2016) 61–72. http://doi.org/10.1016/j.powtec.2016.06.006.

[13] A. Burggraeve, T. Van Den Kerkhof, M. Hellings, J.P. Remon, C. Vervaet, T. De Beer, Evaluation of in-line spatial filter velocimetry as PAT monitoring tool for particle growth during fluid bed granulation, Eur. J. Pharm. Biopharm. 76 (2010) 138–146. http://doi.org/10.1016/j.ejpb.2010.06.001.

[14] C.A.M. Silva, O.P Taranto, Real-time monitoring of gas-solid fluidized-bed granulation and coating process: evolution of particle size, fluidization regime transitions, and psychometric

parameters, Drying Technol. 33 (2015) 1929–1948. http://doi.org/10.1080/07373937.2015.1076000.

[15] J.G. Rosa, R.F. Nascimento, K. Andreola, O.P. Taranto, Influence of drying conditions on the acacia gum particle growth in fluidized bed agglomeration: in-line monitoring of particle size, 21st Drying Symposium Proceedings (2018) 1439–1446. http://doi.org/10.4995/IDS2018.2018.7345.

[16] M. Aghbashlo, R. Sotudeh-Gharebagh, R. Zarghami, A.S. Mujumdar, N. Mostoufi, Measurement techniques to monitor and control fluidization quality in fluidized bed dryers: a review, Drying Technol. 32 (2014) 1005–1051. http://doi.org/10.1080/07373937.2014.899250.

[17] E.M. Hansuld, L. Briens, A review of monitoring methods for pharmaceutical wet granulation. Int. J. Pharm. 472 (2014) 192–201. http://doi.org/10.1016/j.ijpharm.2014.06.027.

[18] A. Burggraeve, T. Monteyne, C. Vervaet, J.P. Remon, T. De Beer, Process analytical tools for monitoring, understanding, and control of pharmaceutical fluidized bed granulation: A review. Eur. J. Pharm. Biopharm. 83 (2013) 2–15. http://doi.org/10.1016/j.ejpb.2012.09.008.

[19] C.A.M. Silva, J.J. Butzge, M. Nitz, O.P. Taranto, Monitoring and control of coating and granulation processes in fluidized beds – A review, Adv. Powder Technol. 25 (2014) 195–210. http://doi.org/10.1016/j.apt.2013.04.008.

[20] D. Petrak, S. Dietrich, G. Eckardt, M. Köhler, In-line particle sizing for real-time process control by fibre-optical spatial filtering technique (SFT), Adv. Powder Technol. 22 (2001) 203–208. http://doi.org/10.1016/j.apt.2010.11.002.

[21] K. Andreola, C.A.M. Silva, O.P. Taranto, Agglomeration process of rice protein concentrate using glucomannan as binder: in-line monitoring of particle size, Chem. Eng. Res. Des. 135 (2018) 37–51. http://doi.org/10.1016/j.cherd.2018.05.019.

[22] J.G. Rosa, R.F. Nascimento, K. Andreola, O.P. Taranto, Acacia gum fluidized bed agglomeration: use of inulin as a binder and process parameters analysis, J. Food Process Eng. 43 (2020) e13409. http://doi.org/10.1111/jfpe.13409.

[23] R.F. Nascimento, J.G. Rosa, M.F. Ávila, O.P. Taranto, Pea protein isolate fluid dynamics and characterization obtained by agglomeration in pulsed fluidized bed, Part. Sci. Technol. (2020) 1–11. http://doi.org/10.1080/02726351.2020.1830209.

[24] M. Langner, I. Kitzmann, A.L. Ruppert, I. Wittich, B. Wolf, In-line particle size measurement and process influences on rotary fluidized bed agglomeration, Powder Technol. 364 (2020) 673–67. http://doi.org/10.1016/j.powtec.2020.02.034.

[25] D. Geldart, Gas fluidization technology, John Wiley & Sons Inc., Hoboken, NJ, 1986.

[26] K. Andreola, C.A.M. Silva, O.P. Taranto, Production of instant rice protein concentrate by rotating pulsed fluidized bed agglomeration using hydrolyzed collagen solution as binder, Chemical Engineering Transactions 49 (2016) 115–120. http://doi.org/10.3303/CET1649020.

[27] M.F. Ávila, J.G. Rosa, R.F. Nascimento, O.P. Taranto, Pea protein isolate moisture content effect on fluid dynamics behavior and particle growth kinetic in fluidized bed, XXXIX Congresso Brasileiro de Sistemas Particulados Proceedings (2019) 1–9.

[28] R.F. Nascimento, J.G. Rosa, K. Andreola, O.P. Taranto, Wettability improvement of pea protein isolate agglomerated in pulsed fluid bed, Parti. Sci. Technol 38 (2019) 511–521. http://doi.org/10.1080/02726351.2019.1574940.

[29] J. Du, A. Bück, E. Tsotsas, Influence of process variables on spray agglomeration process in a continuously operated horizontal fluidized bed, Powder Technol. 363 (2020) 195–206. http://doi.org/10.1016/j.powtec.2020.01.008.

[30] M. Dadkhah, E. Tsotsas, Influence of process variables on internal particle structure in spray fluidized bed agglomeration, Powder Technol. 258 (2014) 165–173. http://doi.org/10.1016/j.powtec.2014.03.005.

[31] M. Roostaei, S.A. Hosseini, M. Soroush, A. Velayati, A. Alkouh, M. Mahmoudi, A. Ghalambor, V. Fattahpour, Comparison of Various Particle-Size Distribution-Measurement Methods, SPE Res. Eval. & Eng. 23 (2020) 1159–1179. http:// doi.org/10.2118/199335-PA.

[32] K.V.S. Sastry, D.W. Fuerstenau, Mechanisms of agglomerate growth in green palletization, Powder Technol. 7 (1973) 97–105. http://doi.org/10.1016/0032-5910(73)80012-9.

[33] M. Butensky, D. Hyman, Rotary drum granulation. An experimental study of the factors affecting granule size. Ind. Eng. Chem. Fundam. 10 (1971) 212–219. http://doi.org/10.1021/i160038a005.

[34] H.S. Tan, A.D. Salman, M.J. Hounslow, Kinetics of fluidised bed melt granulation III: Tracer studies, Chem. Eng. Sci. 60 (2005) 3835–3845. http://doi:10.1016/j.ces.2005.02.009.

[35] P. Vonk, C.P.F. Guillaume, J.S. Ramaker, H. Vromans, N.W.F. Kossen, Growth mechanisms of high-shear pelletisation. Int. J. Pharm. 157 (1997) 93–102. http://doi.org/10.1016/S0378-5173(97)00232-9.

CHAPTER IV

Characterization of spray system to evaluate particle size

enlargement in fluidized bed agglomeration

Nascimento, R.F.; Ávila, M.F.; Taranto, O.P.; Kurozawa, L.E.

Characterization of spray system to evaluate particle size enlargement in fluidized bed agglomeration

Raul F. Nascimento[a], Mariana F. Ávila[b], Osvaldir P. Taranto[b], Louise Emy Kurozawa[a]

[a]Department of Food Engineering, School of Food Engineering, University of Campinas, Monteiro Lobato St. 80, Campinas, SP, Brazil

[b]Department of Process Engineering, School of Chemical Engineering, University of Campinas, Albert Einstein Ave. 500, Campinas, SP, Brazil

HIGHLIGHTS

- The spray profile is intrinsically related to operating parameters.
- The PDI system can provide information about droplet size and velocity.
- The binder concentration and flow rate notably influenced the droplet size formation.
- The CMC particle growth occurs due to operating condition variations.

ABSTRACT

Droplet size is a crucial success factor for increased particle size in agglomeration process. Thus, this work aimed to analyze the physicochemical properties of maltodextrin solutions used as the binder, their influence on the size of the formed droplets, and their relationship to particle growth. Three maltodextrin solutions (5.0%, 20.0%, and 35.0% w/w) were characterized for that in terms of physicochemical properties and droplet size, and following that, the binder concentrations, binder flow rate, and atomizing air pressure were evaluated. There was a large concentration of droplets with small sizes up to 50 μm with velocities reaching about 100 m/s for all tested conditions. The binder solution concentration and binder flow rate displayed similar and positive effects on droplet sizes; in contrast, atomizing air pressure exhibited a negative effect. The binder liquid concentration is the most outstanding parameter for the agglomeration process regarding particle growth under experimental conditions.

Keywords: Droplet size; Phase Doppler Interferometry; Maltodextrin; Particle growth.

4.1. INTRODUCTION

Agglomeration includes transforming the fine particles into semi-permanent granules using a range of equipment, and one of these is a fluidized bed [1]. Generally, a liquid solution is atomized into a solid particle bed for enough time, so the fine particles are wetted, remain in contact with each other, dry, and stay joined in granule format [2,3]. The formation and guarantee of stability of these larger structures are related to the physicochemical properties of both the solid material and the liquid binder and the process parameters [4–6].

The fluidized bed agglomeration process basically consists of atomizing a binding liquid onto the fluidized particle bed. The process is considered as successive humidification and drying operations are performed; at first, the liquid is atomized over the particles, causing liquid bridges to form; then, hot air removes water from the particles, developing solid bridges and thus creating larger granules. Growth only occurs when there is enough liquid to establish bridges or when liquid saturation is sufficient to increase the plastic deformation of the agglomerates [5,7]. Because of that, binder solutions play an essential role in the wet agglomeration process. Mainly because it is only necessary to spray a liquid phase on the solid phase, and then the outer layer of the particles will be deformable and suitable for forming bridges [1].

Furthermore, the first step of the fluidized bed agglomeration process is the wetting of the particles (sometimes, in older research studies, wetting was described jointly with nucleation) as reported in the literature [1,6,8–11]. Sastry and Fuerstenau [12] indicated that a set of forces must act on the system for particle growth to start, including interfacial and capillary forces, which are only present due to the presence of the liquid phase. There must be an instantaneous and homogeneous distribution of the liquid over the solid phase for these forces to act proportionally on all particles, which, in real systems, is impossible to happen. The agglomeration mechanisms depend on the degree of liquid dispersion over powder [6,8]. As Tardos et al. [6] explained, enough binder must be at the point of contact for a bridge to form. Growth is favored if there is an adequate amount for adhesion; otherwise, particles are bounced off. More recently, Iveson et al. [1] inserted another fundamental parameter for wetting, the contact angle and the consequent scattering coefficient of the liquid phase on the solid phase. The kinetics of nuclei formation depends on parameters such as droplet and particle size. If there is a significant drop compared to the particles, the nucleation takes place by immersion of the small particles in the droplet, producing nuclei with saturated pores. On the other hand, if

the drops are tiny, nucleation occurs by the distribution of the droplets on the particle surface, producing nuclei with trapped air inside [1,13].

It is well known that size, size distribution, the shape of solids, surface tension, the viscosity of liquid binder, and the contact angle are critical variables of the agglomeration process since they are used as predictive criteria for operations [14]. The most effective way to insert liquid into the system is through atomizing nozzles when considering wet agglomeration since there is an increase in the surface area of the liquid and a consequent increase in both the wetting and evaporation rates. When it comes to atomizing nozzles and droplet formation, the limiting factors are those related to the physicochemical properties of liquids and gas velocities (or pressure) [15]. Droplet formation is theoretically divided into two steps: liquid disintegration into filaments or large droplets and continued breaking liquid into smaller droplets. The atomizing air pressure and the liquid flow are relevant aspects to consider regarding operating conditions in droplet formation and the uniformity of the droplet size distribution. According to Hede et al. [15] and Lefebvre [16], air pressure and droplet size are inversely proportional, and liquid flow rate directly influences them. Viscosity, liquid density, and surface tension are the most important variables for consideration when dealing with liquid properties. In general, viscosity and surface tension directly affect Sauter diameter droplets because more energy is needed for spray atomization.

On the other hand, liquid density has a complex influence since one must consider the type of atomizer and process variables. Typically, the liquid atomization is divided into three regions, from the closest to the farthest from the nozzle: sheet, ligament, and drops. In some cases, the ligament region may be far below the exit point of the liquid from the nozzle, and in others, depending on the mass flow, a more compact spray can be formed, leading to the formation of large droplets. Meanwhile, the increase in liquid density can reduce the filament region thickness and combined with high relative velocity; the atomization process can be improved [15,16].

Some authors have reported using the spray features to evaluate the drying process. There is a relevant trend line focused on fluidized bed coating, e.g., Duangkhamchan et al. [17] explored the computational fluid dynamics model to describe two-fluid atomization in a fluidized bed coater using the air-blast/air-assisted atomizer model; Hede et al. [18] developed a mathematical model for the top-spray fluid bed coating process; or the evaluation *in situ* of the behavior of aqueous spray produced by a pneumatic nozzle in a fluid-bed process [19].

Other authors related the effect of the droplet size on melt granulation in fluidized beds, e.g., Seo et al. [20], Abberger et al. [21], and Moraga et al. [22].

There is some information in the literature on the effect of process-related variables and physicochemical properties on droplet size and particle enlargement in the agglomeration process [23]. These authors discussed how the solid and liquid parameters favor the granulation or coating; they found that capillary forces drove the granulation process under the addressed conditions. Tan et al. [24] reported a case in which the droplets are smaller than the primary particles. At first, the granules are formed at a high growth rate caused by particle collision due to the thick binder film formed around the particles. Then, there is secondary growth, in a shorter time than the first, due to the rewetting of unsaturated granules. More recently, Kan et al. [25] simulated the effect of droplet size on a particle-particle adhesion by the dynamic liquid bridge. It was explained that, in the approach stage, there is a correlation between the particle motion dissipation energy and the droplet diameter due to the increased capillary pressure force acting as a dissipative force. In contrast, in the separation stage, there is a directly proportional relationship, mainly due to the difference in the liquid bridge shapes formed during particle collision.

Despite everything that has already been reported, clearly, not only the droplet size is a crucial factor for the evaluation of granule growth in the fluidized bed agglomeration process, but also the physicochemical properties of the binder liquids used during the process. The authors understand there is a gap in the literature directly relating the droplet size to the particle size during the agglomeration process. Thus, this work has aimed to analyze the physicochemical properties of maltodextrin solutions used as binder liquids in a fluidized bed agglomeration process, as well as their influence on the size of the droplets formed by spraying and their relationship with the growth of particles during the process. The novelty of this work also lies in using advanced in-line and real-time measurement techniques for particle size, the ability to monitor growth kinetics, and the use of a robust technique for measuring binder liquid droplet size.

4.2. MATERIAL AND METHODS

4.2.1. Material

The binder solutions were prepared at room temperature (around 27 °C) by subjecting distilled water and maltodextrin (MOR-REX® 1910, Ingredion, USA) to magnetic stirring until they were completely dissolved. The concentrations of maltodextrin aqueous solutions were 5.0%, 20.0%, and 35.0 % w/w, and the densities were 1.02 ± 0.01, 1.08 ± 0.01, and 1.14 ± 0.01 g/cm^3, respectively, measured using a digital densimeter (DMA 4500M, Anton Paar, Austria), at 20 °C.

Microcrystalline cellulose (CMC) (Microcel, Blanver Farmoquímica, Brazil) was used in the agglomeration assays. Moisture content, density, and the particle size expressed by the *D10v*, *D50v*, and *D90v* percentiles are $7.28\% \pm 0.05\%$, 1.5485 ± 0.0010 g/cm^3, 147.9 ± 6.8, 295.9 ± 10.0, and 436.6 ± 25.1 µm, respectively. The pore surface area, volume, and radius are 3.708 ± 0.038 m^2/g, 0.0012 ± 0.0001 mm^3/g, and 0.6503 ± 0.0130 nm, respectively, estimated by BET and HK methods.

4.2.2. Characterization of the solutions

4.2.2.1. Surface tension

The surface tension was evaluated by the pendant droplet method using a tensiometer (Tracker-S, Teclis, France) at 25 °C for 2,400 s. An axially symmetric drop of each solution was formed on the needle tip of a syringe inside a cuvette. The needle position inside the cuvette was adjusted aided by a computer. The drop image was monitored by a charge-coupled device camera and scanned. The surface tension was calculated through equipment software by analyzing the drop profile according to the Laplace equation.

4.2.2.2. Rheological behavior of liquid binder solutions

Shear stress curves determined the viscosity of liquid binder solutions as a function of the shear rate. The measurements were done in duplicate for each solution using a strain-controlled rheometer (AR 1500 ex, TA Instruments, England, UK) with double-wall concentric cylinders geometry constructed from aluminum (the inner radius was 15.925 mm, and the outer radius was 17.505 mm). Three flow ramps were obtained at shear rates that ranged from 0 to

300 1/s (first and third curves) and from 300 to 0 1/s (second curve) at 25 °C. Both first curves were necessary to eliminate thixotropic effects if any. The data from the third flow curve were fitted to the empirical model of Newtonian fluids (Eq. 4.1).

$$\sigma = \mu \times \gamma \hspace{4cm} 4.1$$

Where σ is shear stress (Pa), μ is the viscosity (Pa s), and γ is shear rate (1/s).

4.2.2.3. Contact angle and contact area

The CMC pellets (13 mm in diameter) were made by subjecting 200 mg of particulate material to 80 kN of force under vacuum in a hydraulic press (SSP 10A, Shimadzu, Japan) for 5 min. A drop of approximately 3 µL of each liquid binder was deposited on the surface of the solid material pellet. For better visualization, a photograph was taken of the shadow projected of the system formed by the liquid drop and the solid pellet. The angle formed between the solid-liquid interface and the liquid-air interface was defined as the contact angle. The circular area formed by the drop on the solid surface was defined as the contact area. The images were processed and analyzed by the Low Bond Axisymmetric Drop Shape Analysis method utilizing the *drop_analysis* plugin installed in the ImageJ software [26]. The wettability is inversely related to the contact angle, i.e., to angles less than 90°, the liquid spontaneously wets the solid; to angles greater than 90°, the liquid does not wet the solid, and when the angle is equal to 0°, the liquid thoroughly wets the solid surface [27].

4.2.3. Spray system

The spray system was composed of a bi-fluid nozzle (SU12A, Spraying Systems Co., USA) supplied by pressurized air and liquid from a compressor (MSV 40 MAX 10 hp, Schulz, Brazil) and a peristaltic pump (Masterflex L/S 7780-60, Cole Parmer, USA), respectively (Figure 4.1(a)). For the agglomeration tests, the nozzle was positioned inside the fluidized bed chamber in the upper position (Figure 4.1(b)). The atomizing nozzle can be shown in detail in Figure 4.1(c), and the maltodextrin solution typical spray formed at 5% w/w, 4 mL/min, and 20 psi is pictured in Figure 4.1(d).
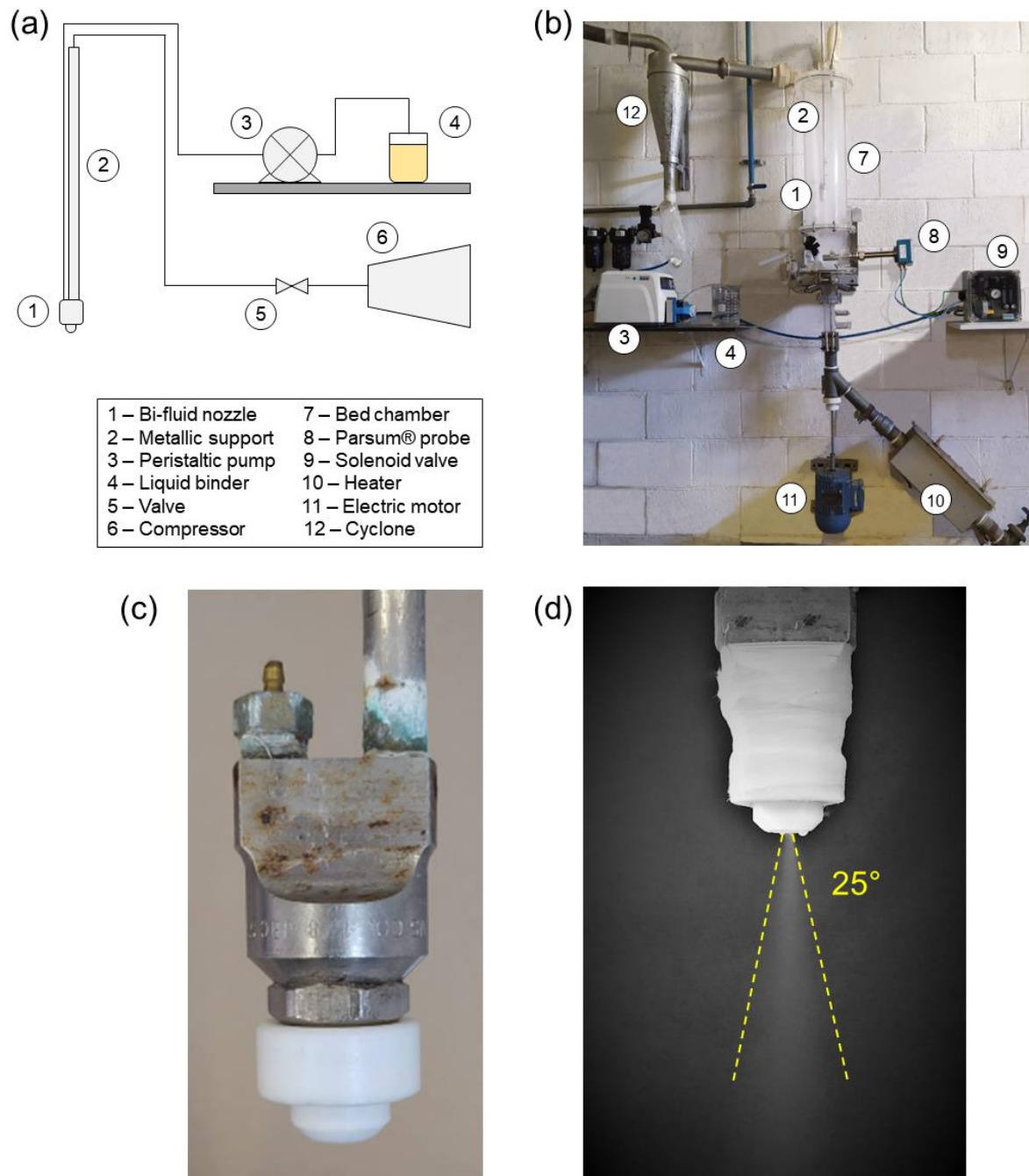
Figure 4.1: (a) spray system; (b) photo of the experimental apparatus; (c) atomizing nozzle in detail; (d) typical maltodextrin solution spray at 5% w/w, 4 mL/min, and 20 psi.

4.2.4. Droplet size and axial velocity data acquisition

The droplet size and axial velocity were monitored by Phase Doppler Interferometry (PDI) (PDI-300 MD, Artium Technologies Inc., USA). According to Bachalo et al. [28], this technique consists of the interferometric measurement of a fringe pattern produced

by the intersection of two laser beams. A single spherical droplet passes through the fringe pattern, causing light reflection or refraction and sending a Doppler signal to the photodetectors. This signal consists of a high-frequency Doppler component (f_D) superimposed on a Gaussian low frequency. The droplet velocity (v_d) is proportional to f_D and the spacing between the fringes (δ) (Eq. 4.2). In turn, δ is expressed by Eq. 4.3 and is proportional to the wavelength (λ) and the intersection angle between two laser beams (γ). A distortion in spacing between the fringes occurs when a droplet, which can be handled by a lens, passes through the interference pattern. Thus, Eq. 4.4 defines the droplet diameter (d_d) that is obtained by the relationship between δ and λ.

$$v_d = f_D \times \delta \qquad\qquad 4.2$$

$$\delta = \frac{\lambda}{2}\left(\sin\left(\frac{\gamma}{2}\right)\right)^{-1} \qquad\qquad 4.3$$

$$d_d = \frac{F\delta}{s\lambda} \qquad\qquad 4.4$$

Where F is the focal distance and s is a calibration factor (dimensionless).

In this current work, there were two laser beam emitting modules (A and B) and one receptor module (C) in the PDI system. Module A emits two laser beams arranged in orthogonal planes with 532 and 473 nm wavelengths. Module B emits a laser beam with a wavelength of 561 nm, which must be aligned to the same plane like the 473 nm laser beam. The laser beams are continuous and produced by Nd:YAG technology, with 300 mJ of power for the 532 nm laser beam and 180 mJ for the other two laser beams. The laser beams are split into two pairs of the same wavelength and aligned to respectively intersect at the focal point of module C, allowing interference fringes to form. There was a 40° angle between modules A and B. This arrangement made it possible to align the 532 nm laser beam from module A to the atomizing nozzle axial direction. Optical filters were used in the photodetector matrixes to separate the signals from beams with different wavelengths and room lighting. There was a 10 cm distance between the atomizing nozzle exit orifice and the point of intersection of the lasers. This distance was chosen by observing the region where the formation of drops in a uniform size was most constant. Higher up, there was the formation of a sheet region and, while lower down, the droplets were too small and dispersed like a fog, making it difficult to obtain accurate readings.

4.2.5. Agglomeration assays

The experimental apparatus used for agglomeration processes have already been described by Nascimento et al. [29]. A conical-cylindrical lab-scale fluidized bed was used to carry out the experiments. The acrylic bed-chamber comprised a conical base (0.075 m inlet air diameter and 0.15 m in height) and a cylindrical column (0.15 m diameter and 0.60 m in height). Andreola et al. [30] and Rosa et al. [31] described the equipment and data acquisition system in details. The Spatial Filter Velocimetry (SFV) probe (Parsum IPP 70S, Chemnitz, Germany) was used to acquire the evolution of the particle diameters in real time. Nascimento et al. [10] and Nascimento et al. [29] have already detailed their position and operating parameters.

The SFV probe is capable of measuring particle size, determined by chord length, using particle velocity, the burst signal frequency, the distance between two optical fibers, and pulse signal duration. The relationship between these parameters was defined by Langner et al. [32] and applied to the same system studied in the current work by Nascimento et al. [10]. As determined by Tyler sieves, particle size and PSD, were collected by the system and sent to the LabVIEW™ 8.16 software every 5.12 seconds using the OPC Server protocol [33]. The retained fractions (% volume) were measured and recorded over time for the following particle size classes, as previously described by Nascimento et al. [10]. Process time was expressed as a percentage of process occurrence (% process) to enable comparison between experiments of varying duration (10, 16, and 40 min).

Five experiments (Table 4.1) were carried out to evaluate the effect of the liquid binder concentration, liquid binder flow rate, and atomizing air pressure on the droplet size sprayed and, consequently, on how the spray features influence the agglomeration process and the particle enlargement. The fluidizing air temperature and velocity, particulate material load, and atomizing nozzle height were kept constant at 60 ℃, 0.12 m/s, 0.4 kg, and 0.30 m, respectively, in all assays. The execution time of each experiment (10, 16, and 40 min) varied according to the liquid binder flow rate to keep the amount of liquid inserted into the bed-chamber constant at 40 mL. Temperature, relative humidity, and pressure drop data were collected by thermoresistance (PT100, Novus, Brazil), thermo-hygrometer sensor (RHT-XS, Novus, Brazil), and differential pressure transmitter (98073–12, Cole Parmer, USA), respectively. The accessories positions were also described by Nascimento et al. [10].

Table 4.1: Experimental operating parameters, levels, mean droplet size d_m, and mean particle size $D50v$.

Assay	Liquid binder concentration (% w/w)	Liquid binder flow rate (mL/min)	Atomizing air pressure (psi)	d_m (µm)	$D50v$ (µm)
E1	5.0	1.0	20.0	34.85 ± 0.20^a	354.5 ± 9.9^{ab}
E2	35.0	1.0	20.0	40.63 ± 0.73^b	378.3 ± 8.6^c
E3	5.0	4.0	20.0	41.10 ± 0.48^b	336.5 ± 10.6^d
E4	5.0	1.0	10.0	38.74 ± 0.39^c	355.8 ± 3.7^a
E5	20.0	2.5	15.0	35.01 ± 0.06^a	344.6 ± 4.2^{bd}

Data are expressed as mean ± standard deviation. According to Tukey's test, values in a column with the same letter were not significantly different (p < .05).

4.3. RESULTS AND DISCUSSION

4.3.1. Liquid binder characterization

The liquid binder solutions were characterized by surface tension, viscosity, and contact angle. The contact area determined due to the contact angle analysis was also presented. The solutions were named *MD5*, *MD20*, and *MD35*, indicating the concentration of maltodextrin in each solution, 5%, 20%, and 35% w/w, respectively. These results are summarized in Table 4.2.

Table 4.2: Maltodextrin solutions characterization.

	MD5	MD20	MD35
Surface tension (mN/m)	29.9 ± 0.7^a	32.5 ± 0.9^b	43.5 ± 1.3^c
Viscosity (Pa s)	0.0016 ± 0.0006^a	0.0050 ± 0.0006^b	0.0270 ± 0.0007^c
Contact angle (°)	41.5 ± 3.4^a	46.8 ± 0.7^a	67.9 ± 3.2^b
Contact area (mm²)	0.066 ± 0.047^a	0.081 ± 0.004^a	0.060 ± 0.004^a

Data are expressed as mean ± standard deviation. According to Tukey's test, values in a line with the same letter were not significantly different (p < .05).

The surface tension increased as the maltodextrin concentration increased. It relates to the increased attraction forces between the water and the maltodextrin.

The rheological behavior for the *MD5*, *MD20*, and *MD35* is presented in Figure 4.2(a). The viscosity increased based on the concentration (Table 4.2). The non-linear behavior close to zero shear rates is associated with the equipment sensitivity limitations. Solutions exhibit a Newtonian behavior in the range of concentrations studied (Figure 4.2(b)) since the empirical Newtonian model firmly fit to the data ($R^2 = 0.98$, $R^2 = 0.99$, and $R^2 = 0.99$ for *MD5*,

MD20, and *MD35* data, respectively). Similar results were found by Dokic et al. [34] and Loret et al. [35].
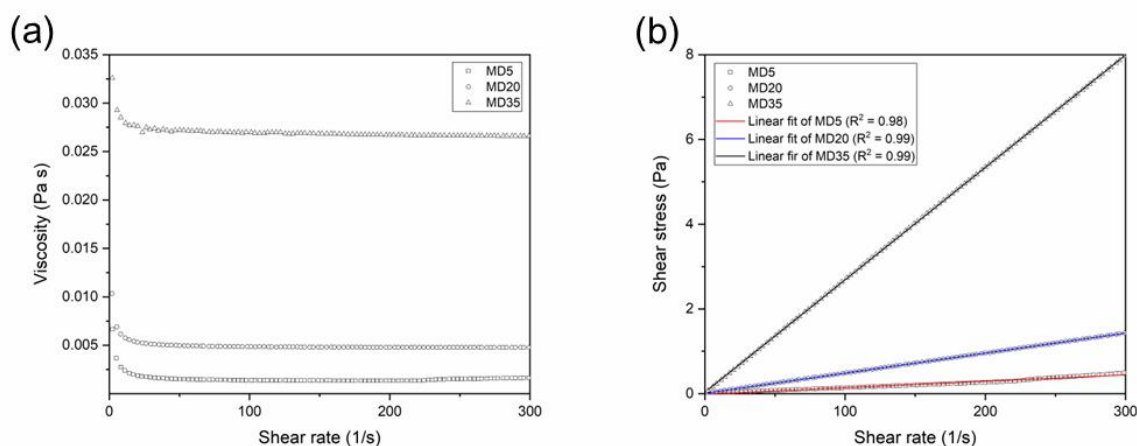
Figure 4.2: (a) rheological behavior and (b) flow curves with respective linear fit to the *MD5*, *MD20*, and *MD35* solutions.

The contact angle between the CMC pellet and maltodextrin solutions was measured to determine the solid material wettability and the liquid-solid contact area, i.e., the more the liquid wets the solid surface, the larger the footprint is left by the liquid on the solid. The solutions presented contact angles numerically directly proportional to the concentration, although there is no significant difference between the contact angles of *MD5* and *MD20* solutions. However, the most notable is that all angles were smaller than 90°, indicating that the liquid spontaneously wets the solid. Regarding the contact area, there is no significant difference in the three cases, implying that the footprint marked on the solid surface is the same size as the analyzed concentration range.

4.3.2. Influence of operating parameters on droplets formation

A characteristic scatter plot of all detected droplets for assay *E1* is shown in Figure 4.3. The most detected droplets are in a size range from 0 to 75 µm. The distributed droplet velocity range for those is from 0 to 125 m/s. There is a large concentration of tiny droplets, mainly up to 30 µm, and their velocities are in all analyzed ranges. However, the highest occurrence of droplets (about 80%) varies from 11 to 33 µm and velocities from 10 to 74.55 m/s. The velocities decreased for droplets with diameters ranging from 33 µm to 75 µm, and

the remaining ranged from 10 to 50 m/s. The number of droplets represents about 20% of the total in that region. After that, some droplets were 175 µm in size, and velocities were around 20, 25, 50, and 85 m/s. These last drops cannot represent the spraying behavior since they seem derived from inconsistencies in the measurements compared to the droplets being examined.
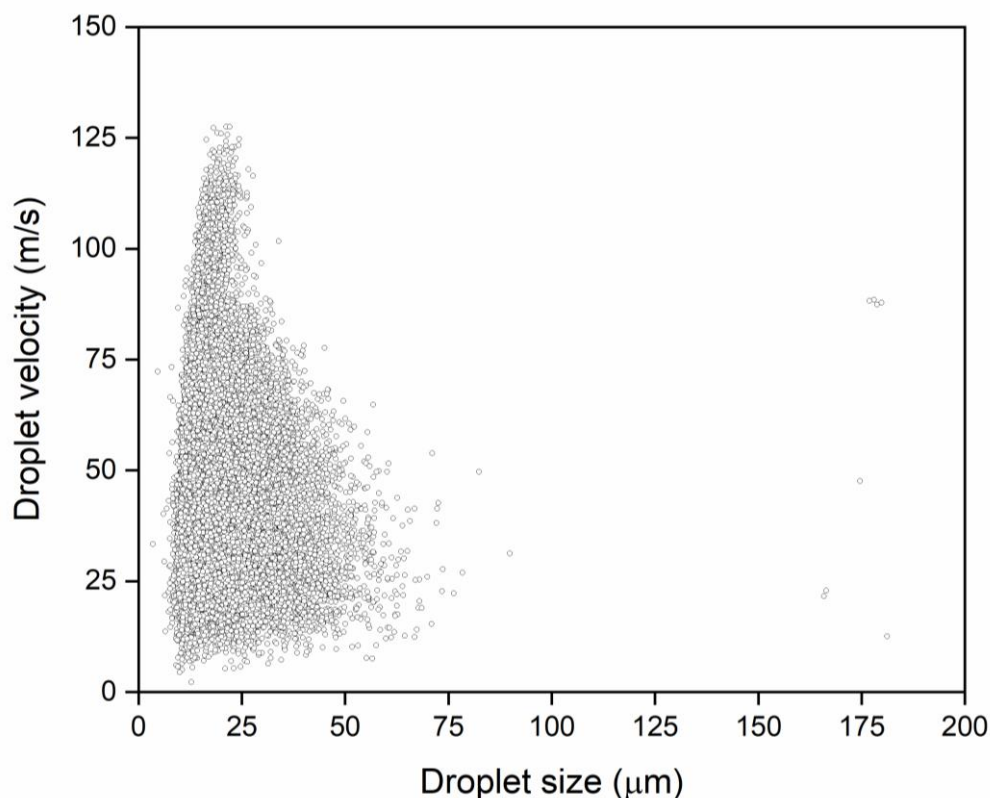
Figure 4.3: Scatter plot and for assay *E1* (*C* = 5.0 % w/w; *Q* = 1.0 mL/min; *P* = 20.0 psi).

The *E2*, *E3*, *E4*, *E5* assay data obtained from the PDI system are presented in Figure 4.4. For these conditions, the velocity distribution based on a function of droplet size displayed similar behavior as assay *E1*, i.e., there is a large number of small-sized droplets up to 50 µm with velocities reaching about 100 m/s (assays *E4* and *E5*) to a little more than 125 m/s (assays *E2* and *E3*). As for assay *E1*, most droplets occurred in a narrow size range. According to what was found in this current work, 80% of the total droplets moved at velocities from 10 to 75 m/s in all cases. It was expected that big droplets move at high and constant velocities; however, in the current work, the opposite behavior occurs, i.e., the big droplets (especially those larger than 50 µm) are concentrated in a velocity range of around 50 m/s or less. It is essential to clarify that the distance they were measured significantly impacts the velocity results. The further away the atomizing nozzle exit is, the more air resistance effect is observed, which

causes a deceleration of the droplets. In other words, tiny droplets are stopped faster than large ones due to air drag [36–39].
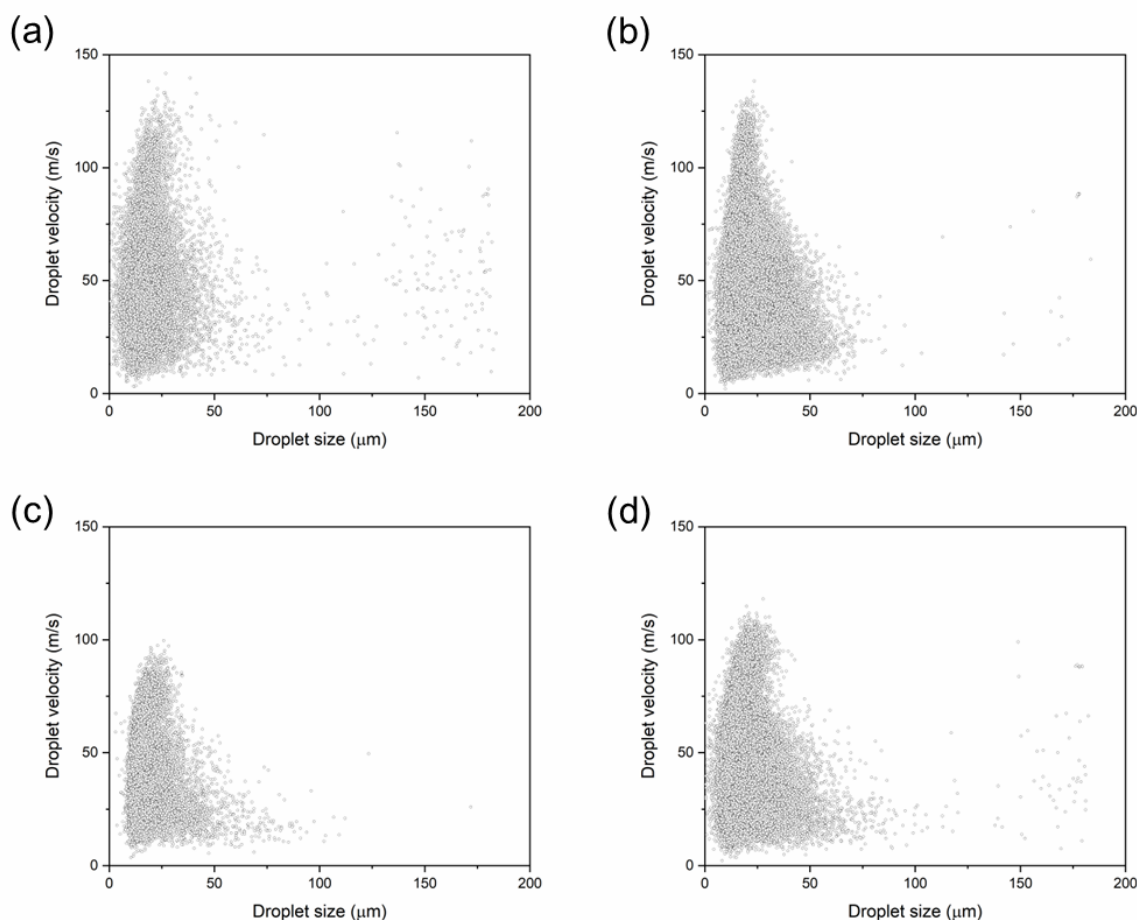
Figure 4.4: Scatter plot for (a) assay *E2* (*C* = 35.0 % w/w; *Q* = 1.0 mL/min; *P* = 20.0 psi), (b) assay *E3* (*C* = 5.0 % w/w; *Q* = 4.0 mL/min; *P* = 20.0 psi), (c) assay *E4* (*C* = 5.0 % w/w; *Q* = 1.0 mL/min; *P* = 10.0 psi), and (d) assay *E5* (*C* = 20.0 % w/w; *Q* = 2.5 mL/min; *P* = 15.0 psi).

Figure 4.5 shows the cumulative DSD for each one of the assays. All experiments have droplets reaching at least 50 µm, except that *E2* shows droplets close to 100 µm. Notably, the liquid binder concentration was the highest in assay *E2*. The shape of the cumulative DSD curve is evident in assay *E2* and achieves higher size values when comparing the cumulative DSD (Figure 4.5) to the scatter plot size in (Figure 4.4). Nonetheless, the same should occur with the cumulative DSD curve of assays *E3* and *E5* since these droplets are larger than 150 µm (Figure 4.4). In this case, there may have been a misunderstanding regarding the PDI measures, indicating these large droplets are not actual measurements. It happens because the signal can undergo a trajectory effect, and the unavoidable slit effect causes system errors [40]. Droplets larger than the sample volume diameter can reflect rather than refract the light, leading

to inaccurate size calculations [41]. Also, the volume fraction of the large droplets is very low compared to the total volume, and then this amount does not appear in the DSD, or it is practically null.
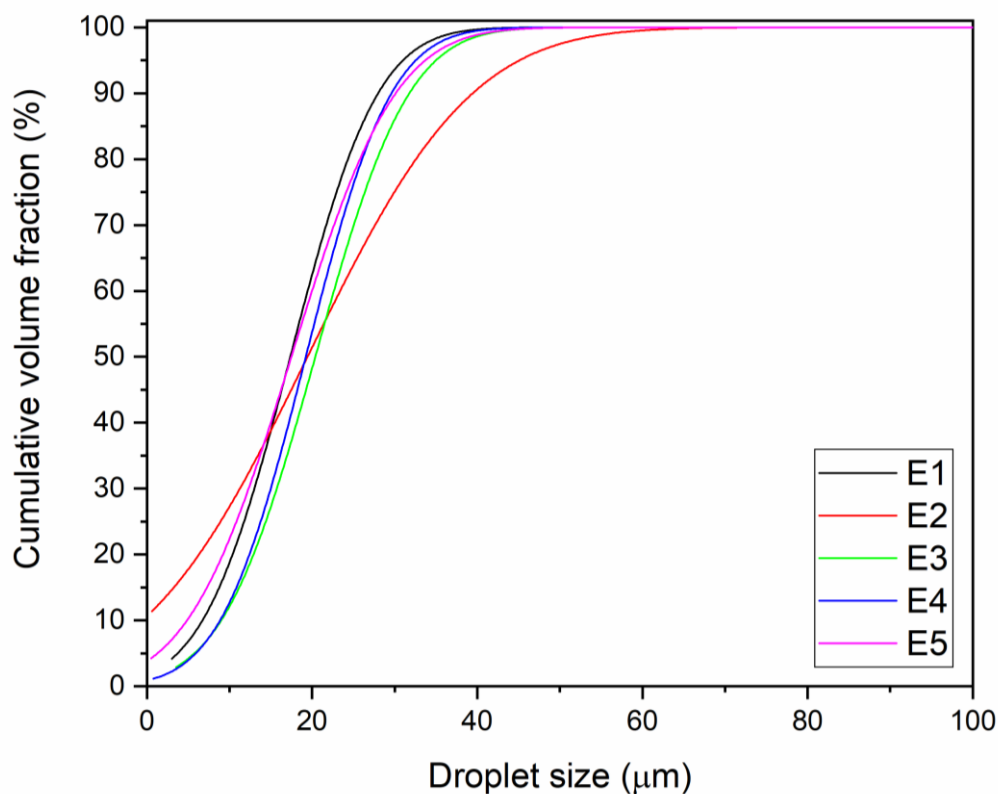
Figure 4.5: Cumulative droplet size distribution for each assay.

Figure 4.5 also displays that most droplet volume fractions presented size values from 20 to 25 µm in all assays. It is possible to note the proximity of the values of d_{10}, d_{50}, and d_{90} for each assay.

The most critical liquid properties influencing the droplet size are viscosity, liquid density, and surface tension [15,16]. These parameters are closely linked to the solution concentration. Process parameters such as liquid flow rate and atomization pressure influence the droplet size. Generally, by lowering both liquid flow rate and solution concentration and increasing atomization pressure, there is a trend of smaller droplet formation [42–44]. This way, assay *E1* was carried out under these conditions and the others assays varied the parameters one-by-one and compared to the assay *E1*. Finally, assay *E5* was executed under mild conditions (Table 4.1).

To verify the effect of solution concentration, the medium sizes for assay *E1* (5.0% maltodextrin) were around 15% smaller than the medium sizes for assay *E2* (35.0% maltodextrin). Higher maltodextrin concentrations implied higher liquid density, surface tension, and viscosity (Table 4.2). This finding abides by the results obtained by Hede et al. [15], Ehlers et al. [19], and Müller and Kleinebudde [45]. The researchers found a directly proportional effect of solution concentration on the droplet size, adhering with the general understanding of the effect of the solution's physicochemical properties on droplet size.

The effect of the solution flow rate was like what was observed in the solution concentrations, as the medium droplet size in assay *E3* (5.0% maltodextrin and 4.0 mL/min) reached values akin to assay *E2* (35.0% maltodextrin and 1.0 mL/min). The percentage increase related to assay *E1* was comparable to what was described above. Lefebvre [16] reported an association between solution flow rate and droplet size by employing the air/liquid mass ratio. The author affirms that a reduction in air/liquid mass ratio causes an increase in droplet size. This conclusion can be applied to this current work, as the air mass was kept constant, and the liquid mass was increased by increasing the liquid flow rate (implying a decreased air/liquid mass ratio). A smaller amount of air compared to the liquid hinders overcoming the viscous and surface tension forces, which jointly interact and interfere with the formation of drops. Excessive air (increase in air/liquid mass ratio) is also not advantageous to forming droplets since the sheet region becomes too large to disintegrate appropriately. Ideally, air/liquid mass ratio values could range from 3 to 5, however, without additional gain for values close to the upper limit [16].

The effect of pressure was the least prominent of the three analyzed parameters. Comparing the assay *E1* (20 psi) to assay *E4* (10 psi), around an 8% variation was noted in the medium size of droplets. Hede et al. [15] have already disclosed an inverse relationship between atomization air pressure and droplet size. This behavior was confirmed by Ehlers et al. [19] and Mueller and Womac [46].

The droplet sizes were close to the *E1* in mild conditions (assay *E5*), as there was no significant difference between them. The joint variation of the analyzed factors appears not to influence the droplet size. That is, the positive change in size caused by the flow rate and concentration of the liquid would be counterbalanced by the negative change caused by the air pressure.

4.3.3. Influence of droplet size on agglomeration process

Some authors have been defining agglomeration as a process in which a solid system is continuously wetted and dried so that the fine primary particles unite and form semi-permanent structures named granules [1,2,6,47]. Furthermore, growth only occurs when there is enough liquid to establish bridges or when liquid saturation is enough to increase the plastic deformation of the agglomerates [5,7]. When the authors list the steps of the agglomeration process in the most recent theories, their explanation starts with wetting. In other words, the wetting step is the starting point without which the agglomeration process does not occur [1,6,10,48,49]. Thus, it is noteworthy that the liquid binder features and their relationship to the solid system are essential for the agglomeration process.

Agglomeration experiments were carried out under the conditions described in Table 4.1. The particle size value expressed by *D50v* (Table 4.1) corresponds to the mean of the last ten measurements performed by the SFV probe. All assays provided particle enlargement compared to the raw material particle size (295.95 µm), from 336.49 µm to 378.34 µm, corresponding to an increased size range of 13.7% and 27.8%. After the agglomeration process and then defining assay *E1* as the experimental basis, the ranking of the particle sizes was *E2 > E4 > E5 > E3*. This classification indicates that the solution concentrations, followed by atomizing air pressure and solution flow rates, are the operating parameters that most impact the particle size in the fluidized bed agglomeration process under the experimental conditions performed in this current work.

These agglomeration operating parameters have been broadly investigated in the fluidized bed process over the years and using the most diverse raw material and binder solutions. In our previous work [10], investigating the agglomeration of CMC with maltodextrin solutions, we also concluded that the solution concentrations were the main parameter that influenced the process. Dacanal and Menegalli [50] also demonstrated the relevance of solution concentration in the agglomeration process of soy protein isolate and maltodextrin solution, as well as Andreola et al. [30] with rice protein concentrate agglomerated by glucomannan solution.

The solution flow rate was also reported as a key factor for powder agglomeration, for example, in a process involving pea protein isolate with gum Arabic solution [51], hydrolyzed collagen with blackberry pulp [52], gum Arabic with water [31], rice protein concentrates with glucomannan solution [30], and soy protein isolates with CMC [53].

However, the influence of atomization air pressure on particle size is a less studied operational parameter. Jiménez et al. [54] described atomizing air pressure analysis combined with other factors to delineate thermal zones and particle growth during agglomeration. Pathare et al. [55] evaluated the atomizing air pressure to produce granola breakfast cereal by the fluidized bed in a technological approach.

The evolution of particle classes can be seen in Figure 4.6 according to the classification delimited by Nascimento et al. [10]. The experiments were monitored the entire time by the SFV probe, and the data were divided into three classes: Class I represents fine particles with $D50v < 300$ µm, Class II represents the intermediate particles with 300 µm $< D50v < 600$ µm, and Class III represents the coarse particles with $D50v > 600$ µm.
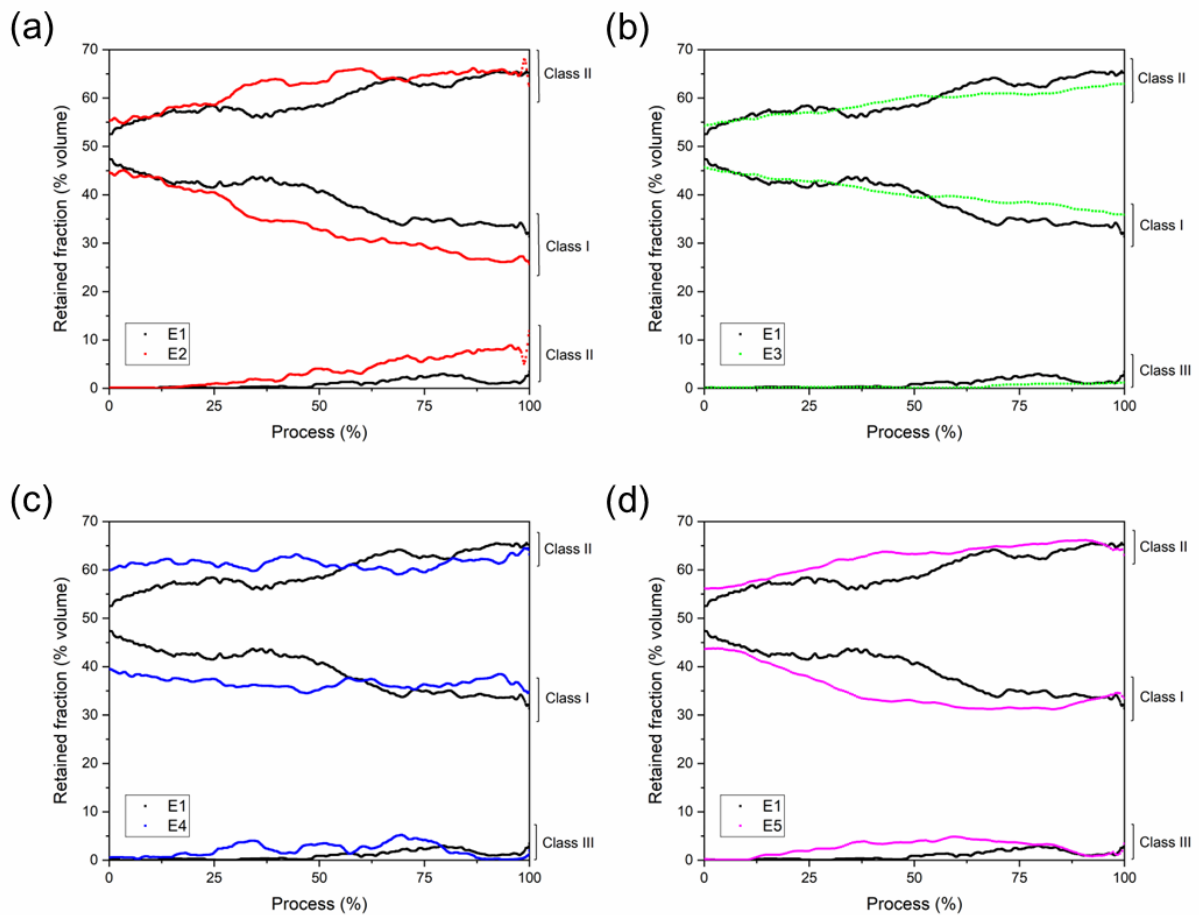
Figure 4.6: Evolution of particle classes. The black lines represent assay *E1* (base experiment; $C = 5.0$ % w/w, $Q = 1.0$ mL/min, $P = 20.0$ psi). Assay *E1* was compared to (a) assay *E2* (red lines, $C = 35.0$ % w/w, $Q = 1.0$ mL/min, $P = 20.0$ psi), (b) assay *E3* (green lines, $C = 5.0$ % w/w, $Q = 4.0$ mL/min, $P = 20.0$ psi), (c) assay *E4* (blue lines, $C = 5.0$ % w/w, $Q = 1.0$ mL/min, $P = 10.0$ psi), and (d) assay *E5* (pink lines, $C = 20.0$ % w/w, $Q = 2.5$ mL/min, $P = 15.0$ psi).

Perhaps, the primordial fact is the emergence of Class III based on the particle class classification since this is linked to the appearance of the larger particles. According to Nascimento et al. [10], this point indicates the beginning of phase 3, named Coalescence and Growth. Regarding assay *E1*, this phase starts after concluding around 50% of the process, i.e., until that point, the particles were properly wetted and sufficiently available for nuclei formation. After nearly 80% of the process, the assay *E1* particles size experienced a slight drop, observed by a decrease in Class III retained fraction and an increase in Class II retained fraction.

By comparing assay *E1* to assay *E2* (Figure 4.6), the binder concentrations were 5.0% and 35.0%, respectively, and the behavior of the particle classes evolution was similar from 0% to 20% of the process. However, in assay *E2*, there was an increase in the coarse particles after 20% of the process. The change in maltodextrin concentration from 5% to 35% w/w caused the start of the growth phase to be continued and reach 30%. Additionally, throughout the process, the number of fine particles for assay *E2* was always lower than in assay *E1*, indicating increased progress in the process when agglomeration was carried out using a liquid binder containing 35.0% of maltodextrin.

Iveson et al. [56] emphasized that the key factor for growth occurrence is the degree of binder dispersion in the powder on a microscale. In the case of this current work, where the droplet size is smaller than the particle size, the growth mechanisms are governed by a layering of a binder-granule by small fine particles. For that reason, it is primordial that there is some binder between two particles at the point of contact. Increasing the binder concentration also increases the formulation dynamic rupture stress, which is related to the increase in surface tension. Also, the granules will become stronger and less deformable as the bond strength between two granules increases during a collision, leading to a higher probability of permanent coalescence.

There is a crushing of the deformable particle surface in less concentrated solutions, and the growth of layers dampens the collision between the granules and does not favor granulation. The relationship is a little more complex regarding the increased viscosity related to increasing binder concentration because there are three key-role processes involved in the granulation rate: binder dispersion, consolidation, and growth. The increase in viscosity is promoted by higher concentration concerning the distribution of the binder that can inhibit atomization and dispersion. Hence, there is probable formation of larger droplets that lead to the formation of larger initial nuclei, which may take longer to disperse evenly through the

powder bed, delaying the start of growth and reducing the consolidation rate. On the other hand, the granules' strength is increased. Coalescence is more likely to be favored once the more viscous binder reaches the particle surface since the collision kinetic energy dissipation is more effective. It reduces pore saturation and the contact area formed during collisions [1,56]. In the case of assays *E1* and *E2*, the decrease in the appearance time of Class III is due to a more significant influence of the binder tension forces on the viscous forces since the positive result of the coalescence in a shorter process time in the case of the assay *E2* was due to the increase in the concentration of binder and consequent increase in surface tension.

Regarding assay *E3* (Figure 4.6(b)), carried out at a higher flow rate (4.0 mL/min) compared to assay *E1* (1.0 mL/min), the appearance of coarse particles occurred after at least 70% of the process, and the evolution of the other classes was practically constant. The retained volume fraction of fine particles varied from 45% to 32% from the beginning until the end of the process, while for intermediate particles, from 55% to 68%. The appearance and maintenance of coarse particles were brief, unable to preserve the formed agglomerates. There was probably a breakage balance that surpassed the formation of stable granules. The same can be inferred from assay *E4* (Figure 4.6(c)), which was carried out at higher air atomization pressure (10 psi) compared to what was used by assay *E1* (20 psi). There was a slight variation in the classes throughout the process, and the classes remained almost constant. This result indicates that the change in pressure level did not provide favorable conditions for the particles to go through the wetting and nucleation phases.

The increased amount of liquid binder, expressed by the high flow rate, increases the maximum pore saturation and the growth rate but not the nature of the growth. In systems with induction growth, as appears to be the case with the assay *E3*, there is a long period of little or no growth, followed by a period of slight growth. Increasing the binder content in systems with slow consolidation generally shortens the duration of the induction period [56]. However, in comparing assays *E1* and *E3*, the increase in the amount of liquid binder extended the induction period. That seems to have happened as the growth did not go beyond the nucleation phase due to the low rate of Class III appearance. Initially, the granules do not deform enough to coalesce during impact. However, as time passed, they slowly consolidated, and if the liquid binder is compressed onto their surfaces, rapid coalescence growth occurs. Probably, compressing the binder on the deformable particle surface was ineffective.

In constant growth systems, the granule growth rate increases rapidly as the binder content increases, which can be observed by comparing assays *E1* and *E4*. The increased

atomization pressure enhances the wetting efficiency of the liquid on the particulate bed. Wet granules tend to be more easily deformable due to reduced interparticle forces, have lower coefficients of restitution, and have more binder availability on their surfaces, which aids in coalescence growth. Increasing the liquid content by adjusting the operating process conditions reduces the amount of consolidation required for the granules to become saturated and generally improves the consolidation rate [56].

In the case of assay *E5* (Figure 4.6(d)), the mild conditions provide an interesting particle class evolution. There was the appearance of coarse particles in nearly 12.5% of the process, but the operating conditions could not maintain the positive development of Class III. Using milder process conditions would be an interesting alternative for saving energy or materials. Still, as seen, such conditions were not enough for the granules to remain stable and intact until the end of the process.

As in assay E5, the mild conditions promoted droplet formation and granulation similar to assay *E1*. The operating parameter levels at which these two assays were performed likely led to the so-called crumb behavior [56], which occurs when the binder formulation is too weak to form permanent granules, but instead forms enough deformable material to cushion the larger granules collisions which are constantly being broken down and remade. In this case, the particle surface saturation by the liquid portion occurs so that the wet particles are not energetically available to remain bound but to bounce back the other particles when they collide.

The concentration of the binder liquids is undoubtedly the most outstanding to be considered in the agglomeration process, among the factors studied. This is mainly because there are intrinsic physicochemical properties for solutions that must be considered and also how these solutions will relate to the solid material during the process.

4.4. CONCLUSIONS

This study explored the effects of process variables and physicochemical properties of a liquid binder on solid particle growth in fluidized bed agglomeration. The influence of solution viscosity (from 0.0016 to 0.0270 Pa s), surface tension (from 29.9 to 43.5 N/m), and contact angle (from 41.5° to 67.9°) were investigated. Additionally, the effect of liquid binder

concentration, flow rate, and atomization air pressure on droplet formation and solid particle agglomeration was examined.

The results indicate that surface tension and viscosity are crucial physicochemical properties of maltodextrin solutions for droplet formation and CMC agglomeration. The contact angle between the solutions and the CMC pellet was less than 90°, indicating that the solutions spontaneously wetted the solid. This spontaneous wetting of the solid material surface suggests that the formation of a wet and sticky layer around the particle is favored.

The PDI system was able to measure the droplet size and velocity. The data analysis indicated that tiny droplets moved at low velocities, up to 75 m/s. Even though large droplets are more likely to move at higher velocities, in this case, they moved at lower velocities than tiny droplets, a fact associated with the measurement execution distance.

Regarding droplet formation, binder solution concentration, and flow rate were the most significant parameters affecting droplet size growth, while atomizing air pressure displayed a lesser impact under the analyzed conditions. However, in the fluidized bed agglomeration process, the operating parameter that displayed the most significant influence on particle size was, in order of importance, solution concentration, atomizing air pressure, and solution flow rate. Thus, particle size growth in fluidized bed agglomeration processes depends on the particulate material and the properties of the binder liquid. Understanding the spray system is crucial for analyzing this process.

ACKNOWLEDGMENTS

FUNDINGS

REFERENCES

[1] Iveson, S.M., Litster, J.D., Hapgood, K., Ennis, B.J., 2001. Nucleation, growth and breakage phenomena in agitated wet granulation processes: a review. Powder Technol. 117(1–2), 3–39. https://doi.org/10.1016/S0032-5910(01)00313-8.

[2] Iveson, S.M., Litster, J.D., 1998. Growth regime map for liquid-bound granules. AlChE J. 44(7), 1510–1518. https://doi.org/10.1002/aic.690440705.

[3] Litster, J.D., Hapgood, K.P., Michaels, J.N., Sims, A., Roberts, M., Kameneni, S.K., Hsu, T., 2001. Liquid distribution in wet granulation: dimensionless spray flux. Powder Technol. 114(1–3), 32–39. https://doi.org/10.1016/S0032-5910(00)00259-X.

[4] Avilés-Avilés, C., Dumoulin, E., Turchiuli, C., 2015. Fluidised bed agglomeration of particles with different glass transition temperatures. Powder Technol. 270, 445–452. https://doi.org/10.1016/j.powtec.2014.03.026.

[5] Lipps, D.M., Sakr, A.M., 1994. Characterization of wet granulation process parameters using response surface methodology. 1 Top-spray fluidized bed. J. Pharm. Sci. 83(7), 937–947. https://doi.org/10.1002/jps.2600830705.

[6] Tardos, G.I., Khan, M.I., Mort, P.R., 1997. Critical parameters and limiting conditions in binder granulation of fine powders. Powder Technol. 94(3), 245–258. https://doi.org/10.1016/S0032-5910(97)03321-4.

[7] Pont, V., Saleh, K., Steinmetz, D., Hémati, M., 2001. Influence of the physicochemical properties on the growth of solid particles by granulation in fluidized bed. Powder Technol. 120(1–2), 97–104. https://doi.org/10.1016/S0032-5910(01)00355-2.

[8] Butensky, M., Hyman, D., 1971. Rotary drum granulation. An experimental study of the factors affecting granule size. Ind. Eng. Chem. Fundam. 10(2), 212–219. https://pubs.acs.org/doi/pdf/10.1021/i160038a005.

[9] Heim, A., Antkowiak, W., 1988. A mathematical model for granulation kinetics. Chem. Eng. Sci. 43(7), 1447–1456. https://doi.org/10.1016/0009-2509(88)85136-4.

[10] Nascimento, R.F., Ávila, M.F., Taranto, O.P., Kurozawa, L.E., 2021. A new approach to the mechanisms of agglomeration in fluidized beds based on Spatial Filter Velocimetry measurements. Powder Technol. 393, 219–228. https://doi.org/10.1016/j.powtec.2021.07.076.

[11] Sastry, K.V.S., 1975. Similarity size distribution of agglomerates during their growth by coalescence in granulation or green pelletization. Int. J. Miner. Process. 2(2), 187–203. https://doi.org/10.1016/0301-7516(75)90021-6.

[12] Sastry, K.V.S., Fuerstenau, D.W., 1973. Mechanisms of agglomerate growth in green pelletization. Powder Technol. 7(2), 97–105. https://doi.org/10.1016/0032-5910(73)80012-9.

[13] Scott, A.C., Hounslow, M.J., Instone, T., 2000. Direct evidence of heterogeneity during high-shear granulation. Powder Technol. 113(1–2), 205–213. https://doi.org/10.1016/S0032-5910(00)00354-5.

[14] Simons, S.J.R., Fairbrother, R.J., 2000. Direct observations of liquid binder–particle interactions: the role of wetting behaviour in agglomerate growth. Powder Technol. 110(1–2), 44–58. https://doi.org/10.1016/S0032-5910(99)00267-3.

[15] Hede, P.D., Bach, P., Jensen, A.D., 2008. Two-fluid spray atomisation and pneumatic nozzles for fluid bed coating/agglomeration purposes: A review. Chem. Eng. Sci. 63(14), 3821–3842. https://doi.org/10.1016/j.ces.2008.04.014.

[16] Lefebvre, A.H., 1980. Airblast atomization. Prog. Energy Combust. Sci. 6(3), 233–261. https://doi.org/10.1016/0360-1285(80)90017-9.

[17] Duangkhamchan, W., Ronsse, F., Depypere, F., Dewettinck, K., Pieters, J.G., 2012. CFD study of droplet atomisation using a binary nozzle in fluidised bed coating. Chem. Eng. Sci. 68(1), 555–566. https://doi.org/10.1016/j.ces.2011.10.022.

[18] Hede, P.D., Bach, P., Jensen, A.D., 2009. Batch top-spray fluid bed coating: scale-up insight using dynamic heat- and mass-transfer modelling. Chem. Eng. Sci. 64(6), 1293–1317. https://doi.org/10.1016/j.ces.2008.10.058.

[19] Ehlers, H., Larjo, J., Antikainen, O., Räikkönen, H., Heinämäki, J., Yliruusi, J., 2010. In situ droplet size and speed determination in a fluid-bed granulator. Int. J. Pharm. 391(1–2), 148–154. https://doi.org/10.1016/j.ijpharm.2010.02.033.

[20] Seo, A., Holm, P., Shaefer, T. 2002. Effects of droplet size and type of binder on the agglomerate growth mechanisms by melt agglomeration in a fluidised bed. Eur. J. Pharm. Sci. 16(3), 95–105. https://doi.org/10.1016/S0928-0987(02)00086-6.

[21] Abberger, T., Seo, A., Schaefer, T., 2002. The effect of droplet size and powder particle size on the mechanisms of nucleation and growth in fluid bed melt agglomeration. Int. J. Pharm. 249, 185–197. https://doi.org/10.1016/S0378-5173(02)00530-6.

[22] Moraga, S.V., Villa, M.P., Bertín, D.E., Cotabarren, I.M., Piña, J., Pedernera, M., Bucalá, V. 2015. Fluidized-bed melt granulation: The effect of operating variables on process performance and granule properties. Powder Technol. 286, 654–667. https://doi.org/10.1016/j.powtec.2015.09.006.

[23] Hemati, M., Cherif, R., Saleh, K., Pont, V, 2003. Fluidized bed coating and granulation: influence of process-related variables and physicochemical properties on the growth kinetics. Powder Technol. 130, 18–34. https://doi.org/S0032-5910(02)00221-8.

[24] Tan, H.S., Salman, A.D., Hounslow, M.J., 2006. Kinetics of fluidised bed melt granulation I: The effect of process variables. Chem. Eng. Sci. 61(5), 1585–1601. https://doi.org/10.1016/j.ces.2005.09.012.

[25] Kan, H., Nakamura, H., Watano, S., 2017. Effect of droplet size on particle-particle adhesion of colliding particles through droplet. Powder Technol. 321, 318–325. https://doi.org/10.1016/j.powtec.2017.08.045.

[26] Stalder, A.F., Kulik, G., Sage, D., Barbieri, L., Hoffmann, P., 2006. A snake-based approach to accurate determination of both contact points and contact angles. Colloids Surf., A 286(1–3), 92–103. https://doi.org/10.1016/j.colsurfa.2006.03.008.

[27] Thakker, M., Karde, V., Shah, D.O., Shukla, P., Ghoroi, C., 2013. Wettability measurement apparatus for porous material using the modified Washburn method. Meas. Sci. Technol. 24(12), 125902. https://doi.org/10.1088/0957-0233/24/12/125902.

[28] Bachalo, W.D., 1980. Method for measuring the size and velocity of spheres by dual-beam light-scatter interferometry. Appl. Opt. 19(3), 363–370. https://doi.org/10.1364/AO.19.000363.

[29] Nascimento, R.F., Rosa, J.G., Ávila, M.F., Taranto, O.P., 2020. Pea protein isolate fluid dynamics and characterization obtained by agglomeration in pulsed fluidized bed. Part. Sci. Technol. 39(7), 809–819. https://doi.org/10.1080/02726351.2020.1830209.

[30] Andreola, K., Silva, C.A.M., Taranto, O.P., 2018. Agglomeration process of rice protein concentrate using glucomannan as binder: in-line monitoring of particle size. Chem. Eng. Res. Des. 135, 37–51. https://doi.org/10.1016/j.cherd.2018.05.019.

[31] Rosa, J.G., Nascimento, R.F., Andreola, K., Taranto, O.P., 2020. Acacia gum fluidized bed agglomeration: Use of inulin as a binder and process parameters analysis. J. Food Process Eng. 43(7), e13409. https://doi.org/10.1111/jfpe.13409.

[32] Langner, M., Kitzmann, I., Ruppert, A.L., Wittich, I., Wolf, B. (2020). In-line particle size measurement and process influences on rotary fluidized bed agglomeration, Powder Technol. 364, 673–67. http://doi.org/10.1016/j.powtec.2020.02.034.

[33] Silva, C.A.M., Taranto, O.P. 2015. Real-time monitoring of gas-solid fluidized-bed granulation and coating process: evolution of particle size, fluidization regime transitions, and psychometric parameters, Drying Technol. 33, 1929–1948. http://doi.org/10.1080/07373937.2015.1076000.

[34] Dokic, P., Jakovljevic, J., Dokic-Baucal, L., 1998. Molecular characteristics of maltodextrins and rheological behaviour of diluted and concentrated solutions. Colloids and Surf., A 141(3), 435–440. https://doi.org/10.1016/S0927-7757(97)00118-0.

[35] Loret, C., Meunier, V., Frith, W.J., Fryer, P.J., 2004. Rheological characterisation of the gelation behaviour of maltodextrin aqueous solutions. Carbohydr. Polym. 57(2), 153–163. https://doi.org/10.1016/j.carbpol.2004.03.026.

[36] Dombrowski, N., Johns, W.R., 1963. The aerodynamic instability and disintegration of viscous liquid sheets. Chem. Eng. Sci. 18(3), 203–214. https://doi.org/10.1016/0009-2509(63)85005-8.

[37] Goering, C.E., Bode, L.E., Gebhardt, M.R., 1972. Mathematical modeling of spray droplet deceleration and evaporation. Transactions of the ASAE 15(2), 220–225. https://doi.org/10.13031/2013.37871.

[38] Nuyttens, D., de Schampheleire, M., Verboven, P., Brusselman, E., Dekeyser, D., 2009. Droplet size and velocity characteristics of agricultural sprays. Trans. ASABE 52(5), 1471–1480. https://doi.org/10.13031/2013.29127.

[39] Sidahmed, M.M., Brown, R.B., Darvishvand, M., 1999. Drop-size/velocity correlations at formation of sprays from fan nozzles. Transactions of the ASAE 42(6), 1557–1564. https://doi.org/10.13031/2013.13320.

[40] Bachalo, W.D., Houser, M.J., 1984. Phase/Doppler spray analyzer for simultaneous measurements of drop size and velocity distributions. Opt. Eng. 23(5), 235583. https://doi.org/10.1117/12.7973341.

[41] Tuck, C.R., Butler Ellis, M.C., Miller, P.C.H., 1997. Techniques for measurement of droplet size and velocity distributions in agricultural sprays. Crop Prot. 16(7), 619–628. https://doi.org/10.1016/S0261-2194(97)00053-7.

[42] Chigier, N.A., 1979. The atomization and burning of liquid fuel sprays. Energy and Combustion Science 21, 183–200. https://doi.org/10.1016/B978-0-08-024780-9.50014-9.

[43] Nguyen, D.A., Rhodes, M.J., 1998. Producing fine drops of water by twin-fluid atomisation. Powder Technol. 99(3), 285–292. https://doi.org/10.1016/S0032-5910(98)00125-9.

[44] Petit, J., Méjean, S., Accart, P., Galet, L., Schuck, P., le Floch-Fouéré, C., Delaplace, G., Jeantet, R., 2015. A dimensional analysis approach for modelling the size of droplets formed by bi-fluid atomisation. J. Food Eng. 149, 237–247. https://doi.org/10.1016/j.jfoodeng.2014.10.022.

[45] Müller, R., Kleinebudde, P., 2008. Comparison study of laboratory and production spray guns in film coating: effect of pattern air and nozzle diameter. Pharm. Dev. Technol. 11(4), 425–433. https://doi.org/10.1080/10837450600770205.

[46] Mueller, T.C., Womac, A.R., 1997. Effect of formulation and nozzle type on droplet size with isopropylamine and trimesium salts of glyphosate. Weed Technol. 11(4), 639–643. https://doi.org/10.1017/S0890037X00043177.

[47] Ennis, B.J., Tardos, G., Pfeffer, R., 1991. A microlevel-based characterization of granulation phenomena. Powder Technol. 65, 257–272. https://doi.org/10.1016/0032-5910(91)80189-P.

[48] Mohan, B., Kloss, C., Khinast, J., Radl, S., 2014. Regimes of liquid transport through sheared beds of inertial smooth particles. Powder Technol. 264, 377–395. https://doi.org/10.1016/j.powtec.2014.05.045.

[49] Vonk, P., Guillaume, C.P.F., Ramaker, J.S., Vromans, H., Kossen, N.W.F., 1997. Growth mechanisms of high-shear pelletisation. Int. J. Pharm. 157(1), 93–102. https://doi.org/10.1016/S0378-5173(97)00232-9.

[50] Dacanal, G.C., Menegalli, F.C., 2010. Selection of operational parameters for the production of instant soy protein isolate by pulsed fluid bed agglomeration. Powder Technol. 203(3), 565–573. https://doi.org/10.1016/j.powtec.2010.06.023.

[51] Nascimento, R.F., Rosa, J.G., Andreola, K., Taranto, O.P., 2019. Wettability improvement of pea protein isolate agglomerated in pulsed fluid bed. Part. Sci. Technol. 38(4), 511–521. https://doi.org/10.1080/02726351.2019.1574940.

[52] Viegas, T.R., Taranto, O.P., 2018. Agglomeration of hydrolyzed collagen with blackberry pulp in a fluidized bed. IDS 2018. 21st International Drying Symposium Proceedings 1447–1454. https://doi.org/10.4995/IDS2018.2018.7347.

[53] Machado, V.G., Hirata, T.A.M., Menegalli, F.C., 2014. Agglomeration of soy protein isolate in a pulsed fluidized bed: Experimental study and process optimization. Powder Technol. 254, 248–255. https://doi.org/10.1016/j.powtec.2014.01.040.

[54] Jiménez, T., Turchiuli, C., Dumoulin, E., 2006. Particles agglomeration in a conical fluidized bed in relation with air temperature profiles. Chem. Eng. Sci. 61(18), 5954–5961. https://doi.org/10.1016/j.ces.2006.05.007.

[55] Pathare, P.B., Baş, N., Fitzpatrick, J.J., Cronin, K., Byrne, E.P., 2012. Production of granola breakfast cereal by fluidised bed granulation. Food Bioprod. Process. 90(3), 549–554. https://doi.org/ 10.1016/j.fbp.2011.08.004.

[56] Iveson, S.M, Wauters, P.A.L., Forrest, S., Litster, J.D., Meesters, G.M.H., Scarlett, B., 2001. Growth regime map for liquid-bound granules: further development and experimental validation. Powder Technol. 117(1–2), 83–97. https://doi.org/10.1016/S0032-5910(01)00317-5.

CHAPTER V

The formation of solid bridges during agglomeration in a fluidized bed: investigation by Raman spectroscopy and image analyses

Nascimento, R.F.; Ávila, M.F.; Silva, A.G.P.; Taranto, O.P.; Kurozawa, L.E.

The formation of solid bridges during agglomeration in a fluidized bed: investigation by Raman spectroscopy and image analyses

Raul F. Nascimento[a], Mariana F. Ávila[b], Adriano G. P. da Silva[b], Osvaldir P. Taranto[b], Louise Emy Kurozawa[a]

[a]Department of Food Engineering, School of Food Engineering, University of Campinas, Monteiro Lobato St. 80, Campinas, SP, Brazil

[b]Department of Process Engineering, School of Chemical Engineering, University of Campinas, Albert Einstein Ave. 500, Campinas, SP, Brazil

HIGHLIGHTS

- Establishing and maintaining solid bridges is crucial to agglomeration success.
- Raman spectroscopy identified the granule surface composition throughout the process.
- Image analysis provided agglomeration visualization and solid bridge formation.
- Data and images made it possible to delimit the stage of the solid bridge formation.

ABSTRACT

Solid bridge formation in the agglomeration process is still not well-understood. This work has aimed to analyze particle class evolution, Raman spectra, and microscopy to comprehend granule formation in a fluidized bed throughout the process. Microcrystalline cellulose was agglomerated by maltodextrin solutions. The experimental statuses were classified in wet and dry conditions according to the combination of operating parameters. The effect of solution concentration (5.0, 20.0, and 35.0% w/w), solution flow rate (1.0 and 4.0 mL/min), and air temperature (30 and 90 °C) on particle size was checked. Afterward, the solution flow rate was increased from 1.0 to 4.0 mL/min while maintaining constant solution concentration and air temperature. Wet conditions led to more effective particle formation since the amount of liquid binder on the particle surface favored the formation of a sticky layer. The examination of data and images made it possible to identify the solid bridge formation and stability.

Keywords: Solid bridges; Raman spectra; Scanning electron microscopy; Fluorescence microscopy; Particle growth.

5.1. INTRODUCTION

Fluidized beds are widely used for some industrial processes dealing with particle enlargement. In turn, increased particle size becomes important for food, chemical, and pharmaceutical industries for producing instant products featuring enhanced physicochemical properties such as water solubility and dispersion. In this aspect, agglomeration (or granulation) is the most common unit operation capable of fulfilling this purpose. Agglomeration consists of increasing particle size by forming granules, which are semi-permanent structures organized in an aggregate form. This formation can only occur by establishing and maintaining solid bridges between primary particles due to the influence of favorable operating conditions. Thus, particle size is the most outstanding factor in the agglomeration process. However, there is a limitation in obtaining the necessary information to understand the process because experimental measurements are usually only taken at the end of the process. Techniques, such as Spatial Filter Velocimetry (SFV), can be useful, when possible, for solving this disadvantage, for example, by taking measurements in real-time and throughout the process, as previously demonstrated by Andreola et al. [1], Rosa et al. [2], and Nascimento et al. [3]. This way, it is noteworthy that other parameters could also be measured while the process takes place to address the monitoring of the product and process quality.

Several technologies have been used to relate to physicochemical properties and final product quality in this context. Near-infrared reflectance (NIR) spectroscopy is commonly used for at-line and online measures [4]. At-line refers to the analysis performed close to the equipment while samples are withdrawn while the process carries on. Errors are possible for this type of measurement due to the disturbance caused by the sample collection process and the manual handling of samples. In online measurements, mistakes are minimized as there is an automatic and systematic collection of samples from the process. The samples are collected, analyzed, and return to the process cyclically while maintaining material integrity [5]. In this context, preferably, no process sampling is performed, and measurements are taken while executing the process in the case of in-line measurements. Portable Raman spectroscopy can achieve the same function as NIR spectroscopy. Plus, there is an advantage as it can be coupled to the fluidized bed chamber, as tested successfully by Walker et al. [4] and Walker et al. [6].

Raman spectroscopy is a non-destructive technique whereby not much sample preparation is required and provides the capability of providing quick responses. Each compound is defined by a unique Raman spectrum derived from the excitation energy of the vibrational molecule modes. Raman spectroscopy is performed by recording the energy profile

of scattered light from a sample produced by a specific laser, i.e., Raman spectroscopy employs inelastic light scattering from molecules excited by an incident photon beam of a particular wavelength [4]. The relation between signal intensity and material concentration on the superficial sample is the most important aspect enabling measurement implementation by Raman spectroscopy, which makes sample composition mapping possible [7].

Currently, there is little information in the literature regarding the use of Raman spectroscopy probes coupled to fluidized bed chambers and in-line and real-time measurements. The previous works did not show how to control the sample volume and used only one stage to record the data, as Walker et al. [4] observed. However, measurements in equipment are still difficult to perform, such as from the fluidized bed, since measurements must be done with as little ambient light as possible to avoid interference. Regarding this, it is still preferable that analyses are carried out online, taking samples during the process execution, even if some minimal damage is caused. Designing, monitoring, and controlling the agglomeration process demands expertise on operating parameters and product features. Conventionally, visual observation and manual procedures are usual ways to monitor agglomeration processes when particle size, moisture content, and bulk and tap density are the main responses. Nonetheless, a considerable amount of material in various stages of the process is required to determine these properties, demanding time consumption and specialized personnel [8].

In the current work, operating parameters (liquid binder concentration, liquid binder flow rate, and fluidizing air temperature) have been monitored during the agglomeration process, and particle enlargement was evaluated. A bench portable Raman spectrometer was used for online spectral acquisition, and the SFV probe was used for measuring the in-line particle size distribution. Furthermore, scanning electronic and fluorescence micrographics were obtained from the samples. The results of both methods combined with the image analysis made it possible to establish the solid bridge formation conditions during the agglomeration process. There are very few publications where Raman spectroscopy was used for this purpose, to the best of the author's knowledge. For this reason, the authors consider this manuscript a useful reference in the particulate system field for achieving outstanding information about granule formation during agglomeration in a fluidized bed.

5.2. MATERIAL AND METHODS

5.2.1. Material

Microcrystalline cellulose (CMC) (Microcel®, Blanver Farmoquímica, Brazil) with moisture content, density, and $D10v$, $D50v$, and $D90v$ percentiles as $7.28 \pm 0.05\%$, 1.5485 ± 0.0010 g/cm^3, and 119.8 ± 9.0, 290.2 ± 6.6, and 517.8 ± 8.5 μm, respectively, was agglomerated with maltodextrin solutions whose concentrations varied from 5.0 to 35.0% w/w, according to experimental conditions. These solutions were prepared by subjecting maltodextrin (MOR-REX® 1910, Ingredion, USA) to magnetic stirring at room temperature until completely dissolved. For each experimental run, 0.4 kg of CMC was fed in the bed chamber.

5.2.2. Equipment and fluidized bed agglomeration process

The agglomeration experiments were carried out in a lab-scale fluidized bed, as described by Andreola et al. [1], Rosa et al. [2], and Nascimento et al. [3]. The fluidized bed-chamber was composed of a conical base (0.075 m inlet air diameter and 0.15 m of height) and a cylindrical column (0.15 m diameter and 0.60 m height), both constructed from transparent acrylic Plexiglass®. At the entrance to the conical part, the air was distributed by a perforated plate in a triangular array. The fluidizing air was supplied by an air blower placed out of the room. The air was heated by an electrical heater. The elutriated particles were collected by a cyclone. A peristaltic pump was used to deliver the liquid binder to the bi-fluid spray nozzle. The liquid binder was sprayed onto the bed and the atomization pressure was provided by a compressor, also located out of the room. The SFV probe (Parsum IPP 70S, Malvern Instruments, Germany) was coupled to the fluidized bed chamber at the conical base, above the air distribution plate, at the position already reported by Nascimento et al. [9] for monitoring the particle size evolution. The SFV probe collected the data every 5.12 sec and exported them to the LabVIEW^{TM} 8.6 software. The particle dimensions defined by chord size were calculated according to Nascimento et al. [3]. The accessories collected the temperature, relative humidity, and pressure drop data, as depicted by Nascimento et al. [3]. The median particle size ($D50v$) was estimated as the average of the last ten measurements.

In the beginning, the agglomeration experiments were performed under dry and wet conditions, according to Table 5.1. In this current work, dry condition (DC) was defined by the

combination of a lower solution flow rate (1.0 mL/min) and higher air temperature (90 °C), and wet condition (WC) by the combined use of higher solution flow rate (4.0 mL/min) and lower temperature (30 °C). The solution concentration was varied in three levels for each condition: 5.0, 20.0, and 35.0% w/w. The total amount of liquid inserted into the bed chamber was 120 mL for each experiment. In this way, the execution time of each experiment varied according to the solution flow rate (30 min for 4.0 mL/min and 120 min for 1.0 mL/min). The operating parameters were defined abiding by what was proposed in our previous work [3], except for using the lowest temperature level. The Raman spectra of samples were collected at the end of the process and analyzed to verify the presence (or not) of maltodextrin on the particle surface.

Table 5.1: Experimental conditions and response based on mean particle size *D50v*.

Exp.	Concentration (% w/w)	Solution flow rate (mL/min)	Air temperature (°C)	Experimental status	*D50v* (µm)
E1	5.0	4.0	30	WC	378.3 ± 6.8^a
E2	5.0	1.0	90	DC	352.3 ± 3.9^b
E3	20.0	4.0	30	WC	377.9 ± 0.2^a
E4	20.0	1.0	90	DC	415.9 ± 2.1^c
E5	35.0	4.0	30	WC	449.9 ± 1.0^d
E6	35.0	1.0	90	DC	408.8 ± 1.0^e

Data were expressed as mean ± standard deviation. According to Tukey's test, values in the same letter column were not significantly different ($p < .05$). WD: wet condition; DC: dry condition.

Afterward, an experiment was carried out in which the maltodextrin solution flow rate was increased from 1.0 to 4.0 mL/min, by increments of 0.5 mL/min every 10 min, maintaining a constant solution concentration and air temperature at 20.0% and 30 °C, respectively. Samples were taken every 10 min and analyzed by Raman spectrometry and scanning electron microscopy. At the end of the process, the agglomerated product was analyzed by fluorescence microscopy.

5.2.3. Raman spectroscopy

Raman spectra were collected on the Avantes Spectrometer (AvaSpec, ULS2048I-TEC-RS-USB2) utilizing a 785 nm laser. The data were recorded at room temperature for all samples in the spectral range from 300 to 1500 cm^{-1}. The laser potency was 900 mV and measured ten integration times at 10 s each, totaling 100 s. The spectral subtraction between the specific spectrum and the base spectrum was performed to verify the existence (or not) of

any difference between the collected spectra in an experimental condition and that of the raw material.

5.2.4. Particle morphology

Particle morphology was evaluated by scanning electron microscopy (SEM). The samples were examined under an LEO 440i scanning electron microscope (LEO Electron Microscopy Ltd., Oxford, England). The SEM microscope was operated at a magnification ranging from 100×, 250×, and 1000× at 10 kV and 50 pA.

5.2.5. Fluorescence microscopy

The fluorescence microscopy was performed employing a microscope (Axioscope 5, Zeiss, Germany) utilizing a coupled camera to capture images (Axioscam 503 color, Zeiss, Germany). Three milliliters of Calcofluor White solution (0.1 g/L) were mixed with the binder solution and atomized by the spray nozzle into the bed chamber during the process. Samples that were collected at the end of the process were analyzed to identify where the maltodextrin solution remained deposited on the particle surface.

5.3. RESULTS AND DISCUSSION

5.3.1. Granule growth kinetics for dry and wet conditions

The data from each experimental run was separated into particle classes for analyzing the granule kinetic growth, according to Nascimento et al. (2021). Class I corresponds to the particles with $D50v$ < 300 µm; Class II, 300 µm $\leq D50v$ < 600 µm; and Class III, $D50v$ $\geq$ 600 µm, named fine, intermediate, and coarse, respectively. The evolution of particle classes throughout the process is displayed in Figure 5.1. The agglomeration phase classification was also performed, as stated by Nascimento et al. [3].

The most important aspect in the evolution of particle classes is the emergence of Class III, the consequent sharp decline of Class I, and the smooth alteration of Class II. The fine and intermediate particles are available for wetting and ready for agglomerating and forming the coarse particles when the process begins. Maintaining the amount of Class III

particles is preferable to guarantee a high granule growth rate throughout the process and stable granules at the end of the process.

Regarding the executed experiments and the evolution of particle classes (Figure 5.1), it is clear that to conditions set in *E4*, *E5*, and *E6* provided the emergence of Class III. Two of these experiments (*E5* and *E6*) were carried out at a high maltodextrin concentration level (35.0% w/w), and the other (*E4*) at an intermediate level (20.0% w/w), associated with the dry condition (lower flow rate and higher temperature).

In the case of *E4* (C = 20.0% w/w, Q = 1.0 mL/min, T = 90 °C), the emergence of coarse particles occurred after around 30% of the process jointly with the considerable reduction of fine particles, characterizing the outset of Coalescence and Growth phase (Nascimento et al., 2021). The particles, in that case, reached a mean size of 415.9 ± 2.1 µm (Table 5.1) at the end of the process, while after 90% of the process, the mean particle size was considered stable. Regarding *E5* (C = 35.0% w/w, Q = 4.0 mL/min, T = 30 °C) and *E6* (C = 35.0% w/w, Q = 1.0 mL/min, T = 90 °C), the emergence of Class III occurred after around 5% and 10% of the process, respectively. The first case initiated the Stabilization phase expeditiously after approximately 25% of the process continued until the process ended. The particle enlargement reached a size of 449.9 ± 1.0 µm (Table 5.1). The second case was different; the mean particle size reached 408.8 ± 1.0 µm (Table 5.1) in a process that Coalescence and Growth phase occurred up after around 70% of the process, followed by the Stabilization phase.

The other three experiments (*E1*, *E2*, and *E3*) did not display the evolution of particle classes, according to Figure 5.1, since the data corresponding to Class III practically oscillated around zero percent of the retained fraction. For *E3*, the retained fraction of coarse particles was slightly larger than zero but not enough to understand this behavior as an emergent class. The operating conditions for these experiments (*E1* and *E2*) were at the lower concentration level (5.0% w/w), and intermediate concentration level (20.0% w/w) associated with wet conditions (higher flow rate and lower temperature) for the other experiment (*E3*). The final particle sizes for *E1*, *E2*, and *E3* were 378.3 ± 6.8 µm, 352.3 ± 3.9 µm, and 377.9 ± 0.2 µm, respectively (Table 5.1), about only 20% larger than the raw material size.
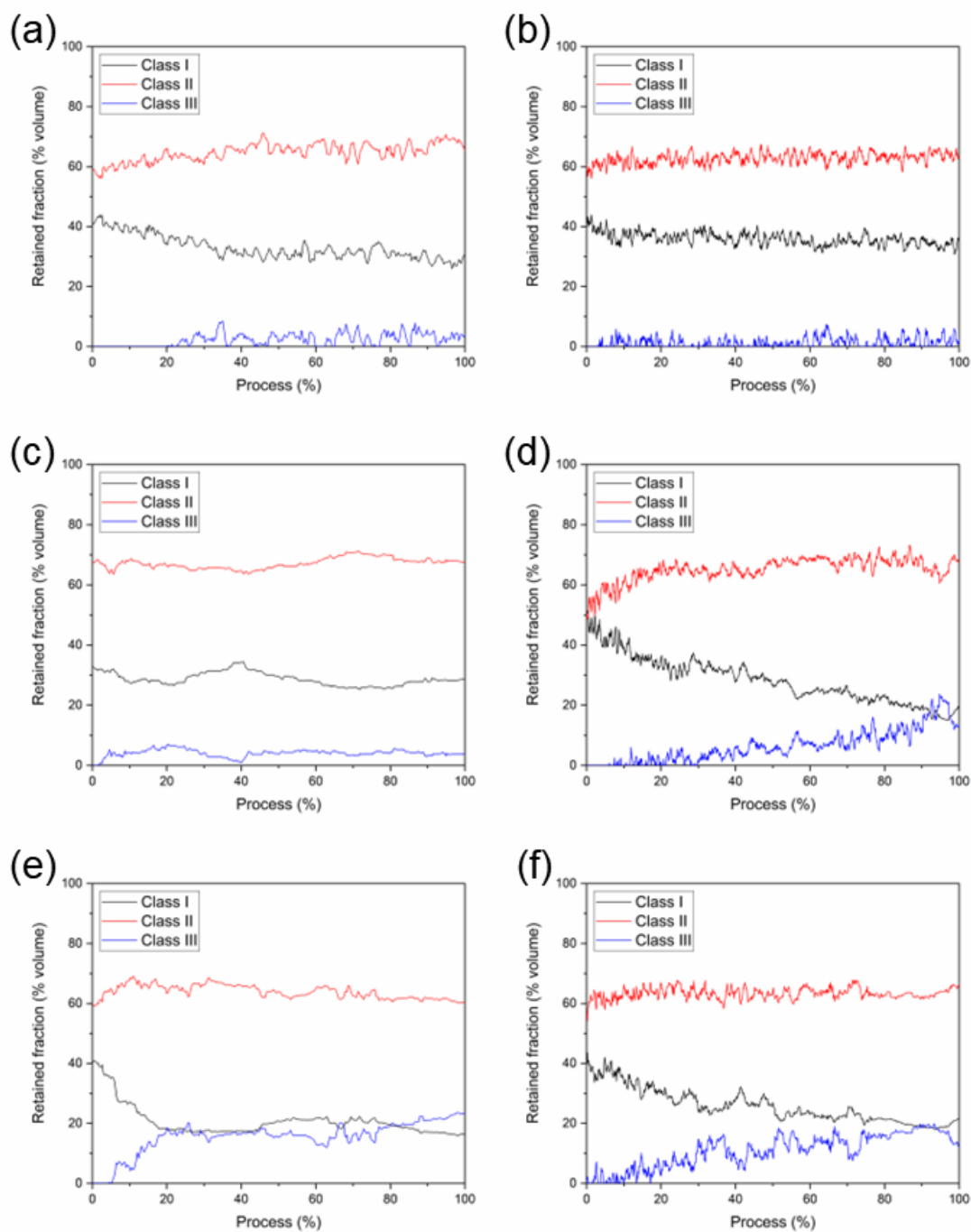
Figure 5.1: Evolution of particle classes for the experiments: (a) *E1* ($C = 5.0\%$ w/w, $Q = 4.0$ mL/min, $T = 30\ ^\circ$C), (b) *E2* ($C = 5.0\%$ w/w, $Q = 1.0$ mL/min, $T = 90\ ^\circ$C), (c) *E3* ($C = 20.0\%$ w/w, $Q = 4.0$ mL/min, $T = 30\ ^\circ$C), (d) *E4* ($C = 20.0\%$ w/w, $Q = 1.0$ mL/min, $T = 90\ ^\circ$C), (e) *E5* ($C = 35.0\%$ w/w, $Q = 4.0$ mL/min, $T = 30\ ^\circ$C), and (f) *E6* ($C = 35.0\%$ w/w, $Q = 1.0$ mL/min, $T = 90\ ^\circ$C).

The effect of conditions (dry or wet) can be seen when the experiments are compared two at a time, especially contrasting *E3* and *E4*. In the other pairs (*E1-E2* and *E5-E6*), the effect of binder concentration was much more evident and overlapped the dry or wet

experimental condition. Nascimento et al. [3] have already reported that binder concentration was the most prominent operating variable that caused particle enlargement in the case of the CMC agglomeration in a fluidized bed. In the current work, this effect also remained evident since no evolution occurred in the *E1* and *E2* particle classes ($C = 5.0\%$ w/w), and the evolution is clear for *E5* and *E6* ($C = 35.0\%$ w/w) (Figure 5.1). The binder concentration level is the difference between these two pairs of experiments.

Experiments were carried out at a medium level of binder concentration for *E3* and *E4* ($C = 20.0\%$ w/w) there was an opposite effect of wet or dry conditions as to what has already been reported in the literature. The wet and dry conditions referred to the expected state of the internal environment of the bed chamber according to the set operating variables, i.e., high temperature and low binder flow rate provided dry conditions, and low temperature and high binder flow rate provided wet conditions. The operating variables provided a dry environment that also improved particle size enlargement (*E4*), even though the binder concentration was not higher. Oppositely, the wet environment obtained in *E3* has not shown particle size enlargement at the set levels of the operating variables.

Wet conditions (higher flow rate and lower temperature) may have led to more effective particle formation since the amount of liquid binder under the particle surface made the sticky layer creation available. Furthermore, more liquid in the bed chamber allowed the wet-active zone enough moisture so the particles could coalesce, favoring the growth rate and the agglomeration. Authors such as Dacanal and Menegalli [10], Hirata et al. [11], Machado et al. [12], and Nascimento et al. [13] reported experimental results that corroborated the influence of wet conditions on the agglomeration of powdered materials.

The effect of temperature on particle enlargement and growth rate was already addressed in the literature regarding dry conditions (lower flow rate and higher temperature) by Rosa et al. [2], Hirata et al. [11], Machado et al. [12], and Nascimento et al. [13]. According to those authors' results, the higher the temperature, the smaller the granule size would be at the end of the process. They explained this relation between increasing temperature and decreasing granule size due to the fast drying of the liquid binder at high temperatures and the improved heat transfer and drying rate. Sometimes, the binder droplets could not even reach the solid particle bed by top spraying since the droplets were evaporated before touching the solid surface. The relative humidity of the air in the bed chamber decreased, interfering with the droplet action, and then the particles were not as sticky and wetted, preventing bridge formation.

For agglomeration to occur, an amount of binder must be present at the point of contact for bridge formation to occur. If there is enough for adhesion, growth is favored, otherwise, the particles are rebounded. The granule growth and quality (features related to the bridge formation and stability) are linked to the liquid binder viscosity and the amount of this liquid adhered to the particle surface at the points of contact [14] and the state of particle pores saturation [15].

During the process, the liquid bridges formation is guaranteed by the kinetic energy viscous dissipation of colliding particles [14]. In order for them to collide and stay together, the liquid surface tension is the first most important force. However, during the process, these can be exchanged for others, especially during drying phase. In this case, van der Waals forces and chemical bonds can take the place of surface tension, depending on the type of particulate material and the nature of the liquid binder [16]. A limiting factor, then, is the fact that, in real situations, it is impossible for instantaneous and uniform distribution of liquid to occur over the particulate bed. Particles that are wetted first form a granule with an outer layer of excess moisture. This liquid incorporates more particles until there is no more excess liquid. That is, the agglomeration mechanisms depend on the degree of liquid dispersion over the powder [14,16].

In addition, the liquid bridges formed must be able to give rise to solid bridges by solvent evaporation, making the granules remain stable on drying phase [17]. Agglomeration is the result of a controlled compaction process that occurs due to the rubbery state that is produced at a critical viscosity state above the glass transition temperature. Under the specific conditions of agglomeration in a fluidized bed, the amorphous components pass through the glass transition, causing a decrease in viscosity and the appearance of a rubbery state. Agglomeration requires particle surface plasticization, which can be the result of increased temperature or variation in humidity. Particles with plasticized surfaces form granules by creating liquid bridges [17]. In this case, DC can favor the appearance of liquid bridges by increasing the temperature even with low binder flow, but they do not guarantee the permanence of the stability of the bridges with the process progress.

The liquid bridges formation, the transition from the state of liquid bridges to that of solid bridges, and the solid bridges stability should not be understood with the analysis of isolated operating parameters. By interpreting what has already been discussed, there is no doubt about the non-triviality of the parameters' joint analysis, mainly because the factors that were correlated in the dry and wet states have opposite effects on the particulate material

plasticization for the liquid bridges formation and on solvent evaporation for the maintenance of solid bridges. It was also seen that the liquid binder concentration (and, to a certain extent, its nature) also has a great influence on the mechanisms discussed here.

Figure 5.2(a) showed representative Raman spectra of fluidizing particles, whereas the vertical axis was the scattered light intensity, and the horizontal axis was the frequency. The spectra corresponded to the raw material (CMC) for each experiment (*E1* to *E6*) and maltodextrin. In the CMC spectra, the peaks at 250–550 cm^{-1} corresponded to skeletal bending of C–C–C, C–O–C, O–C–C, or O–C–O groups, methine bending (C–C–H or O–C–H), or skeletal stretching (C–C or C–O); the H–C–C and H–C–O bending occurred at ~900 cm^{-1}; the 950–1180 cm^{-1} band peaked around 1100 cm^{-1} was the influence of C–C and C–O stretching and H–C–C or H–C–O skeletal bending; the 1180–1500 cm^{-1} band could be divided into four regions: until ~1270 cm^{-1} represented the skeletal stretching and methine bending, 1270–1350 cm^{-1} depicted the H–C–C and H–C–O bending range, 1350–1430 cm^{-1} expressed the C–O–H bending, and the H–C–H bending up to 1500 cm^{-1} [18,19].

Also, according to the maltodextrin spectra in Figure 5.2(a), the 300–700 cm^{-1} band corresponded to skeletal vibrations, and the 485 cm^{-1} peak was assigned to the pyranose rings of the C–C backbone stretch modes; the 800–1200 cm^{-1} band, in turn, represented the C–C, C–O, C–OH vibration, and C–O–C groups in pyranose units, the 852 cm^{-1} peak was the C–O–C glycosidic linkage, 1082 cm^{-1}, and 1124 cm^{-1} depicted the C–O and C–C symmetric stretching vibration and C–OH deformation. Furthermore, at 950–1200 cm^{-1}, the band expressed the C–O–C and C–C glycosidic symmetric stretching vibration, and at 1200–1500 cm^{-1}, the –CH_2 and C–OH deformation. The 1256 cm^{-1}, 1338 cm^{-1}, 1380 cm^{-1}, and 1495 cm^{-1} peaked in this last region that represented the –CH_2 twisting vibration, the C–O symmetric stretching vibration, and the C–H deformation, the –CH_3 symmetric bending vibration, and the –CH_2 deformation, respectively [20,21].
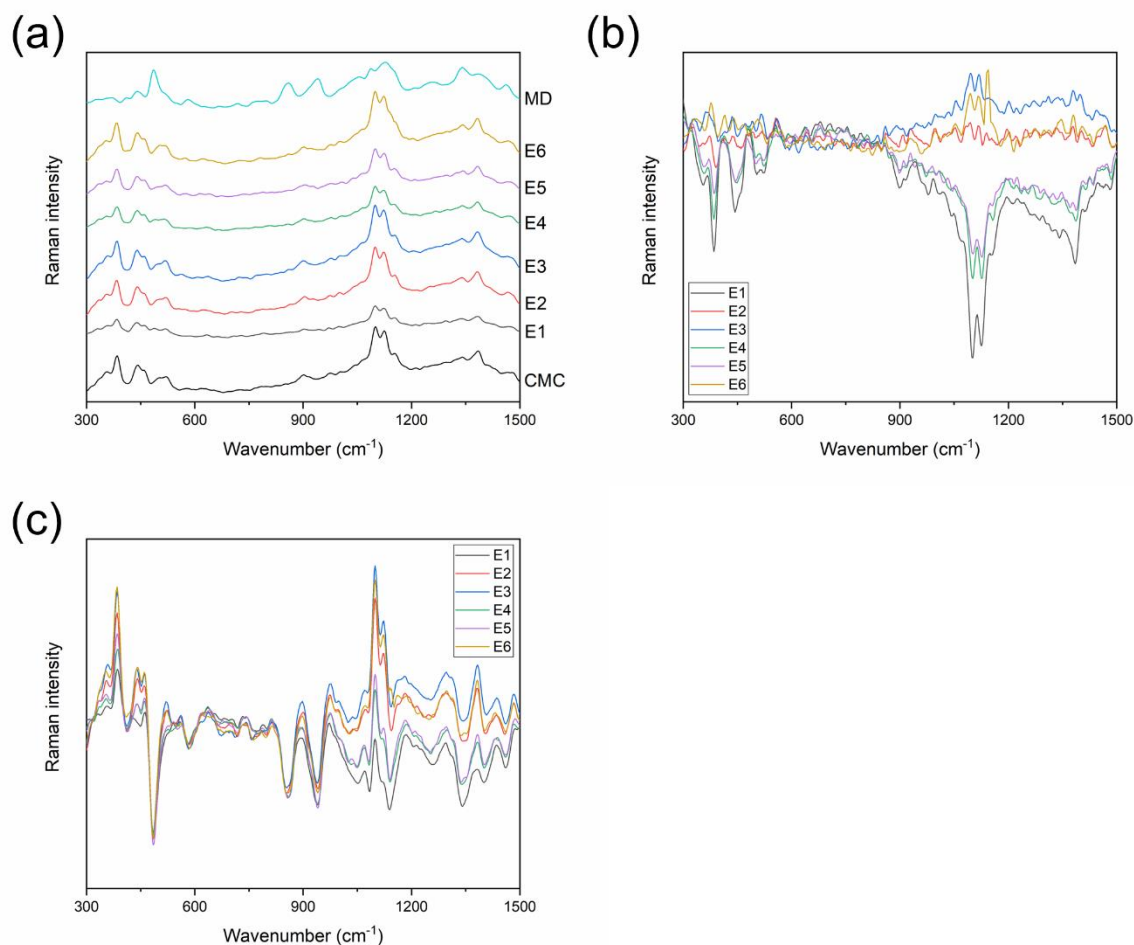
Figure 5.2: (a) Raman spectra for microcrystalline cellulose (CMC) for each experimental run (*E1* to *E6*) after the process and maltodextrin (MD). (b) Raman spectra difference between each experiment and the CMC spectrum, and (c) Raman spectra difference between each experiment and the MD spectrum. Operating conditions: *E1* (C = 5.0% w/w, Q = 4.0 mL/min, T = 30 °C); *E2* (C = 5.0% w/w, Q = 1.0 mL/min, T = 90 °C); *E3* (C = 20.0% w/w, Q = 4.0 mL/min, T = 30 °C); *E4* (C = 20.0% w/w, Q = 1.0 mL/min, T = 90 °C); *E5* (C = 35.0% w/w, Q = 4.0 mL/min, T = 30 °C); *E6* (C = 35.0% w/w, Q = 1.0 mL/min, T = 90 °C).

According to Walker et al. [6], the absolute signal height directly indicated the amount of a given constituent in an analyzed sample. The intensities of the relative band reflected the relative proportions of the constituents present in the sample. Figure 5.2(a) also showed the Raman spectra for each agglomerated sample obtained from the experimental runs (Table 5.1) after the process, additionally with the spectra for the previously discussed raw materials. This analysis intended to verify each applied experimental condition to verify if it was possible to identify the presence of maltodextrin (liquid binder) on the particle surface at the end of the experiments.

Compared to all performed experiments, the *E1* (C = 5.0% w/w; Q = 4.0 mL/min; T = 30 °C; wet condition), *E4* (C = 20.0% w/w, Q = 1.0 mL/min, T = 90 °C; dry condition), and *E5* (C = 35.0% w/w; Q = 4.0 mL/min; T = 30 °C; wet condition) experiments showed the highest attenuation of peaks corresponding to CMC (Figure 5.2(b)). On the contrary, *E2* (C = 5.0% w/w; Q = 1.0 mL/min; T = 90 °C; dry condition) showed little spectrum variation compared to CMC. The *E6* (C = 35.0% w/w; Q = 1.0 mL/min; T = 90 °C; dry condition) experiment also abided by the same behavior as experiment *E2*, even though the highest liquid binder concentration was used. That could indicate that the effect of the conditions caused by the variation of air temperature and liquid binder flow rate overlapped the effect of liquid binder concentration. According to Figure 5.2(c), comparing the maltodextrin spectrum, the experimental spectra were confused until reaching the 1000 cm^{-1} region; after that, the spectra separated from each other but abided by the same shape. The spectral difference was zero for none of them, i.e., no spectrum was completely equal to the maltodextrin spectrum.

The 5.0% w/w and 35.0% w/w concentrations, the wet conditions favored decreased CMC peaks, indicating that there was more binder on the particles' surface. In the case of the 20.0% w/w concentration, the dry condition (*E4*, C = 20.0% w/w; Q = 1.0 mL/min; T = 90 °C) favored decreased CMC peaks; however, in reality, the peaks for these two conditions (*E4* and *E5*) were practically the same, or with very little variation.

The liquid binder tended to remain on the particle surface under wet conditions, mainly in a saturation state near 100% [22]. The saturation rate was increased by adding more liquid binder and/or internal porosity reduction due to consolidation, and the enlargement process was intimately linked to it. The combined influence of liquid binder flow rate and air temperature on the saturation state in the fluidized bed was explained by Jiménez et al. [23]. They also defined three zones: the wetting-active zone, the isothermal zone, and the heat transfer zone. The first was classified as a lower temperature and higher humidity zone close to the atomizer nozzle. The particles were wetted, and there was high humidity and temperature gradients in that region; consequently, the wetting and drying operations occurred more efficiently, favoring agglomeration. These gradients became smaller as they moved away from the center of the fluidized bed, reaching the lowest values when they touched the equipment walls. The second zone was surrounded by the wetting-active zone, characterized by a homogeneous temperature, minimum (or null) temperature and humidity gradients, and equilibrium between mass and heat transfers. Finally, the third zone was called the heat transfer zone. It was located above the air distribution plate, where the temperature was high just over

the plate and decreased as it rose through the bed, as there was energy absorption by the particles that came from the wetting-active zone.

These three zones were theoretically defined, and their sizes varied according to the operating parameters. The agglomeration efficiency was enhanced only if the particles could penetrate the wetting-active zone because their surfaces would be wetted by droplets and could collide. Larger wetting-active zones promoted better agglomeration since more particles were moving through them. Changes in temperature and flow rate also caused the wetting-active zone size to vary. The combination of low air temperature and high liquid flow increased the wetting-active zone, possibly even overlapping the heat transfer zone. Lowering the temperature limits the evaporation of the atomized liquid, and the liquid flow rate determined the drying conditions [24–26].

5.3.2. Granule growth kinetics for the experiment with increment in the liquid binder flow rate

In this second part, experiments were carried out in which the maltodextrin solution flow rate increased from 1.0 to 4.0 mL/min, by increments of 0.5 mL/min every 10 min while maintaining the constant solution concentration and air temperature at 20.0% and 30 °C, respectively. These conditions were selected because, based on the Raman spectra analysis, they provided increased chances of depositing liquid binder solution on CMC particle surfaces. Although the experiment did not achieve the greatest attenuation of the peaks, there was the emergence of characteristic peaks of maltodextrin ranging from 600 to 1000 cm^{-1}. Additionally, in the end of the process, the experiment was continued without atomizing the liquid binder for 10 min to evaluate the particle size behavior under that condition. This step was named the drying phase in this current work. The increased liquid binder flow rate was proposed to confirm whether there would be a change or not in the spectra throughout the process by adding binder liquid and, consequently, more maltodextrin in the same time interval. Figure 5.3 displayed the particle class evolution for this experiment. The Raman spectra were obtained for each liquid binder flow region and drying phase (Figure 5.4(a)), as well as SEM micrographs (Figure 5.5). The SEM micrographs displayed in Figure 5.5 are related to 1000× magnification. The other magnifications (100× and 250×) can be seen in Supplementary Material. Figure 5.6 shows the images taken by fluorescence microscopy.

According to Figure 5.3 and the classification reported by Nascimento et al. [3], the evolution of particle classes demonstrated the occurrence of the Wetting phase in up to approximately 8% of the process and the fine retained fraction and intermediate retained fraction fluctuating from around 40% to 60%, respectively. At that moment, no coarse particles were present ($D50v \geq 600$). Additionally, the Raman spectrum for the sample collected at this stage was very like the raw material spectrum but slightly less intense (curves corresponding to 1.0 mL/min and raw material in Figure 5.4(a)). Also, it was possible to notice the difference in Figure 5.4(b) between the CMC and 1.0 mL/min spectra was the lowest, and the difference in maltodextrin spectrum was the highest (Figure 5.4(c)) that inferred the non-existence of maltodextrin on particles' surface in that process phase. Figure 5.5(b) shows the particles obtained at this point of the process, characterized by single and loose particles, also extremely analogous to the raw material particles (Figure 5.5(a)).
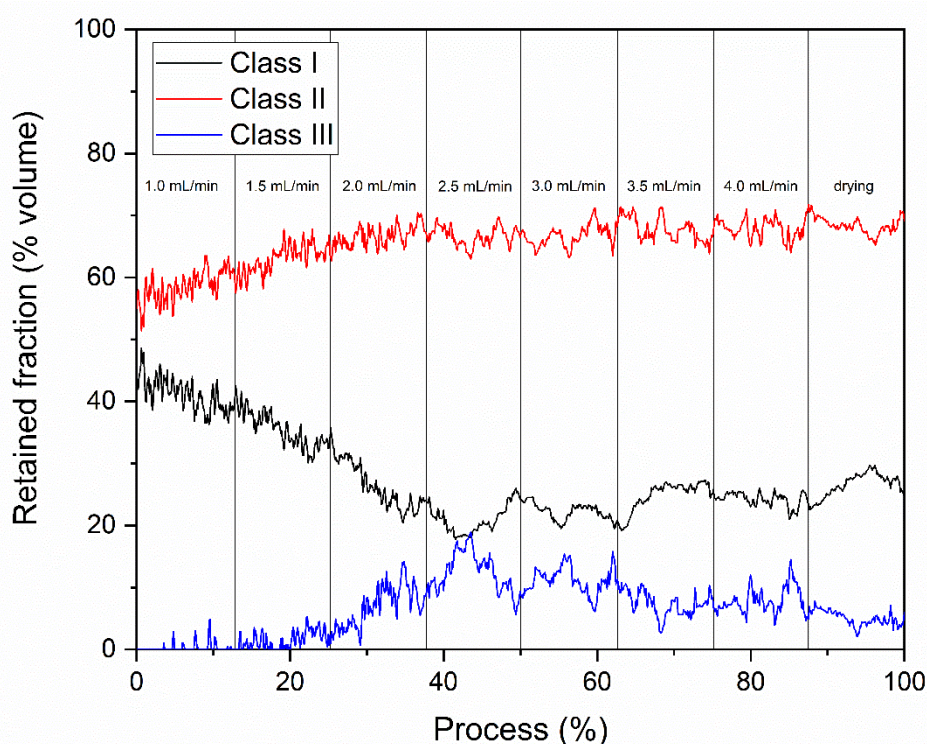
Figure 5.3: Evolution of particle classes for the experiment in which liquid binder flow rate varied from 1.0 mL/min to 4.0 mL/min, at $C = 20.0\%$ w/w and $T = 30\ °C$.

In general, the spectral differences presented in Figures 5.4(b) and (c) showed the low binder flow rates; the spectra resembled the CMC spectrum and differed much more than the maltodextrin spectrum, indicating that at the beginning of the process, there was less binder solution on the particles' surface. The spectral differences between maltodextrin and the

experiments decreased while the process occurred, while those between CMC increased. This indicates maltodextrin may have been deposited on the surfaces as the flow rate of the binder solution increased.

There is the occurrence of the Nucleation phase of the process ranging from 8% to 20%, marked by the continuous increase in the fine retained fraction, which reached almost 65%, and decreased in the fine particles retained fraction, reaching a little over 35%. The emergence of coarse particles marked the end of this phase and, consequently, the beginning of the next one. The Raman spectrum corresponded to the 1.5 mL/min curve in Figure 5.4(a), abiding by the same trend as the preceding phase, as there was little modification in the Raman intensity. That indicated that the major constituent of the particles was still CMC, which was also verified by the low spectral difference in Figure 5.4(b). In Figure 5.5(c), the particles remained separated, like the previous step. It is important to state that it was not possible to verify the surface composition through SEM micrographs; thus, the Nucleation stage was predominant despite knowing that from the evolution curves of Figure 5.3. This confirmation was not possible to do by image analysis.

The most important phase of the agglomeration process corresponded to the Coalescence and Growth phase, which took place after 20% of the process when the coarse particles emerged and continued until approximately 42% of the process, marked by the beginning of the apparent growth stabilization (Figure 5.3). In that phase, the fine particles of the retained fraction decreased by up to 20% compared to the increase of coarse particles in the retained fraction that was up to around 20% as well. The retained fraction of the intermediate particles did not show large variation and always remained around 65% during that phase. The Raman spectra for this phase (the curve corresponded to 2.0 mL/min in Figure 5.4(a)) appeared to be less intensive than the previous, characterizing the decrease in CMC availability. Figure 5.4(b) confirms this information. That could indicate that the liquid binder was coating the particles.

Moreover, Figure 5.5(d) and the Supplementary Material show that the particulate system a more homogeneous size, with few tiny fragments on surfaces, probably due to the fine particle elutriation by dragging or their incorporation on the larger particles. It is important to highlight the details in Figure 5.5(d), which present the contact point between two particles. At this point, if there were enough liquid binder and favorable conditions, a solid bridge may have been formed.
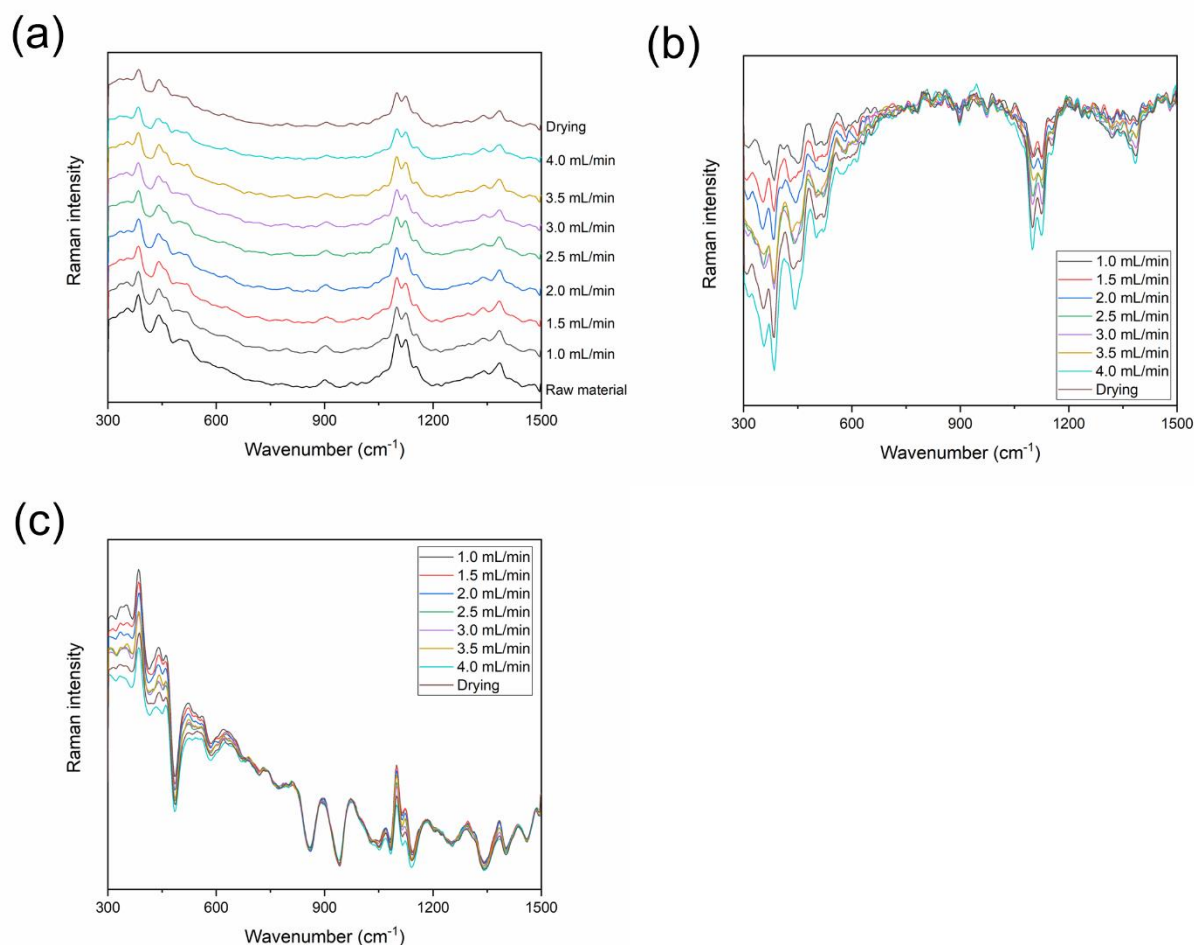
Figure 5.4: (a) Raman spectra for microcrystalline cellulose agglomerated with maltodextrin solution. The maltodextrin solution flow rate increased from 1.0 to 4.0 mL/min by increments of 0.5 mL/min every 10 min. (b) Raman spectra difference between each experiment and the CMC spectrum, and (c) Raman spectra difference between each experiment and the MD spectrum.

The evolution behavior of particle classes indicated that the Stabilization phase occurred and ranged from 42% to 87.5% of the process, mainly due to the linearity of retained fractions (Figure 5.3). The liquid binder flow rate increased in this phase from 2.5 mL/min to 4.0 mL/min, which was the largest identified phase in this experiment and achieved these already disposed condition. The increase in liquid binder flow rate favored the wetting of large particles by the liquid binder, which could make the particles return to the Wetting and Nucleation phases, starting the process again cyclically. However, that did not happen, at least not on a large scale, since the Raman spectra corresponding to this phase showed the decrease in the peak intensity indicating that the liquid binder was more evident on the surface particles. There was no agglomeration of new particles in this phase, and the SEM micrographs confirmed

no changes in the particle structures from the previous phase (Figure 5.5(c)-(f)). These images display contact points between particles when lower liquid binder flow rates (1.5 mL/min to 3.0 mL/min) were used and better-established solid bridges were defined for liquid binder flow rates at 3.5 mL/min at 4.0 mL/min (Figure 5.5(g) and (h)).
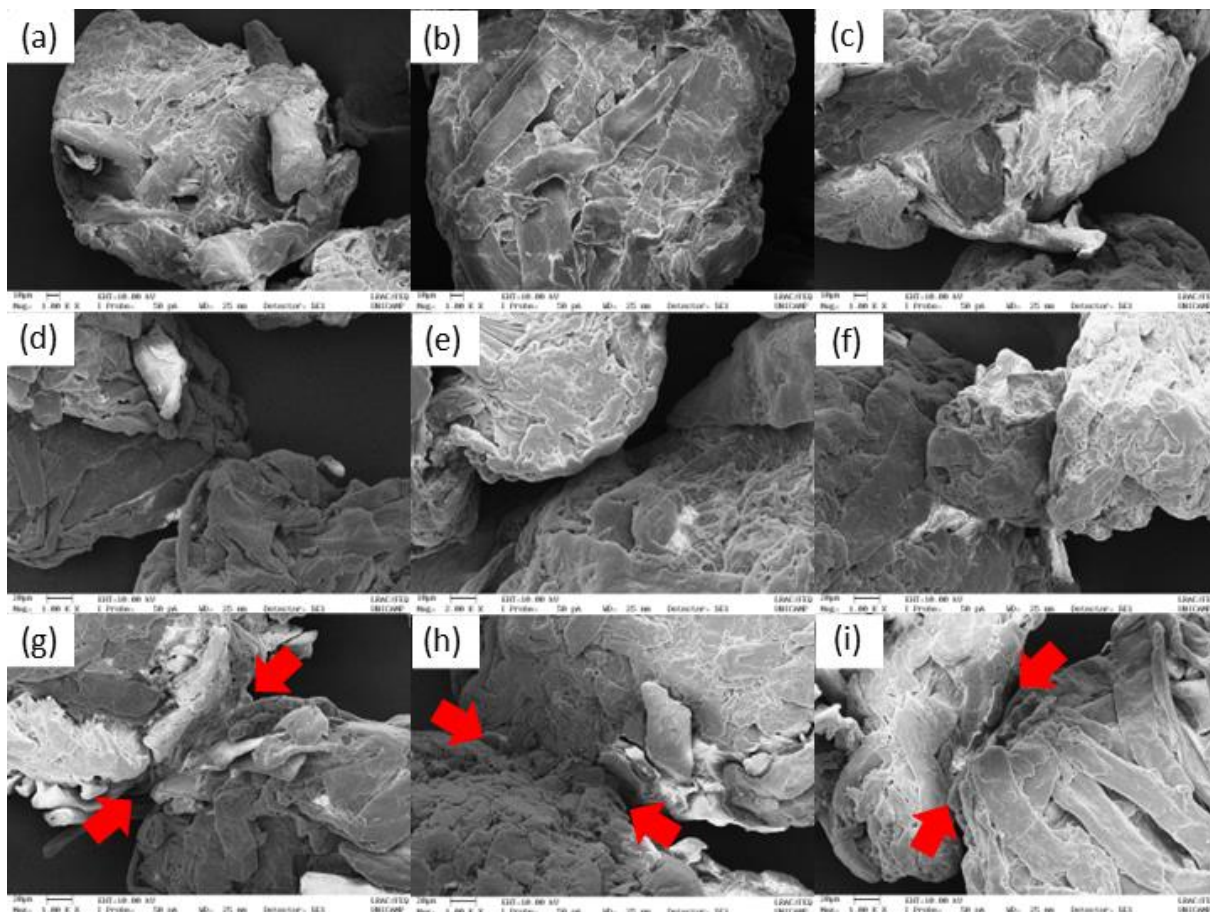
Figure 5.5: SEM micrographs of (a) raw material samples collected during the experiment while varying liquid binder flow rates as (b) $Q = 1.0$ mL/min, (c) $Q = 1.5$ mL/min, (d) $Q = 2.0$ mL/min, (e) $Q = 2.5$ mL/min, (f) $Q = 3.0$ mL/min, (g) $Q = 3.5$ mL/min, (h) $Q = 4.0$ mL/min, and at (i) drying phase, at $1000\times$ magnification, $C = 20.0\%$, and $T = 30$ °C. The red arrows indicate the solid bridges.

There was a slight decrease in the coarse retained fraction in the drying phase, as opposed to a small increase in the fine retained fraction and no change in the intermediate retained fraction (Figure 5.3). This behavior may have been related to the fragmentation of large particles by particle-particle or particle-chamber attrition. Also, during the drying phase, since the liquid binder atomization was turned off and the operating conditions were maintained, there was water evaporation from the particle surfaces and consequent particle shrinkage. The Raman intensity was slightly higher again than in the previous step, indicating that more CMC

may have been available on the particle surface. This fact can also be related to the water evaporation from the liquid binder solution deposited on the particles, leaving only well-defined points with available maltodextrin (Figure 5.4(a)). Figure 5.5(i) depicts the solid bridge formed between two CMC particles. Figure 5.6 displays the blue regions corresponding to where the maltodextrin solution was deposited by atomization on the particle surface. The contact point between particles could be observed where the maltodextrin solution remained after the end of the process. These contact points were also the places where the solid bridges were established. In some cases, the particles were completely covered by the maltodextrin solution, indicated by the blue color on most particle surfaces. Regardless of how much the binder solution covered the particle surface, there are two important points: first, the atomization of the binder solution was effective in the initial process phases (Wetting and Nucleation), and second, the formation of solid bridges occurred in stages where the binder solution was proven to be, even after the final stages of the agglomeration process (Consolidation and Growth) and the drying phase.
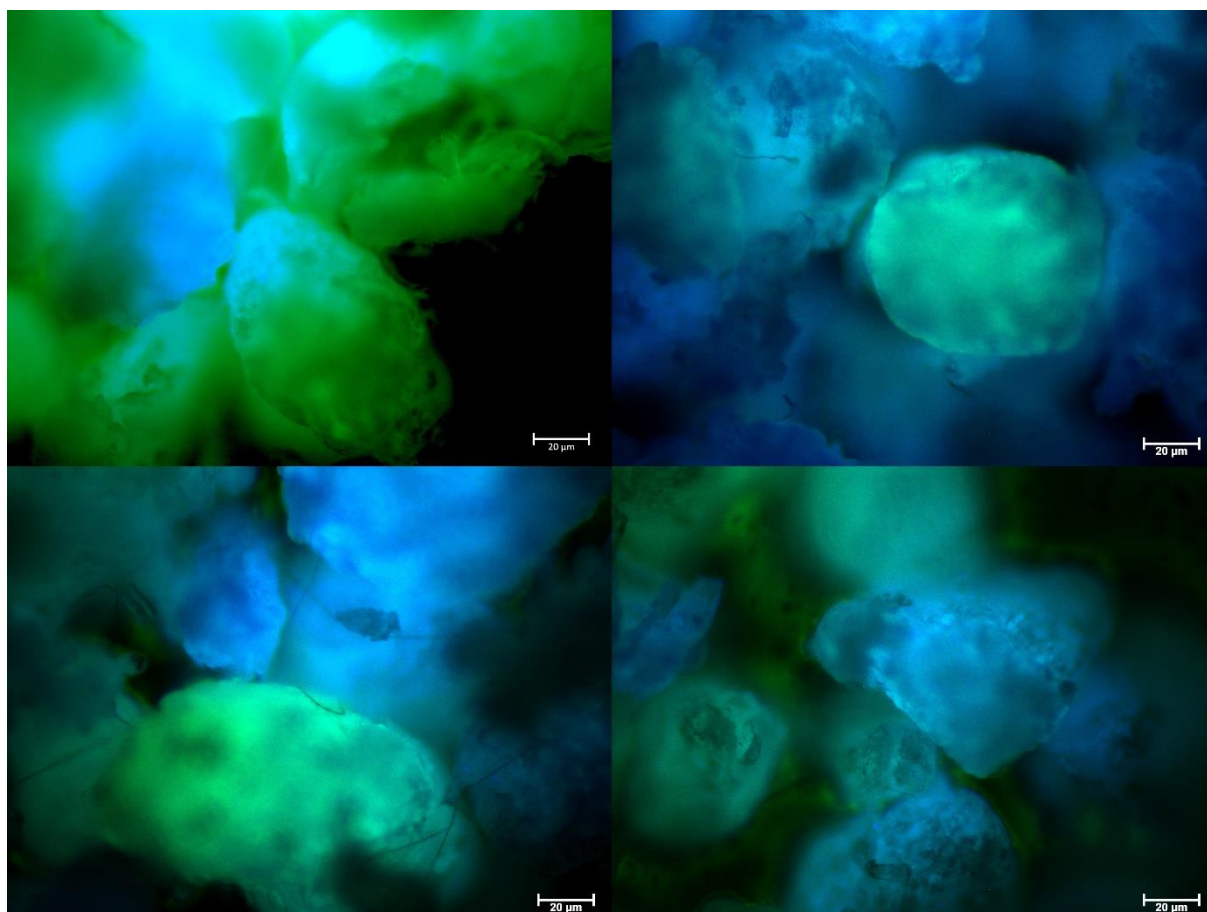
Figure 5.6: Fluorescence micrographs of agglomerated CMC at the end of the process. The green regions correspond to CMC, and the blue regions correspond to where the maltodextrin solution was deposited.

5.4. CONCLUSIONS

It could be concluded that the fluidized bed agglomeration of CMC with maltodextrin solutions has been proven efficient in increasing the mean particle size from based on what has been discussed. The analysis of the size classes was equally efficient in delimiting the steps of the agglomeration process according to the existing literature.

Raman spectroscopy was an extremely useful tool first to identify the composition of the surface of the granules after the process and, secondly, the deposition evolution of the maltodextrin solution on the surface of the granules.

The image analysis provided the visualization of agglomeration and solid bridge formation between CMC particles submitted to increased liquid binder flow rate conditions. There was a stage when the formation of bridges and stabilization of the granules became more evident, as indicated by the particle size class stabilization.

The combined use of the presented techniques proved to be appropriate for identifying mechanisms of granule formation in fluidized bed agglomeration and is a potential tool for further studies in this field.

REFERENCES

[1] K. Andreola, C.A.M. Silva, O.P. Taranto, Agglomeration process of rice protein concentrate using glucomannan as binder: in-line monitoring of particle size, Chem. Eng. Res. Des. 135 (2018) 37–51. http://doi.org/10.1016/j.cherd.2018.05.019.

[2] J.G. Rosa, R.F. Nascimento, K. Andreola, O.P. Taranto, Acacia gum fluidized bed agglomeration: use of inulin as a binder and process parameters analysis, J. Food Process Eng. 43 (2020) e13409. http://doi.org/10.1111/jfpe.13409.

[3] R.F. Nascimento, M.F. Ávila, O.P. Taranto, L.E. Kurozawa, A new approach for the agglomeration in fluidized bed mechanisms based on Spatial Filter Velocimetry technique, Powder Technology 393 (2021) 219–228. https://doi.org/10.1016/j.powtec.2021.07.076.

[4] G.M. Walker, S.E.J. Bell, K. Greene, D.S. Jones, G.P. Andrews, Characterisation of fluidized bed granulation processes using in-situ Raman spectroscopy, Chemical Engineering Science 64 (2009) 91–98. https://doi/org.10.1016/j.ces.2008.09.011.

[5] A. Burggraeve, T. Monteyne, C. Vervaet, J.P. Remon, T. De Beer, Process analytical tools for monitoring, understanding, and control of pharmaceutical fluidized bed granulation: A review, Eur. J. Pharm. Biopharm. 83 (2013) 2–15. http://doi.org/10.1016/j.ejpb.2012.09.008.

[6] G. Walker, S.E.J. Bell, M. Vann, D.S. Jones, G. Andrews, Fluidised bed characterisation using Raman spectroscopy: Applications to pharmaceutical processing, Chemical Engineering Science 62 (2007) 3832–3838. https://doi.org/10.1016/j.ces.2007.04.017.

[7] D.S. Hausman, R.T. Cambron, A. Sakr, Application of online Raman spectroscopy for characterizing relationships between drug hydration state and tablet physical stability, International Journal of Pharmaceutics 299 (2005) 19–33. https://doi.org/10.1016/j.ijpharm.2005.03.005.

[8] M. Alcalà, M. Blanco, M. Bautista, J.M. González, Online monitoring of a granulation process by NIR spectroscopy, Journal of Pharmaceutical Sciences 99 (2010) 336–345. https://doi.org/0.1002/jps.21818.

[9] R.F. Nascimento, J.G. Rosa, M.F. Ávila, O.P. Taranto, Pea protein isolate fluid dynamics and characterization obtained by agglomeration in pulsed fluidized bed, Part. Sci. Technol. (2020) 1–11. http://doi.org/10.1080/02726351.2020.1830209.

[10] G.C. Dacanal, F.C. Menegalli, Selection of operational parameters for the production of instant soy protein isolate by pulsed fluid bed agglomeration, Powder Technol. 203 (2010) 565–573. http://doi.org/10.1016/j.powtec.2010.06.023.

[11] T.A.M. Hirata, G.C. Dacanal, F.C. Menegalli, Effect of operational conditions on the properties of pectin powder agglomerated in pulsed fluid bed, Powder Technol. 245 (2013) 174–181. https://doi.org/10.1016/j.powtec.2013.04.047.

[12] V.G. Machado, T.A.M. Hirata, F.C. Menegalli, Agglomeration of soy protein isolate in a pulsed fluidized bed: experimental study and process optimization, Powder Technol. 254 (2014) 248–255. http://doi.org/10.1016/j.powtec.2014.01.040.

[13] R.F. Nascimento, J.G. Rosa, K. Andreola, O.P. Taranto, Wettability improvement of pea protein isolate agglomerated in pulsed fluid bed, Parti. Sci. Technol 38 (2019) 511–521. http://doi.org/10.1080/02726351.2019.1574940.

[14] G.I Tardos, M.I. Khan, P.R. Mort, Critical parameters and limiting conditions in binder granulation of fine powders, Powder Technol. 94 (1997) 245–258, 1997. http://doi.org/10.1016/S0032-5910(97)03321-4.

[15] S.M. Iveson, J.D. Litster, K. Hapgood, B.J. Ennis, Nucleation, growth and breakage phenomena in agitated wet granulation processes: a review, Powder Technol. 117 (2001) 3–39. http://doi.org/10.1016/S0032-5910(01)00313-8.

[16] M. Butensky, D. Hyman, Rotary drum granulation. An experimental study of the factors affecting granule size, Ind. Eng. Chem. Fundam. 10 (1971) 212–219. http://doi.org/10.1021/i160038a005.

[17] C. Avilés-Avilés, E. Dumoulin, C. Turchiuli, Fluidised bed agglomeration of particles with different glass transition temperatures, Powder Technol. 270 (2014) 445–452. http://doi.org/10.1016/j.powtec.2014.03.026.

[18] J.H. Wiley, R.H. Atalla, Band assignments in the Raman spectra of celluloses, Carbohydrate Research 160 (1987) 113–129. https://doi.org/10.1016/0008-6215(87)80306-3.

[19] G. Socrates, Infrared and Raman characteristic group frequencies: tables and charts, 3. ed. Wiley and Sons, 2001.

[20] Y. Beldengrün, J. Aragon, S.F. Prazeres, G. Montalvo, J. Miras, J. Esquena, Gelatin/Maltodextrin water-in-water (W/W) emulsions for the preparation of cross-linked enzyme-loaded microgels, Langmuir 34 (2018) 9731–9743. https://doi.org/10.1021/acs.langmuir.8b01599.

[21] R. Rózyło, M. Szymańska-Chargot, U. Gawlik-Dziki, D. Dziki, Spectroscopic, mineral, and antioxidant characteristics of blue colored powders prepared from cornflower aqueous extracts, Food Chemistry 346 (2021) 128889. https://doi.org/10.1016/j.foodchem.2020.128889.

[22] P.R. Mort, Scale-up of binder agglomeration processes, Powder Technol. 150 (2005) 86–103. https://doi.org/10.1016/j.powtec.2004.11.025.

[23] T. Jimenez, C. Turchiuli, E. Dumoulin, Particles agglomeration in a conical fluidized bed in relation with air temperature profiles, Chemical Engineering Science 61 (2006), 5954–5961. https://doi.org/10.1016/j.ces.2006.05.007.

[24] S.J. Maronga, P. Wnukowski, Establishing temperature and humidity profiles in fluidized bed particulate coating, Powder Technol. 94 (1997), 181–185. https://doi.org/10.1016/S0032-5910(97)03353-6.

[25] S. Heinrich, J. Blumschein, M. Henneberg, M. Ihlow, L. Mörl, Study of dynamic multi-dimensional temperature and concentration distributions in liquid sprayed fluidized beds, Chemical Engineering Science 58 (2003), 5135–5160. https://doi.org/10.1016/j.ces.2003.08.010.

[26] C. Turchiuli, T. Jimenèz, E. Dumoulin. Identification of thermal zones and population balance modelling of fluidized bed spray granulation, Powder Technol. 208 (2011) 542–552. https://doi.org/10.1016/j.powtec.2010.08.057.

CHAPTER VI

General discussion

Fluidized bed agglomeration is a widely employed process in the food industry for producing instant products and achieving better particulate material features. The final product, generally, displays an improved ability for dispersion and solubilization, porosity, flowability, and size. Adjusting the operating parameters is required to achieve experimental success since fluidized bed agglomeration is a complex process involving mutual unit operations and sensitive mass and heat transfer phenomena. Fluidized bed agglomeration consisted of continuous top liquid binder atomization on the moving particle bed promoted by the heated air stream for the purposes addressed in this current work. The studied parameters are among the operating ones related to the particulate material and liquid binder. The literature has reported parameters such as fluidized air velocity, fluidized air temperature, particulate material load, particulate material initial moisture content, liquid binder concentration, liquid binder flow rate, liquid binder atomizing pressure, atomizing nozzle height, and to a lesser extent, bed chamber geometry and the usage of pulsation, for example.

A theoretical study on trends in the area was carried out and presented in **Chapter II - Agglomeration in fluidized bed: bibliometric analysis, a review, and future perspectives** before starting to analyze the mechanisms related to the fluidized bed agglomeration process. A bibliometric survey was performed in the Web of Science database to identify the main articles that reported themes on agglomeration in fluidized beds. Among the 1,148 papers, only the top most cited 20 were selected for the posterior bibliographic analysis to facilitate the interpretation. Two trendlines were identified: Granulation and Combustion. This discussion will not emphasize the second trendline as further information can be obtained in the respective discussion in the chapter.

Regarding Granulation, the most cited papers cover the respective process, the range of techniques and equipment used, or its practical application for experimental or simulated products. Those publications also recognize that fluidized bed agglomeration is an outstanding unit operation and provides several applications in food products, pharmaceuticals, fertilizers, chemicals, and energy conversion. Moreover, without exception, all highlighted particle enlargement for improving end-use handling properties by agglomeration.

Regarding the microscale, agglomeration is defined as the aggregation of fine particles in more porous structures where the primary structure can still be distinguished. These aggregates are held together by solid bridges formed from liquid bridges. In turn, the liquid bridges are created by contact among wetted particles driven by the sticky layer and viscous and capillarity forces. Broadly, the agglomeration mechanisms have been reported as a

sequence of events that involves wetting, nucleation, coalescence, growth, stabilization, and breakage. Meanwhile, the beginning and end of these mechanisms are not strictly defined, and these steps may overlap or even occur concomitantly.

First, the CMC fluid dynamic behavior and which operating parameters that most influenced the process were defined to identify the fluidized bed agglomeration steps. After that, the main results in **Chapter III - A new approach for the agglomeration in fluidized bed mechanisms based on spatial filter velocimetry technique** were related to the data obtained by the SFV probe. It was possible to establish which and how the operating parameters influence the particle enlargement during the process, using an experimental Plackett-Burman design and its statistical analysis. Among the seven independent variables, liquid binder concentration, initial moisture content, and liquid binder flow rate caused positive effects on the particle size, and fluidizing air temperature caused a negative effect. The positive effect variables relate to the liquid binder features such as viscosity, how this forms a sticky layer around the particles, and the amount of liquid that remains on the already wet particle surface. The negative effect variable relates to water evaporation and the solid bridges' strength.

The most prominent innovative concept addressed in this chapter was the definition of the mechanisms for agglomeration based on the particle size classes from the analysis of the SFV data. It is a new approach based on the existing literature and the obtained data. The data classification by particle size classes made identifying a standard particle growth profile possible. Thus, this new approach was structured as a four-step sequence: Wetting, Nucleation, Coalescence and Growth, and Stabilization and/or Breakage.

The liquid binder features directly influenced the agglomeration process, as seen either through their operating variables or physicochemical properties. In the case of the experiments reported in this work, the liquid was inserted into the fluidized bed employing spray atomization performed by a bi-fluid atomizing nozzle at the top of the chamber. Indeed, there is little information found in the literature on how the spray droplets promote the wetting of the particulate material, even more so, considering that, based on the importance of what has already been discussed, the size of the droplets is a crucial factor for the evaluation of the particle growth in fluidized bed agglomeration. The results are reported in **Chapter IV – Spray system characterization for evaluating particle size enlargement in fluidized bed agglomeration**. The influence of operating parameters on droplet formation by PDI analysis was evaluated after the liquid binder characterization. Liquid binder concentration and flow rate influenced the droplet size more than the atomizing pressure under the studied conditions. The

growth only occurs if there is enough liquid to make the formation of liquid bridges possible. The limiting step for agglomeration is wetting, as noticed from the results and the literature. This chapter also used the particle size class strategy to understand the agglomeration process and classify the particle growth. The key reported factor was the degree of binder dispersion on the particle surface and how particles can contact and remain together. The variation in the liquid binder concentration was a noticeable impact on the agglomeration process mainly due to its associated physicochemical properties.

The solid bridge formation results from the drying of liquid bridges by water evaporation. The solution solid constituent tends to remain on the particle surface after solvent evaporation. Thus, bridge formation was expected to happen in the places where the liquid binder was deposited. Some technologies can be applied to visualize the presence of solid bridges and the superficial granule composition. The joint use of size measurement techniques and analysis of composition and images were addressed in **Chapter V – The formation of solid bridges during agglomeration in a fluidized bed: investigation by Raman spectroscopy and image analyses**. Some experiments were carried out under dry and wet conditions for that reason. These conditions were chosen based on the preliminary results already reported in this thesis. They were established according to the combination of fluidized air temperature and liquid binder flow rate. The other evaluated operating parameter was liquid binder concentration. SFV data and Raman spectroscopy were used to verify the binder presence on the particle surface. Also, that is how the studied conditions impact the agglomeration process as an effort to the effectiveness of the liquid binder deposition. The wet conditions were noticed to provide the sticky layer creation more effectively than dry conditions. These factors are very relevant for particulate material agglomeration since they have been found to favor coalescence and growth. The Raman spectroscopy assists in the confirmation of the binder deposition due to the shift observed in the collected spectra for each experimental run.

Subsequently, another experiment was carried out, now using image analysis. Since the deposition of material on the particle surface was confirmed in the previous experimental set by Raman spectroscopy, it was now possible to visualize the points of contact with the presence of the binder material and bridges formed at these points. It was possible to delimit a definite stage from which solid bridges are formed by confronting particle growth kinetics, Raman spectra, and image analysis. Indeed, solid bridges formed in stages where liquid binder

was confirmed to be, even after the final stages of the process and drying. It was only possible due to the effective binder solution atomization in the initial phases of the process.

Overall, these studies highlight the operating parameters' role in the fluidized bed agglomeration process. More specifically, how the operating conditions could contribute to the definition of process mechanisms, as well as an understanding of how the droplet size influences the appearance of granules and help to elucidate if there is a definite stage of the process when the particles tend to coalesce into granules. It is worth noting that all this was only possible, and it is considered the great advance of this thesis for this field of study, due to the joint use of advanced techniques of particle size measurement in real-time, measurement of droplet size, Raman spectroscopy, and image acquisition. Furthermore, it allows applying the knowledge gained here to actual materials, which is important to the industry.

CHAPTER VII

General conclusion

This research aimed at experimentally identifying the constituent stages of the fluidized bed agglomeration process through real-time monitoring of the process parameters listing the mechanisms governing the agglomeration process and the consequent formation of granules. Furthermore, the study aimed to propose which operating parameters are most suitable for the establishment and permanence of solid bridges. Finally, this study intended the joint use of advanced techniques for measuring particle size, droplet size, and image analysis for identifying solid bridges in agglomerated powder.

In the first phase of this research, the bibliometric analysis was performed to recognize the most frequent keywords, influential journals, the most cited papers, productive countries, and network collaboration according to co-authorship, and innovation trends in granulation and combustion research based on the top 20-most-cited articles surveyed in the Web of Science database. The studies examined theoretical approaches and experimental and/or numerical applications regarding granulation and combustion. The bibliographic review revealed a considerable range of fluidized bed applications, whether for producing foodstuffs or using gas combustion to separate inherent greenhouse gases. The duality of particle agglomeration was also identified, which is desirable for granulation, as the objective is to increase particle size for improved handling properties. In contrast, combustion is undesirable, as the particle increase negatively impacts reactor efficiency. Thus, it represents an opportunity to identify new potential ways of employing this technique in industrial processes.

The second phase of this research demonstrated by an experimental design that the agglomeration process is technically feasible for improving the CMC particle size. This process occurs due to the pulverization of a maltodextrin solution, used as a liquid binder, on the surface of CMC particles. Particle surfaces were wetted and dried, forming the agglomerated structure consolidation, leading to particle enlargement. Increased concentration, initial moisture content, and binder flow rate result in the production of larger granules. Additionally, when the fluidizing air temperature increased, D50v decreased. These data were confirmed by growth kinetics obtained from the SFV technique. This technique proved efficient and effective for real-time particle size monitoring in the CMC agglomeration with maltodextrin. In addition, PSD curves are considered one of the critical parameters in the particulate material agglomeration and, thus, process in-line follow-up and introduce relevant advances in this research field. Finally, a physical parameter was defined to delimit the previously proposed agglomeration steps in the literature. The most significant progress in this work was to present

a new approach considering particle size classification of particulate material divided into size classes and the joint use of the SFV technique.

In the third stage, the physicochemical properties of the maltodextrin solutions were verified as they are critical for droplet formation and CMC agglomeration. Moreover, the solutions spontaneously wet the solid by the analysis of the contact angle, suggesting that a wet and sticky layer is formed surrounding the particle. The data analysis of droplet size and velocity indicated that tiny droplets moved at low speeds, even though large droplets are more likely to move at higher velocities, according to the PDI data. Also, solution concentration and flow rate were the most prominent parameters in the droplet size enlargement, followed by the atomizing air pressure, with the least effect under the analyzed conditions. In the case of the fluidized bed agglomeration process, the operating parameter order was solution concentration, atomizing air pressure, and solution flow rate. In this way, particle enlargement depends on the particulate material and the liquid binder features.

Finally, the analysis of the particle size classes efficiently delimited the steps of the agglomeration process according to the existing literature. Furthermore, Raman spectroscopy was a useful tool to identify the composition and the deposition of the maltodextrin on the granule surface. The image analysis provided the visualization of agglomeration and solid bridge formation between CMC particles submitted to increased liquid binder flow rate conditions. There was a stage when the formation of bridges and stabilization of the granules became more evident. The combined use of the techniques related to this stage proved to be pertinent for identifying mechanisms of granule formation in fluidized bed agglomeration and is a potential tool for further studies in this field.

The application of the new approach to agglomerate real materials was proposed as a suggestion for future work, for example, proteins, carbohydrates, and fats used in food formulations. Additionally, all subsequent analyzes carried out for the CMC could be applied to these actual materials, being able to verify the influence of the type of particulate material in the agglomeration process. It would also be interesting to analyze other kinds of binder liquids, how they interact with particulate material, and whether the inferences caused by maltodextrin as related to granule formation hold true for these other liquids. Implementing joint techniques as a granule surface analysis protocol is also suggested.

References

[1] S.M. Iveson, J.D. Litster, K. Hapgood, B.J. Ennis, Nucleation, growth and breakage phenomena in agitated wet granulation processes: a review, Powder Technol. 117 (2001) 3–39. https://doi.org/10.1016/S0032-5910(01)00313-8.

[2] P.C. Knight, Structuring agglomerated products for improved performance, Powder Technol. 119 (2001) 14–25. https://doi.org/10.1016/S0032-5910(01)00400-4.

[3] C. Avilés-Avilés, E. Dumoulin, C. Turchiuli, Fluidised bed agglomeration of particles with different glass transition temperatures, Powder Technol. 270 (2014) 445–452. http://doi.org/10.1016/j.powtec.2014.03.026.

[4] A.M. Sakr, Characterization of wet granulation process parameters using response surface methodology, 1 Top-Spray Fluidized Bed, J. Pharm. Sci. 83 (1994) 937–947. https://doi.org/10.1002/jps.2600830705.

[5] G.C. Dacanal, F.C. Menegalli, Selection of operational parameters for the production of instant soy protein isolate by pulsed fluid bed agglomeration, Powder Technol. 203 (2010) 565–573. http://doi.org/10.1016/j.powtec.2010.06.023.

[6] V. Pont, K. Saleh, D. Steinmetz, M. Hémati, Influence of the physicochemical properties on the growth of solid particles by granulation in fluidized bed, Powder Technol. 120 (2001) 97–104. https://doi.org/10.1016/S0032-5910(01)00355-2.

[7] G.C. Dacanal, T.A.M. Hirata, F.C. Menegalli, Fluid dynamics and morphological characterization of soy protein isolate particles obtained by agglomeration in pulsed-fluid bed, Powder Technol. 247 (2013) 222–230. http://doi.org/10.1016/j.powtec.2013.07.001.

[8] V.G. Machado, T.A.M. Hirata, F.C. Menegalli, Agglomeration of soy protein isolate in a pulsed fluidized bed: experimental study and process optimization, Powder Technol. 254 (2014) 248–255. http://doi.org/10.1016/j.powtec.2014.01.040.

[9] K. Andreola, C.A.M. Silva, O.P. Taranto, Agglomeration process of rice protein concentrate using glucomannan as binder: in-line monitoring of particle size, Chem. Eng. Res. Des. 135 (2018) 37–51. http://doi.org/10.1016/j.cherd.2018.05.019.

[10] J.G. Rosa, R.F. Nascimento, K. Andreola, O.P. Taranto, Acacia gum fluidized bed agglomeration: use of inulin as a binder and process parameters analysis, J. Food Process Eng. 43 (2020) e13409. https://doi.org/10.1111/jfpe.13409.

[11] R.F. Nascimento, J.G. Rosa, K. Andreola, O.P. Taranto, Wettability improvement of pea protein isolate agglomerated in pulsed fluid bed, Part. Sci. Technol. 38 (2020) 511–521. https://doi.org/10.1080/02726351.2019.1574940.

[12] R.F. Nascimento, J.G. Rosa, M.F. Ávila, O.P. Taranto, Pea protein isolate fluid dynamics and characterization obtained by agglomeration in pulsed fluidized bed, Part. Sci. Technol. 39 (2021) 809–819. https://doi.org/10.1080/02726351.2020.1830209.

[13] K.V.S. Sastry, D.W. Fuerstenau, Mechanisms of agglomerate growth in green palletization, Powder Technol. 7 (1973) 97–105. http://doi.org/10.1016/0032-5910(73)80012-9.

[14] A. Heim, W. Antkowiak, A mathematical model for granulation kinetics, Chem. Eng. Sci. 43 (1988) 1447–1456. https://doi.org/10.1016/0009-2509(88)85136-4.

[15] M. Butensky, D. Hyman, Rotary drum granulation. An experimental study of the factors affecting granule size. Ind. Eng. Chem. Fundam. 10 (1971) 212–219. http://doi.org/10.1021/i160038a005.

[16] G.I. Tardos, M.I. Khan, P.R. Mort, Powder technology critical parameters and limiting conditions in binder granulation of fine powders, Powder Technol. 94 (1997) 245–258. http://doi.org/10.1016/S0032-5910(97)03321-4.

Appendices

APPENDIX A: Supplementary data referring to Chapter III
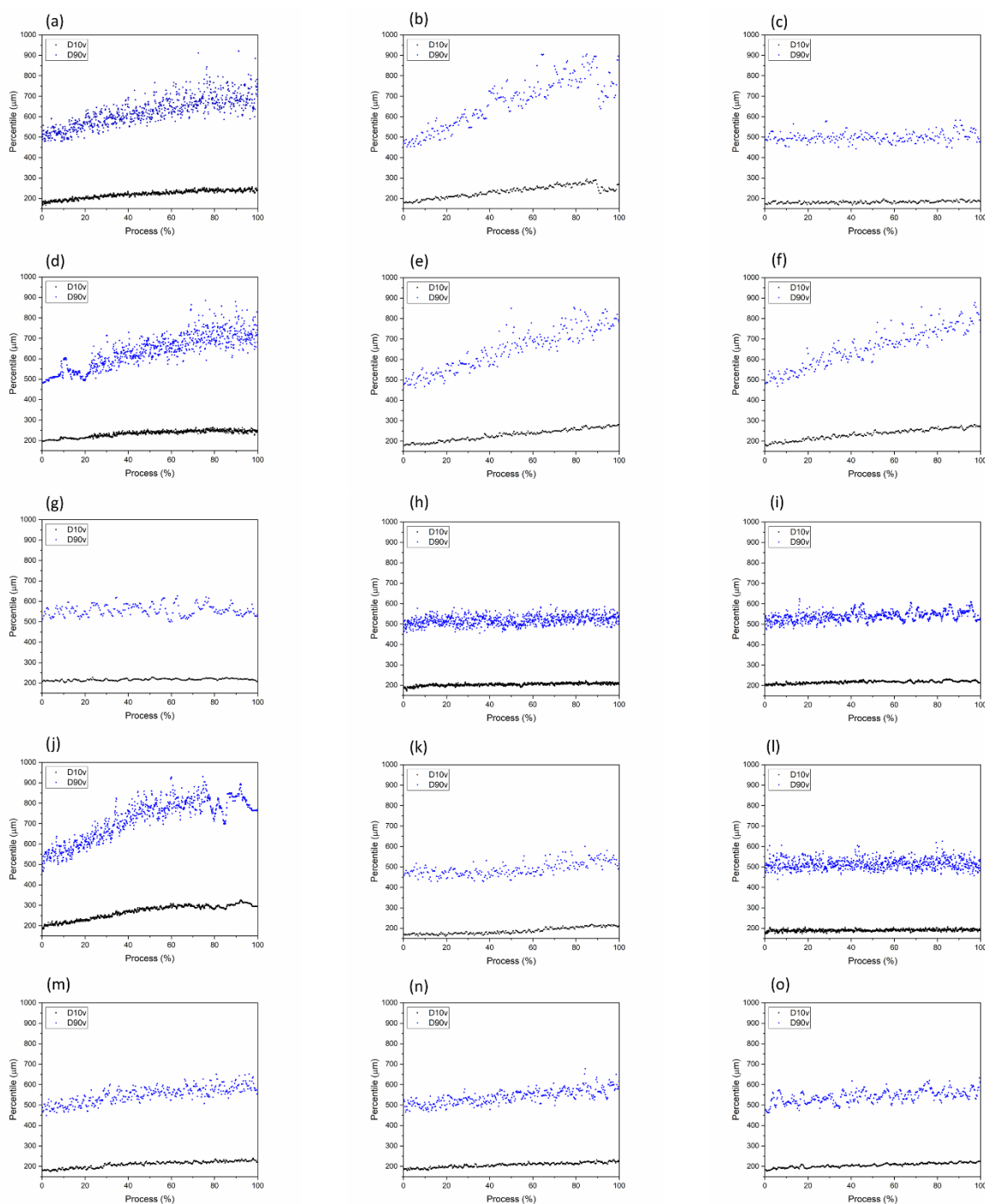
Supplementary material A: The particle growth kinetics for each run of the Plackett-Burman experimental design: (a) runs 1; (b) run 2; (c) run 3; (d) run 4; (e) run 5; (f) run 6; (g) run 7; (h) run 8; (i) run 9; (j) run 10; (k) run 11; (l) run 12; (m) run 13; (n) run 14; (o) run 15. The black dots correspond to the *D10v* percentile and the blue dots correspond to the *D90v* percentile.

APPENDIX B: Supplementary data referring to Chapter V
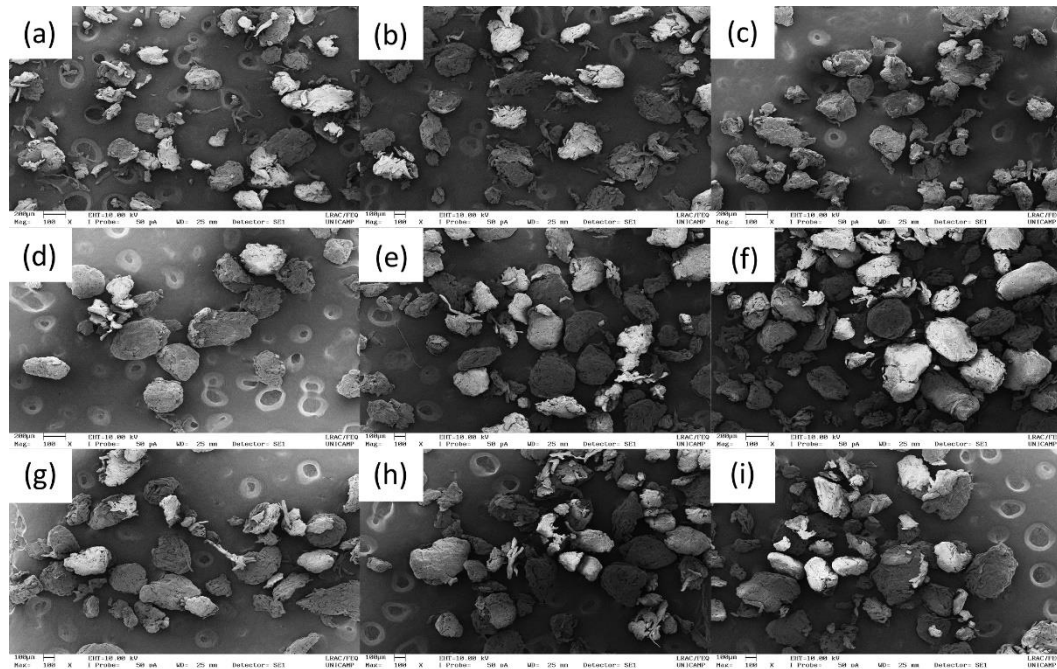
Supplementary material B1: SEM micrographs of (a) raw material samples collected during the experiment while varying liquid binder flow rates at (b) $Q = 1.0$ mL/min, (c) $Q = 1.5$ mL/min, (d) $Q = 2.0$ mL/min, (e) $Q = 2.5$ mL/min, (f) $Q = 3.0$ mL/min, (g) $Q = 3.5$ mL/min, (h) $Q = 4.0$ mL/min, and at (i) drying phase, at $100\times$ magnification, $C = 20.0\%$, and $T = 30$ °C.
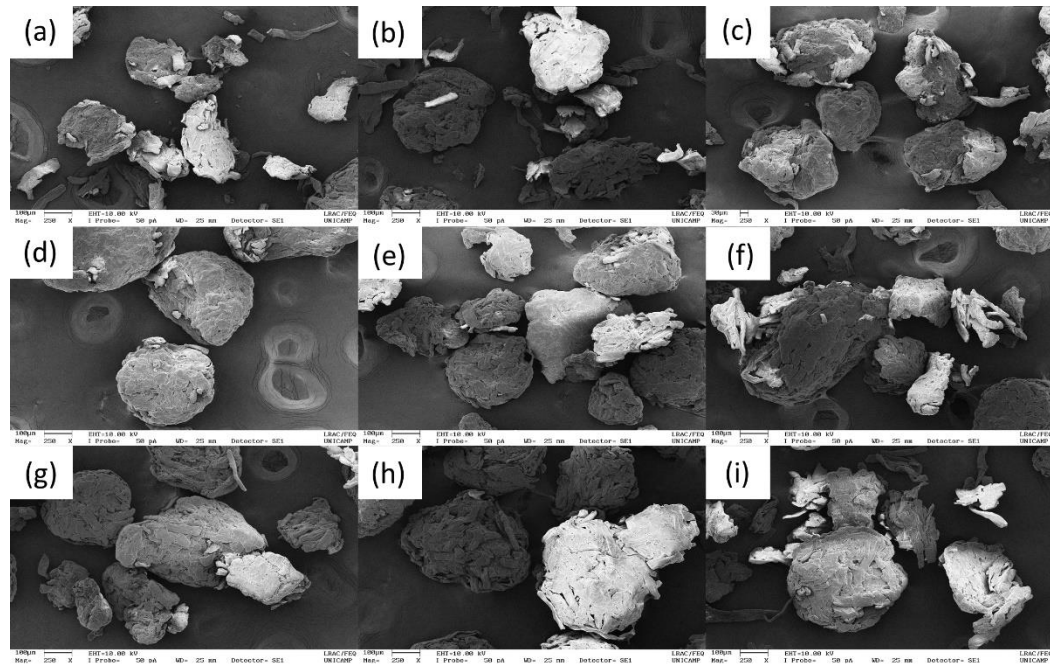
Supplementary material B2: SEM micrographs of (a) raw material samples collected during the experiment while varying liquid binder flow rates at (b) $Q = 1.0$ mL/min, (c) $Q = 1.5$ mL/min, (d) $Q = 2.0$ mL/min, (e) $Q = 2.5$ mL/min, (f) $Q = 3.0$ mL/min, (g) $Q = 3.5$ mL/min, (h) $Q = 4.0$ mL/min, and at (i) drying phase, at $250\times$ magnification, $C = 20.0\%$, and $T = 30$ °C.

APPENDIX C: Publisher authorization

Supplementary material C1: E-mail from Elsevier about the authorization to use the paper "*Agglomeration in fluidized bed: bibliometric analysis, a review, and future perspectives*" as part of the doctoral thesis.

Supplementary material C2: E-mail from Elsevier about the authorization to use the paper "*A new approach to the mechanisms of agglomeration in fluidized beds based on Spatial Filter Velocimetry measurements*" as part of the doctoral thesis.

Supplementary material C3: E-mail from Elsevier about the authorization to use the paper "*The formation of solid bridges during agglomeration in a fluidized bed: investigation by Raman spectroscopy and image analyses*" as part of the doctoral thesis.

APPENDIX D: Original writing verification report

Supplementary material D: Screenshot of the originality verification of the unpublished parts of the doctoral thesis (*Chapter I: General Introduction, Objectives, and Thesis Structure*; *Chapter IV: Characterization of spray system to evaluate particle size enlargement in fluidized bed agglomeration*; *Chapter VI: General discussion*; and *Chapter VII: General conclusion*). Verification performed by Turnitin® software via institutional access.